MOMENTUM TRANSPORT IN PACKED COLUMNS USING STOCHASTIC MODELS

by

Charles Burrell Schriver

A Dissertation Submitted to the
Graduate Faculty in Partial Fulfillment of
The Requirements for the Degree of
DOCTOR OF PHILOSOPHY

Major Subject: Chemical Engineering

Approved:

Signature was redacted for privacy.
In Charge of Major Work

Signature was redacted for privacy.
Head of Major Department

Signature was redacted for privacy.
Dean of Graduate College

Iowa State University
Of Science and Technology
Ames, Iowa

1963

TABLE OF CONTENTS

INTRODUCTION

The increased use of both fixed and fluidized beds by the process industries makes a knowledge of the fundamental behavior of such beds extremely important. A few examples involving such beds are adsorptive dryers, ion exchange columns, catalytic reactors, gravity filters, fluidized ore reduction processes, and towers bringing physical or chemical changes by contact means. While heat and mass transfer occur in many of these processes, momentum transport often plays a dominant role, and therefore it is important to understand the nature of momentum transport in these processes. The prediction of pressure drop or momentum loss in packed columns is a difficult problem and one that deserves continued study. Part of the difficulty lies in the extremely complex nature of porous media. Actually the Navier-Stokes equations, if they could be integrated, would completely describe the flow of a fluid through porous media. The boundary conditions required to integrate these equations could be formulated if the equation of the surfaces bounding the pore spaces could be found. At present, this is an impossible task, and the simpler geometry of a model is resorted to. Part of the difficulty lies in separating the influence of the variables from one another. For example, porosity has long been recognized as a very important variable affecting pressure drop in packed beds. Yet if porosity is to be studied over reasonably wide ranges, then both the particle diameter and particle shape must be varied, and the effects of porosity become confounded with the effects of other variables.

The attack on the problem has been from three main directions. First is the use of purely mathematical techniques in analyzing the bed structure and the flow through the bed. For the most part, these efforts have met with limited success but have been extremely valuable in understanding the basic nature of the problem. The second approach is the use of dimensional analysis or allied techniques to obtain working correlations. The relative success of this approach probably illustrates the similarity of the internal structure of many types of porous media. Finally there is the recent application of some statistical theory in analyzing the random nature of the flow. Almost no work has been done on the random nature of the porous medium itself. The apparent failure of the purely theoretical approach indicates an incomplete understanding of the basic nature of momentum transport.

The main purpose of this study was to investigate the usefulness of a few stochastic methods and models in determining momentum loss for laminar flow in packed columns. By its nature, this work is exploratory, and no attempt is made to investigate all aspects of the problem. A second purpose of this study was to provide some data on the internal characteristics of some typical packed columns that might be useful in future studies. It was felt that this work, in addition to investigating a new approach, would indicate the areas that require more intensive investigation.

This work may be divided into two main parts. In the first part, several experimental beds were constructed using cork packing, having typical commercial packing shapes, and wax. These beds were then

sectioned and sampled to provide frequency distributions of such bed properties as local porosity and local hydraulic radius. The radial variation of porosity was also determined for these beds. Some of these results were compared with the work of other investigators. Pictures of the experimental bed sections were taken so that they would be available for any future studies that might require such information.

The second part of this study was the construction and evaluation of two stochastic models. The calculations for the models were performed with a digital computer and made use of the distributions of bed properties obtained by sampling the experimental beds. The first of these models was a homogenous model while the second model was a two-region model with each region having its own distributions of bed properties. These models were used to predict mean momentum loss, in the region of low velocity laminar flow where inertial effects are negligible, for each one of the experimental beds studied. The models were also used to predict the variation in momentum loss between beds having the same superficial bed properties. The model predictions for mean momentum loss and variation between similar beds were compared with the predictions of Carman and Rose.

LITERATURE SURVEY

Introduction

The amount of literature dealing with flow through porous media and packed beds or columns is immense. One book on the subject, by Scheidegger (56), alone contains some two thousand references covering almost all aspects of fluid flow through porous media. Much of the literature dealing with this subject is discussed in books by Muskat (47), Carman (12), Collins (19), and Scheidegger (56). The book by Scheidegger is particularly valuable as it covers both laminar and turbulent flow, single and two-phase flow, and reviews much of the work done by Russian investigators.

This review will be limited to the more important aspects of single phase incompressible flow through unconsolidated porous media. The review is divided into two main parts. The first part is a historical review covering mainly flow through packed columns, while the second part is a review of the Kozeny-Carman type of equations and some of the experimental work connected with them. Laminar and turbulent flow are not treated separately, but the flow region in which a particular equation or correlation is valid will be indicated.

Historical Review

One of the first workers in the field, D'Arcy (22), was able to show empirically that for water flowing through uniform beds of sand, the following relation held

$$u_o = K_1 \frac{\Delta P}{L} \tag{1}$$

Here u_o is the superficial bed velocity.

K_1 is the permeability of the system and is defined as the rate of water flow across a unit cube of sand at unit pressure.

$\frac{\Delta P}{L}$ is the pressure drop per unit length of bed.

A common modification of this equation is to separate the influence of the porous medium from that of the fluid on the permeability. Thus

$$u_o = \frac{K_2}{\mu} \frac{P}{L} \tag{2}$$

where K_2 is the specific permeability and has the units of length squared. The specific permeability is supposed to depend only on the properties of the porous medium. This assumption has been verified by experiment. Equation 2 is often generalized to three dimensions in the following form

$$\underline{u_o} = \underline{\underline{K_2}} \cdot \nabla \left(\frac{P}{\mu L} \right) \tag{3}$$

where $\underline{\underline{K_2}}$ is now the specific permeability tensor. For an isotropic medium, this reduces to the familiar form

$$\underline{u_o} = \frac{K_2}{\mu} \nabla P \tag{4}$$

An excellent discussion of the D'Arcy law and its significance is given by Hubbert (35). Dupuit (23), realizing that the apparent or superficial bed velocity was less than the true velocity in the pores of the bed, extended the D'Arcy law by assuming that the porosity was constant throughout the bed and that

$$u = \frac{u_o}{\epsilon} \tag{5}$$

where ϵ is the porosity and u is the average pore or channel velocity. The modified D'Arcy law now becomes

$$u_o = K_3 \frac{\epsilon}{\mu} \frac{\Delta P}{L} \tag{6}$$

Equation 6 is useful only if the specific permeability can be related to the physical properties of the porous medium. Because of the extreme geometrical complexity of porous media, theoretical considerations are often based on simplified versions of the porous media called models. Actually the Navier-Stokes equations, if they could be integrated, would completely describe the flow of a fluid through porous media. This requires the formulation of a boundary condition that states that the velocity of the fluid at the walls of the pores or channels must be zero. This boundary condition could be written if the equation of the surfaces bounding the pore spaces could be found. At present, this is an impossible task, and the simpler geometry of a model is used. Some of the ways in which investigators have attempted to relate the specific permeability to the properties of porous media are

A. Empirical Correlations

B. Models

a. Capillaric models

straight capillary
parallel capillary
serial capillary
branching capillary

b. Drag theory models

C. Hydraulic Radius Theories

D. Mathematical and Statistical Theories

The most successful of these methods have been those based on simple capillary models or dimensional analysis. Pure mathematical or statistical methods have not been as successful in correlating results, but have aided in understanding the physical basis of flow in porous media.

The earliest models are those of the "sphere pack" variety. Slichter (60) considered the flow through a uniform bed of spheres. He considered the bed as analogous to a lattice structure with a unit cell repeated throughout the structure. He then obtained a correlation between the shape of this unit cell and porosity. Slichter finally obtained a modification of Poiseuille's law for laminar flow in capillaries of the following form

$$u_o = \frac{10.2}{K_4} \frac{D_p^2}{\mu} \frac{\Delta P}{L} \tag{7}$$

where K_4 is a function of porosity. The main objection to Slichter's treatment is that he assumed a mode of packing for the spheres. His work, however, led to the use of particle diameter as a measure of pore diameter and pointed out the importance of using porosity.

Terzaghi (65), using a modification of Slichter's treatment, obtained a relationship between permeability and porosity that agreed fairly well with experiment. His expression is

$$u_o = K_5 \frac{D_p^2}{\mu} \left(\frac{\epsilon - 0.13}{\sqrt[3]{1-\epsilon}} \right)^2 \frac{\Delta P}{L} \tag{8}$$

K_5 is an empirical constant that varies between 6.03 and 10.5 for all sands.

Emersleben (67) assumed that the granular bed could be approximated by a series of long cylinders that were equally spaced and parallel to the direction of flow. In his attempt to derive the fundamental D'Arcy law, Emersleben obtained values of permeability that did not agree with those derived by previous investigators.

The early mathematical methods described previously were not particularly successful in establishing a connection between Poiseuille's law for capillary flow and D'Arcy's empirical law. Greater correlation success has been obtained by the use of semi-empirical methods, such as dimensional analysis, to establish a connection between the variables. Many workers have accepted the idea of a granular bed being composed of a group of capillaries or channels parallel to the flow, and have attempted to relate the bed permeability to the bed porosity and some measure of channel diameter.

Stanton (62) applied dimensional analysis to flow in tubes and obtained the following result

$$R = K_6 \rho u^2 \left(\frac{D u \rho}{\mu} \right)^{n-2} \qquad (9)$$

where R is the resistance per unit area to flow, and n is 1.0 for laminar flow and 2.0 for fully developed turbulent flow.

The general method of applying dimensional analysis to packed beds is illustrated by the work of Blake (6). Blake's analysis of flow through packed beds led to the following equation.

$$\frac{g_c D_p \Delta P}{\rho u_o^2 L} = K_7 \left(\frac{D_p u_o \rho}{\mu} \right)^{n-2} \qquad (10)$$

This equation has an obvious similarity to Equation 9. Note that u_o is not the actual velocity of flow in the packing and that the particle diameter D_p is only a measure of the true pore diameter. Blake was able to show that his equation held true for a constant diameter packing. However, the dimensionless groups of Equation 10 did not correlate the data for various size packings, indicating that the particle diameter D_p must be modified in some way to account for the effects of porosity. He accounted for this effect by replacing D_p by the mean hydraulic radius $m = \epsilon/S$. Here S is the surface area per unit volume of packed bed. Blake also included the Dupuit assumption that the pore velocity is best represented by $u = u_o/\epsilon$. With these assumptions, Equation 10 becomes

$$\frac{g_c \Delta P \epsilon^3}{\rho L u_o^2 S} = K_7 \left(\frac{u_o \rho}{\mu S} \right)^{n-2} \tag{11}$$

If S is replaced by $S_o(1-\epsilon)$, Equation 11 becomes

$$\frac{\Delta P}{L} = \frac{K_7}{g_c} u_o^n \mu^{2-n} S_o^{3-n} \rho^{n-1} \frac{(1-\epsilon)^{3-n}}{\epsilon^3} \tag{12}$$

where n is 1.0 for laminar flow and 2.0 for turbulent flow, and S_c is the surface per unit volume of particle. For the laminar region, with n = 1.0, Equation 12 may be written

$$K_7 = \frac{g_c \Delta P \epsilon^3}{L u_o \mu S_o^2 (1-\epsilon)^2} \tag{13}$$

This equation is also referred to as the Kozeny equation and K_7 as the Kozeny constant. Blake (6), Fair and Hatch (26), and Kozeny (37) developed this equation at about the same time. Carman (13) has modified the Kozeny equation and collected numerous data in support of it. The Kozeny equation

and some of the assumptions connected with it are discussed in the next section of this literature survey. Blake used Equation 11 and obtained a suitable correlation for his data on the flow of air and water through cylinders, spheres, pumice, and rings although the data for rings did not correlate well. Only a small range in porosity was considered.

Most investigators have supplemented dimensional considerations with modifications of their own to obtain a particular equation. The method of correlation, however, is usually some type of friction factor versus Reynolds number (Re) plot.

Several early investigators, while not employing the equations developed by dimensional analysis in their complete form, did construct various types of friction factor versus Re correlations. Their work, however, was limited mainly to air and water flow through lead shot and various types of sand. Correlation was sometimes based on particle diameter alone and not on porosity. These investigators include Bakhmeteff and Feodoroff (4), Chalmers, Taliaferro, and Rawlins (16), Fancher and Lewis (28), Givan (31), and Hatfield (33).

Burke and Plummer (10) assume that the total resistance of the bed is the sum of the separate resistances of the individual particles in it, as measured free fall. This view is in direct opposition to the assumption that the bed is equivalent to a group of parallel channels. They obtained as a general expression for spheres

$$\frac{\Delta P}{L} = \frac{K_8}{g_c} u_o^n S^{3-n} \mu^{2-n} \rho^{n-1} (1-\epsilon)^{n-2} \epsilon^{-n-1} \qquad (14)$$

This equation is similar to the Kozeny equation except for the porosity function. They correlated their results with a friction factor versus Re plot, except that the term $\epsilon/1-\epsilon$ was considered to be close to unity for the range of porosity considered (i.e. ϵ = 0.4 to 0.5) and was dropped from their correlation. Their data were for air flow through beds of spheres and covered a range of modified Reynolds number ($\rho u_o/\mu S$) of approximately 0.002 to 8.

Furnas (29) conducted extensive research on flow through beds of broken solids and on the nature of the wall effect. He stated that the method of dimensionless groups was inadequate. He attempted to replace this method by a general law and recommended the following form for gases

$$\frac{\Delta P}{L} = AG^B \tag{15}$$

where G is the mass flow rate. Furnas found that A and B were complex functions of temperature, particle size, fluid density and viscosity, and porosity of the bed. B is 1.0 for laminar flow and 2.0 for fully developed turbulent flow. Most of Furnas' data were obtained for flow in the transition region. Chilton and Colburn (18) have objected to the use of this type of equation. They state that the type of flow depends on the modified Reynolds number ($D_p u_o \rho/\mu$). If the flow is in the turbulent range, with a value of 2.0 for B, then either a decrease in particle size or an increase in viscosity will change the flow to laminar, and B will have a value of 1.0 even though the mass velocity remains unchanged.

Chilton and Colburn (18) considered the flow of a fluid through a granular bed as the flow through conduits of irregular cross section, and

that the pressure drop was due to the sum of the frictional resistance of the particle surfaces and the head loss due to expansion and contraction. They also assumed that the actual velocity could be represented by u_o/F_a and that the channel diameter was approximately the same size as the particle diameter. F_a, the fractional effective free area, is not the bed porosity or the total free cross sectional area. It is that portion of the total free cross sectional area that is effective in transmitting the flow. They also included a correction for the wall effect as given by Furnas (29). Their resulting equation was

$$\frac{\Delta P}{L} = \frac{2f\rho u_o^2 A_f}{g_c D_p} \tag{16}$$

where A_f is a wall correction factor. The friction factor f was found to be a complex function of F_a and the ratio A_1/A_2 in both the laminar and turbulent regions. The factor A_1/A_2 is the ratio of the largest to the smallest opening of a void. Chilton and Colburn correlated their data by plotting f versus $D_p u_o \rho/\mu$. Since the factors F_a and A_1/A_2 are not easily evaluated, these variables were not included in their correlation. They believed that the accuracy of their equations and the use of the wall-effect correction, based on the work of Furnas (29), did not justify the use of a porosity function. Their data were for gas flow through balls and granules and were taken in the transition and turbulent region.

Gamson, Thodos, and Hougen (30) studied heat, mass, and momentum transfer for gas flow through spheres and cylinders at Re ranging from 100-4000. They correlated their results with friction factor and j-factor plots, but were unable to obtain a decent correlation of the pressure

drop results. A similar study is reported by Morcom (46) who passed various gases through beds of granular materials.

Oman and Watson (49) studied air flow through commercial tower packings and granules in the transition and turbulent regions and used a modified Blake method to correlate their results.

Coppage and London (20) investigated heat transfer and fluid friction characteristics of wire screens and spheres in the transition flow region, but experienced difficulty in correlating their pressure drop data.

Brownell, Dombrowski, and Dickey (9) assumed that the bed could adequately be described in terms of a shape factor, bed porosity, and diameter of the particles. The method of correlation was a plot of modified Re versus a modified Fanning friction factor. The modifying factors, F_{Re} and F_f, were given by plots of modifying factor versus porosity with particle shape or sphericity as the parameter. The use of charts rather than equations may lead to considerable inaccuracy when a function is changing rapidly. Their data were for liquid flow through various commercial packings and covered a range of modified Re from approximately 0.01 to 10,000 and a range of porosity from 0.4 to 0.93.

Rose (53), (54) applied dimensional analysis to the problem and performed a series of careful experiments with spheres to discover how the resistance to flow depended on the various dimensionless groups. When he attempted to apply his friction factor-Re correlation to nonspherical particles, he found that an additional shape factor, based on the maximum and minimum dimensions of the particle, was required. Rose also derived a correction factor for the wall effect and proposed a new porosity function.

Leva and coworkers (38), (39), (40) have made a thorough study of pressure drop for gas flow through packed beds using a variety of commercial packing materials and covering a range of Re from 200 to 10,000. Both smooth and rough surfaces were considered. By analogy to flow through empty tubes and the use of a shape factor (i.e. ratio of area of particle to area of a sphere of equivalent volume), the following general equation was developed

$$\frac{\Delta P}{L} = \frac{K_9}{g_c}\left(\frac{D_p G}{\mu}\right)^n \left(\frac{\mu^2}{\rho}\right)\left(\frac{\lambda^{3-n}}{D_p^3}\right)\frac{(1-\epsilon)^{3-n}}{\epsilon^3} \qquad (17)$$

The value of the constant K_9 depends on the surface roughness of the packing. Here n is the state of flow factor and varies from 1.0 for laminar flow to a value of 2.0 for turbulent flow. Leva found that surface roughness had a large effect in the turbulent region. A number of experiments were carried out on the prediction of voids in packed tubes.

Ranz (51), from a consideration of a rombhedral arrangement of spheres, developed the expression

$$4 f Re^2 = 1.11 C_D Re^{*2} \qquad (18)$$

Here Re^* is the Reynolds number based on the actual fluid velocity on the front faces of the spheres, and C_D is a resistance coefficient from a consideration of the packing geometry. Ranz concluded that $Re^*/ Re = 10.73$. He suggested that since 10.73 is a value for ordered packing, values of Re^*/ Re for other packings could be determined from pressure drop data. His plot of $C_D Re^{*2}$ versus Re^* shows good agreement with friction factors given by other investigators.

Ergun (24), (25) considered a two term equation to represent the pressure loss caused by simultaneous viscous and kinetic losses. His equation may be written

$$\frac{\Delta P}{L} g_c = 72\alpha \frac{\mu u_o}{D_p^2} \frac{(1-\epsilon)^2}{\epsilon^3} + \frac{3}{4}\beta \frac{\rho u_o^2}{D_p} \frac{(1-\epsilon)}{\epsilon^3} \quad (19)$$

Here α and β are constants indicative of the fact that the kinetic losses are statistically related to the number of particles per unit length of bed. From a consideration of the available data on granular materials, Ergun placed an average value of 150 on 72α and 1.75 on $3/4\beta$. This type of equation is desirable as it is applicable over the entire viscous, transition, and turbulent region.

Stepochkin (63) developed a two term equation similar to that of Ergun, and discussed the general nature of such equations. His equation may be written

$$\Delta P^* = \phi (A_o \, Re + B_o \, Re^2) \quad (20)$$

Here ΔP^* is a dimensionless pressure drop, A_o and B_o are constants developed from a consideration of an ideal bed of parallel cylindrical channels, Re is a modified Reynolds number, and ϕ is a hydrodynamic correction factor that must be determined by experiment.

Recently, several investigators have reviewed the available correlations and performed experiments to determine the most accurate of these correlations. Smith and Roper (61) studied air flow through granular materials for Re in the transition region. They concluded that although the Ergun equation gave the most consistent results, no correlation was

sufficiently accurate for engineering purposes. Their results may be open to question, however, as they found that a decrease in porosity was accompanied by a decrease in pressure drop. Wagstaff and Nirmaier (68) studied air flow through wooden blocks at Re from 100 to 400 and found the correlation of Ergun to be the most accurate.

Fan (27) has developed an equation similar to that of Ergun and has collected data covering a wide range in porosity and Re in support of his equation. Fan, using a semi-empirical method, was able to predict how the laminar and turbulent constants (e.g. α and β of Equation 19) in such a two term equation should vary with bed and packing properties.

Andersson (2) has made a thorough study of air and water flow through beds of spherical particles, covering a range of modified Reynolds number ($D_p u_o \rho / \mu(1-\epsilon)$) from 0.1 to 2000. He analyzed the two term equation employed by Ergun and, based on his data, determined how the factors, α and β, of Equation 19 varied with bed properties. Andersson also investigated the wall effect and end effects for these beds of spheres.

A few workers have attempted to investigate the effect of orientation on pressure drop. Wentz and Thodos (69) have conducted experiments on air flow through packed and distended beds of spheres, arranged in various cubic arrays, at porosities ranging from 0.354 to 0.882 and Re from 2,550 to 64,900. They found that their friction factors were less than those of Ergun and explained this discrepancy on the basis of a surface roughness effect. They also found that the particular cubic arrangement used had no effect on the value of the friction factor.

Martin, McCabe, and Monrad (44) studied pressure drop in stacked

spheres. Their results covered six different stacking arrangements and a range of Re from 1 to 10,000. They found that in addition to the regular friction factor, a semiempirical stacking constant was needed to corelate the results.

Several recent investigators have found the usual correlation methods inadequate and have attempted statistical or pure mathematical approaches to flow through porous media. Iberall (36) applied a drag theory approach to a model of a random distribution of circular fibers of diameter d and obtained the following expression for permeability

$$K = \frac{3}{16} d^2 \frac{\epsilon}{1-\epsilon} \frac{2-\ln(du_o\rho/\mu)}{4-\ln(du_o\rho/\mu)} \tag{21}$$

This equation predicts the slow variation of permeability with flow rate. This effect has actually been observed.

Brinkman (7), (8) analyzed the pressure drop exerted on a single pellet surrounded by a swarm of pellets which constitute a medium of permeability k. His equation may be written

$$\nabla P = -\frac{\mu}{k} \underline{u}_o + \mu \nabla^2 \underline{u}_o \tag{22}$$

where the second term on the right hand side accounts for viscous stresses on the solid surfaces. Brinkman solved his equation to obtain the factor

$$z = \frac{\text{force on N isolated particles}}{\text{force on a swarm of N particles}}$$

for laminar flow. From his calculations, Brinkman obtained a modification of Stokes' law and the following expression for permeability

$$K = \frac{R^2}{18}\left(3 - \frac{4}{1-\epsilon} - 3\sqrt{\frac{8}{1-\epsilon} - 3} \right) \qquad (23)$$

Here R is the radius of the sphere. Verschoor (66) has found that Brinkman's equation accurately fits the data for beds of sand fluidized by air, water, and toluene.

Prager (50) applied a variational technique to the problem of minimizing the energy dissipation in a porous medium and obtained an estimate of the lower bound for the resistance of the medium.

Scheidegger (55), (57), using a statistical approach, considered the path of a fluid particle through a porous medium. Under the assumption that there is no correlation between any two successive steps during the motion of the particle, a Gaussian distribution for the particle position is arrived at. Scheidegger then related the average displacement to the external field of forces and arrived at the fundamental differental equation

$$\epsilon \frac{\partial \rho}{\partial t} = \nabla^2 (\epsilon \rho D) + \nabla \cdot (\rho \frac{k}{\mu} \nabla P) \qquad (24)$$

In this equation, D is a factor of dispersion which is subject to the ordinary diffusion equation and is a property of the packing characteristics. The second term on the right hand side of this equation is a form of the D'Arcy law. Scheidegger states that laminar flow may be considered as the superimposing of two effects: the first is the average flow through a set of small channels and the second is a dispersivity effect. None of the assumptions in the capillary models of previous investigators lead to any such dispersivity effect.

Recently a number of authors, Childs and Collis-George (17), Millington and Quirk (45), Wyllie and Gardner (71), and Marshall (43), have proposed methods for calculating the laminar permeability of a porous medium from its pore size distribution. In these methods, a column of the porous media, having unit cross section, is sectioned and then randomly reassembled. By considering sequences of pairs of pores of all sizes, a mean neck or flow area may be calculated as the sum of a series of terms. While this method appears to give satisfactory predictions of saturated and relative permeabilities, it would appear to be best suited to porous media composed of actual channels such as sandstone. Also, the method requires reliable data on size distribution of the pores.

The Kozeny-Carman Equation

This section will be devoted to a discussion of the type of equation commonly referred to as Kozeny-Carman equations and some of the assumptions and experimental work connected with them. Equation 13 is an example of this type. Again, no attempt is made to provide a complete discussion of the subject, and only the more important modifications and experimental work connected with the Kozeny equation will be considered.

Kozeny's (37) method of derivation was to consider the porous medium as a collection of channels having various cross sections and some definite length. He then solved the Navier-Stokes equations simultaneously for all channels normal to the mean flow in the porous medium. The permeability of the medium is then expressed in terms of a hydraulic radius

and usually involves the specific surface of the medium. Complete details of this derivation are given by Kozeny (37), or a summary of the method may be found in Scheidegger (56). Kozeny's result may be written as follows

$$u_o = g_c \frac{k}{\mu} \frac{\Delta P}{L} = g_c \frac{\epsilon m^2}{k_o} \left(\frac{L}{L_e}\right)^2 \frac{\Delta P}{L} \qquad (25)$$

where k is the specific permeability

m is a hydraulic radius = ϵ/S (S is the specific surface of the porous medium)

L is the bed length

L_e is the actual length of path travelled by the fluid

k_o is a constant for laminar flow in conduits, whose value depends on the shape of the conduit

It can be seen from this equation that the porous medium may be regarded as equivalent to a single capillary whose properties are the average properties of the medium. The group of constants, $k_o (L_e/L)^2$, in the above equation is commonly referred to as the Kozeny constant, and the term $(L_e/L)^2$ is called the tortuosity.

In deriving his equation, Kozeny made the explicit assumption that there was no tangential component of the fluid velocity in the cross section normal to the flow. That is, he assumed that there was no torsional flow. Certain implicit assumptions were also made. These assumptions have been discussed by Carman (14) and may be listed

a. no pores sealed off

b. pores distributed at random

c. pores reasonably uniform in size

d. porosity not too high

e. fluid clings to walls of pore

f. porous medium equivalent to a batch of capillaries

Fortunately, these assumptions are fairly well met for most unconsolidated porous media, but may fail for certain consolidated media. Most of these assumptions are evident except for perhaps (c) and (d). Assumption (c) requires that the pores be reasonably uniform in size. That this is necessary, may be demonstrated by considering the hydraulic radius term, m^2, in Equation 25. The proper term here is really $(m^2)_{avg}$, but since one usually determines m_{avg} from gross bed properties, $(m_{avg})^2$ is used. These terms are exactly equivalent when there is only one pore size. This same reasoning may be applied to other terms in the Kozeny equation. Small deviations from uniformity do not seem to be serious. Childs and Collis-George (17), however, are opposed to the Kozeny theory on the basis of the assumption of uniformity and give a more complete discussion of the consequences of violating this assumption. Assumption (d) requires that the porosity not be too high. Numerous experiments, with high porosity fiber beds, indicate that the value of k_o in Equation 25 increases rapidly at these high porosities. This assumption, however, is met for most all beds of granular materials, in which the porosity is approximately 0.3 to 0.5, so that k_o may be regarded as fairly constant for this type of bed.

The most extensive use and modification of Kozeny's equation has been made by Carman (11). Both Kozeny and Carman chose the following

definition for hydraulic radius

$$m = \frac{\text{volume of capillary}}{\text{wetted surface of the capillary}} = \frac{\epsilon}{S} \qquad (26)$$

where S is the surface per unit volume of the bed. The following definition is equally satisfactory and could have been chosen instead of the previous one.

$$m = \frac{\text{area of cross section of capillary}}{\text{perimeter of cross section of capillary}} \qquad (27)$$

Both definitions are equivalent for circular capillaries, but may not be for packed beds. Harmson (32) has discussed these two definitions and has shown that, for a homogenous bed, the ratio of m defined by Equation 26 to m defined by Equation 27 is a constant, $\pi/4$. Harmson has also argued that the definition according to Equation 27 may be the more applicable, especially for capillary rise phenomena. In any event, the Kozeny constant must be determined experimentally, and any other constants arising will be absorbed in the experimental value of the Kozeny constant.

Carman derived Equation 25 by starting with Poiseuille's law for laminar flow in a capillary. Since k_o varies between 2.0 and 3.0 for conduits, Carman chose an average value of 2.5 for k_o, and based on visual observation of dye flow through glass beads, chose a value of $\sqrt{2}$ for L_e/L. This gives the Kozeny constant, $k_o(L_e/L)^2$, a value of 5.0, which is a commonly accepted value. Carman also replaced S by $S_o(1-\epsilon)$, where S_o is the surface to volume ratio of the particle, and included a shape factor or sphericity so that the hydraulic radius now becomes

$$m = \frac{\epsilon}{S} = \frac{\epsilon}{S_o(1-\epsilon)} = \frac{\phi\, d\, \epsilon}{6(1-\epsilon)} \qquad (28)$$

Here ϕ is a sphericity factor which is 1.0 for spheres and less than 1.0 for other shapes and 6/d is the value of S_o for a sphere of diameter d. A correction factor for the total specific surface S, due to the wall effect, was also included in Carman's equation.

In support of his equation, Carman (11), (13) has collected the data of several investigators and has taken numerous data of his own. Muskat and Botset (48) forced air at very high pressure differences across beds of glass spheres. Carman then employed a differential form of the Kozeny equation to calculate the Kozeny constant. For laminar flow, this constant was found to have a value of 4.65. Schriever (58) performed experiments with hot oil and various size glass spheres and found a mean value of 5.06 for the Kozeny constant. Carman's interest in the Kozeny equation was in determining its usefulness for evaluating the specific surface of various powders and granular materials. His data were for laminar flow of liquids through rings, saddles, sand, and wire crimps. After correcting for wall and end effects, Carman found that the Kozeny constant was approximately 5.0. He later modified his experimental technique to apply to fine powders and used it to determine the specific surface of quartz, celite, zinc, and cement powders. His results compare reasonably well with the specific surface determined by nitrogen adsorption methods.

Other workers have derived equations similar to Equation 25 by making assumptions slightly different from those of Carman. Fair and Hatch (26) derived a Kozeny type of equation by a reasoning similar to that of

Carman's. They did not, however, include an explicity tortuosity term in their equation. Bartell and Osterhof (5) derived Equation 25 by assuming that the channels were circular (i.e. $k_o = 2.0$) and that $L_e/L = \pi/2$. This gives a value of 4.9 for the Kozeny constant, which is in fair agreement with experimental data. Hickox (34) derived an expression similar to Carman's by assuming a shape factor of 1.0 and a value of 1.3 for L_e/L. He found that his formula gave good agreement with his experimental data taken for water flow through various sands.

For Equation 25 to be completely useful, one should be able to correctly predict values for k_o, $(L_e/L)^2$, and S a priori. Unfortunately, this is impossible in most cases, and the procedure is to test the equation under a variety of conditions to determine the variation in the Kozeny constant. An average value of this constant is then used as the basis of future predictions. Various workers, however, have attempted to predict or independently measure the factors in the Kozeny constant.

Sullivan and Hertel (64) introduced a tortuosity factor defined as $(\cos^2\theta)_{avg}$, where θ is the angle formed by the axis of the bed and a streamline at some point P. They claimed that $(\cos^2\theta)_{avg}$ would be extremely difficult to measure, but where inertia effects were negligible, this factor could be represented by $(\sin^2\phi)_{avg}$, where ϕ is the angle between a normal to the packing surface and the axis of the bed. They were able to calculate this factor for certain ideal cases of fiber orientation, but in general evaluation of this factor will not be possible. Sullivan and Hertel also measured the permeability of various beds of wool, cotton, and glass fibers. They found that, for intermediate values

of porosity, k_o had an average value of 3.0, rather than the value of 2.5 assumed by Carman, and at high porosities, k_o increased rapidly. They found also that the particular value of k_o depended on the orientation of the fibers. They concluded, however, that with a correction for fiber orientation, reasonably accurate values of the specific surface of powders, fibers, and other unconsolidated porous media could be calculated from Carman's equation.

Adamson (1) has performed experiments on the permeability of fiber beds. He found that the Kozeny constant increased with increasing porosity and claimed that the Kozeny equation was good only for low pressures and smooth surfaces.

Wiggins, Campbell, and Maass (70), however, found that a Kozeny type equation accurately predicted the specific surface of a number of fiberous materials.

Arthur et al. (3) studied air flow through charcoal granules using a Kozeny-Carman equation and found that their equation gave values of specific surface that agreed with values determined by other methods. However, they found that the pressure drop in these beds was influenced by the tube diameter to particle diameter ratio and by the manner in which the air was introduced.

Lorenz (41) has discussed the nature of tortuosity in porous media. On the basis of a simplified pore geometry, he derived a relationship between the electrical conductivity of a porous medium, saturated with a conducting fluid, and the pore geometry. His results appear more applicable to media having actual channels, such as sandstones, rather than

unconsolidated granular materials.

Macmullin and Muccini (42) investigated the characteristics of porous beds and structures using a refined electrical conductivity method. They correlated their results by the following equation

$$m^2 = KP\ R/R_o \qquad (29)$$

Here m is the hydraulic radius

K is a constant for all media

P is a permeability coefficient

R/R_o is the resistivity ratio and is the ratio of the resistance of the porous medium saturated with a conducting fluid to the resistance of the fluid occupying a volume equal to that of the medium

It can be seen that R/R_o is equivalent to the tortuosity $(L_e/L)^2$. The investigations mentioned above are typical of the many that have been carried out for the purpose of indepently measuring a tortuosity factor.

Attempts to predict k_o have not been nearly as successful as attempts to predict tortuosity. Many workers have used the theoretical results of Emersleben (67) who derived k_o on the basis of a model in which the fluid flows parallel to rows of equally spaced cylinders. These workers find, however, that they must usually modify Emersleben's values of k_o by semi-empirical means in order to reach agreement with experiment. Fortunately k_o remains reasonably constant in the porosity ranges covered by granular materials.

Coulson (21) performed a series of comprehensive experiments in which

oil was passed through beds of spheres, cylinders, cubes, plates, and prisms. After correcting for wall effects, Coulson found that the Kozeny constant varied from 3.5 to 6.0 with an average value of 4.5 for all packings. These experiments point out the danger in using the specific surface as determined from individual particle measurements as suggested by Carman. When packed into a column, flat surfaces tend to mate and reduce the actual surface exposed to the fluid. For spheres, having only point contacts, this is no problem, but Coulson found that the variation in the Kozeny constant was greatest for packings having flat surfaces such as cubes and plates.

Wyllie and Gregory (72) investigated the effect of particle size and shape on the Kozeny constant. They found that particle shape had a large effect on this constant, especially for packings having flat surfaces. The minimum variation in the Kozeny constant occurred at a porosity of 0.4 where the value was found to be 5.0 ± 0.5. Wyllie and Gregory also made independent measurements on the effective surface area of their packings by sectioning some of the packed beds and then employing a statistical pin dropping technique to calculate the surface to volume ratio. A similar study is reported by Chalkey, Cornfield, and Park (15) who tested this pin dropping technique on wooden blocks embedded in paraffin. Their interest was in determining the surface to volume ratios of tissue cells.

In conclusion, it would seem that a Kozeny-Carman type of equation may be used when dealing with beds of ordinary granular materials. That this is possible, is probably due to the fact that most granular materials have a similar structure. However, in view of the fact that only an

average value of the Kozeny constant can be predicted for these beds, an approximate variation of 10%-15% in the results must be acceptable. For beds of materials having widely varying configurations, porosity, or surface properties, such as beds of fibers and plates, special corrections will be needed if a Kozeny-Carman equation is to be used.

PREPARATION AND SAMPLING OF EXPERIMENTAL BEDS

General Description of Beds

To determine the internal characteristics of certain packed beds, a total of ten wax-cork experimental beds were prepared. Eight of these beds were sectioned perpendicular to the axis of the bed to investigate local hydraulic radius and porosity, and the remaining two beds were sectioned lengthwise so that the longitudinal distribution of the packing could be examined. The packings chosen, spheres, cylinders, and Raschig rings, represent common industrial packings that offer a reasonable variation in size, shape and bed porosity. Of the eight beds constructed for hydraulic radius and porosity measurements, four were for spheres, two were for cylinders, and two were for Raschig rings. Spheres were considered a most important packing hence both the tube diameter to particle diameter ratio (D_T/D_p) and two methods of packing were investigated. For cylinders, two values of D_T/D_p and one method of packing were considered. Raschig rings seemed to offer the greatest variation in packing characteristics, and therefore two methods of packing and one value of D_T/D_p were used. For all beds, only one value of bed length to tube diameter ($L/D_T \doteq 2.5$) was considered. This was done in order to limit the number of beds to a reasonable number and because it was felt that D_T/D_p was a more important variable than L/D_T. The characteristics of each bed and each type of packing are summarized in Tables 6 and 7 in the Appendix.

Preparation of Beds

The actual preparation of the beds was carried out as follows. A cardboard tube, having the required diameter, was cut to the desired length. The tube was then inspected to insure that it was perfectly cylindrical and free from any structural defects. After sanding, the tube was given two coats of lacquer to prevent wax seepage and then cemented to a wooden base. After the lacquer and cement had dried, the tube height and diameter were determined by averaging eight vernier caliper measurements of each dimension.

The tube was then packed with the desired packing. The packings were made from grade XXX cork and were supplied by the Manton Cork Co. Because of small deviations from the nominal dimensions, the actual dimensions of each type of packing were determined by vernier caliper measurements on a random sample of 100 pieces of packing. In this work, only two methods of packing were considered. In the first method, each piece was hand dropped from a height of approximately six inches. This allows each piece of packing to come to an equilibrium position before the next one is dropped and gives a more dense and even type of packing. The second method consisted of randomly dumping the packing into the tube. This method gives a loose type of packing and allows bridging of the particles to occur, especially with rough surfaces such as cork. After packing the tube, according to a particular method, the top of the bed was leveled by rearranging a few pieces of packing and covered with a wire screen to hold the packing down during the pouring operation. At this time, molten

paraffin (m.p. 58°C), preheated to 100°C, was slowly poured into the bed. The wax used was colored with small amounts of Methyl Red and Thymol Blue dyes to aid in the color contrast between the wax and cork. After pouring, the bed was allowed to soak at 120°C for approximately two hours to remove any air pockets. After the soaking period, the bed was allowed to cool at room temperature until solidified. As paraffin wax contracts on cooling, molten wax was added to the bed as needed during the cooling period. When the bed had completely cooled, it was cut into a number of sections, perpendicular to the axis of the bed, using a band saw. The thickness of these sections was determined mainly by the diameter of the bed. In general, the larger beds were cut into sections 1/2 inch thick and the smaller beds into sections 1/4 inch thick. After cutting, the sections were scraped and sanded so that the faces were smooth and approximately level. Each section was then photographed on black-white 35 mm. film (Kodak TX 135-20) using a Lica III-G camera and a close-up attachment. The approximate photographic conditions were a camera speed of 1/250 second with an f10 setting and a light meter reading of 65. After developing the film, slides were prepared from the film negatives for enlarging purposes. Photographs of a typical section from each bed are shown on pages 75 and 77. Before the sections could be sampled, they had to be enlarged to some convenient size for making measurements. This was accomplished by projecting the slides onto a flat surface and tracing the image onto a piece of paper. The magnification of the resulting enlargement was determined by dividing the average diameter of the enlarged section by the actual column diameter. Apparent variations in particle shape due to defects in the cork structure

were eliminated during this tracing. This master tracing was then used to make Xerox copies for measuring purposes. This method seemed superior to the usual photographic enlarging procedure as it could produce copies of the enlargement easily and gave a surface that could be written on with pencil.

Sampling of Beds

Before sectioning, each bed was marked with red and black lines running lengthwise so that the individual sections could be realigned after cutting. The individual sections were then labeled in the following manner. First each bed was given a letter designation according to the type of packing it contained. Thus

B designates spheres, 1/2 inch nominal diameter

C designates spheres, 3/8 inch nominal diameter

D designates Raschig rings, 1/2 x 1/2 x 1/4 inch nominal diameter

E designates cylinders, 3/8 x 3/8 inch nominal diameter

Next each bed, having a given packing material, was given a number showing which bed it was. Finally the sections were numbered consecutively starting at the top with one. Thus, a section labeled C3-5 would designate the fifth section from the top of the third bed made with C type packing.

In order to limit the measurements made to a reasonable number, not

all sections from a given bed were used and then only part of each sampled section was used. For each bed, the top 1/2 inch and bottom 1/2 inch were excluded from the sampling. This procedure was adopted because the presence of the tube base and the top retaining screen tends to orientate the packing. These conditions are not representative of the conditions for most of the bed, in which the packing is random, and would not be important unless the beds were extremely short.

The sections were sampled by a method that was partially systematic and partially random. In all random sampling, a table of random numbers was employed. First, it was assumed that the properties of the top half of the bed were similar to the properties of the lower half. Then a section was randomly selected from say, the top half of the bed. The properties of this section were assumed to be similar to the corresponding section in the lower half of the bed, and therefore the section in the lower half was not considered during the remainder of the sampling. This procedure was repeated, alternately choosing sections in a random manner from the upper and lower halves of the bed, until the required number of sections was obtained. In each sampled section, every exposed packing face was given a number. These numbers were then used to randomly sample within each section. At least 25% of each section was sampled. The method for determining the approximate sample size was as follows. A sample was taken, and a histogram of some function calculated from the sampled quantities, such as hydraulic radius, was constructed. Sampling was repeated until the cumulative percent frequency of each class interval of the histogram changed very little. This method, while arbitrary, was

adopted as an approximate procedure. A sample size of approximately 120 was usually obtained.

THEORY AND DESCRIPTION OF MODELS

Introduction

Because of the extreme geometrical complexity of porous media, theoretical considerations are often based on simplified versions of the porous media called models. These simplifications are necessary since the complexity of the porous media does not allow formulation of the boundary conditions necessary to solve the Navier-Stokes equations. One possible general classification of these models is listed on page 6 of the literature survey. No attempt is made in this section to give a complete exposition or general theory of models. Rather, the development and calculation procedures for two specific models are discussed. This section is divided into three main parts. In the first part, some important general considerations for the models are discussed. In the remaining two parts, a description of two specific models and the calculation procedures associated with each are discussed. Any nomenclature that is used occasionally or only once is listed when required.

General Considerations

The description of the nature of porous media, even if this description is completely empirical, is a difficult one. For this reason it would be well to consider first some general aspects of flow in porous media that would be common to many models. A general classification for models is also given.

Consider first a section of straight conduit having only friction drag, that is, there is no momentum loss due to expansion and contraction or form drag. Then

$$F_{drag} = \tau_w A_w = \tau_w Z \ell = (-\Delta P) S \tag{30}$$

where F_{drag} = drag force

τ_w = shear stress at the wall

A_w = area of the wall

Z = constant perimeter of the conduit

ℓ = length of conduit

S = constant cross sectional area of the conduit

Rearranging gives

$$-\frac{\Delta P}{\ell} = \tau_w \frac{Z}{S} = \frac{\tau_w}{R_h} \tag{31}$$

Thus the classic definition of hydraulic radius, R_h, is

$$R_h = \frac{\text{cross sectional area available for flow}}{\text{wetted perimeter}} = \frac{S}{Z}$$

If this particular definition is applied to a packed bed, expansion and contraction and form drag must be accounted for separately, if their effects are important.

Consider now the more general case of steady state flow through a void or pore having smooth continuous surfaces but arbitrary shape. Such a pore might appear as

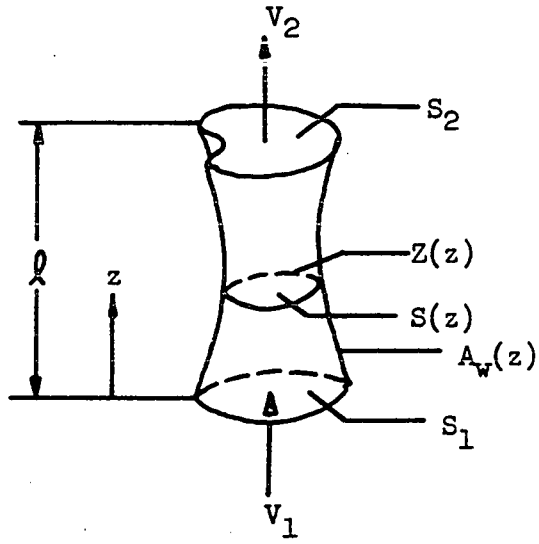

Figure 1. Arbitrary pore

Here V is an average velocity, and now the wall area, wetted perimeter, and cross sectional area are all functions of distance along the channel, z. At steady state, the following balance may be written

$$\underline{F}_{drag} = -\Delta\left[\frac{\langle v^2\rangle}{\langle v\rangle^2}\ \underline{w}\right] - \Delta(PS) + \rho\,\underline{g} \qquad (32)$$

where Δ = condition at 2 - condition at 1

P = pressure

w = mass flow rate = ρVS

v = point velocity

V = average pore velocity at height z

The underline represents a vector quantity. The following may also be written.

$$\underline{F}_{drag} = \underline{F}_{viscous\ drag} + \underline{F}_{form\ drag} \qquad (33)$$

and

$$\underline{F}_{drag} = \int_{A_w} \tau_w dA_w + \int_{A_w} P_w dA_w \qquad (34)$$

where τ_w = z component of the tangential shear stress

P_w = z component of the normal pressure force

Expanding Equation 32 and equating to Equation 34 gives

$$\int_{A_w} \tau_w dA_w + \int_{A_w} P_w dA_w = -\Delta(\rho VSK) - \Delta(PS) \qquad (35)$$

where $K = \langle v^2 \rangle / \langle v \rangle^2$

If $S_1 \neq S_2$, then

$$\Delta(PS) = P_2S_2 - P_1S_1 = (P_1 - \Delta P)S_2 - P_1S_1$$
$$= P_1(S_2 - S_1) + (\Delta P)S_2$$

or

$$\Delta P = \frac{\Delta(PS)}{S_2} - \frac{P_1(S_2 - S_1)}{S_2}$$

and Equation 35 becomes

$$-\frac{\Delta P}{\ell} = \frac{P_1(S_2-S_1)}{\ell S_2} + \frac{\left[\int_{A_w} \tau_w dA_w + \int_{A_w} P_w dA_w + \Delta(\rho V^2 KS)\right]}{\ell S_2} \qquad (36)$$

Equation 36 is a general equation for pressure drop in any pore. It includes the contribution of viscous drag, form drag, and expansion and contraction. The object is now to make

$$\frac{\Delta P}{\ell} = \Phi(V, R_n, \ell, \eta, \text{system geometry ratios})$$

That is, the real pressure drop is desired in terms of easily measured or defined variables. Unfortunately, since τ_w and P_w are generally not known as functions of pore height z, exact solutions to the problem may be found

for only a few situations involving simple geometry, such as a circular tube or annulus. While exact solutions are not usually possible, any semi-theoretical model must in some way account for the effects of viscous drag, form drag, and expansion and contraction when these effects become important.

In constructing any model or physical description of flow in porous media, two problems immediately become apparent. The first of these is the actual construction of the physical or geometrical model, or more specifically, the descriptions and definitions of such quantities as pore width, pore length, orientation of pores, etc. The second problem involves formulating some rule or criteria for the way in which the incoming fluid will distribute itself among the pores. Both of these problems are outlined and discussed in a general way below and will be discussed more fully later on.

While there are many models and means of describing porous media, it is convenient to classify them into the following five groups. Many variations are of course possible.

I. Quasi-homogenous, non-intersecting, non-momentum-diffusion model

In this, the simplest class of models, the bed is regarded as being more or less homogenous in nature. The flow channels in the bed are considered as non intersecting and independent of each other. Also there is no diffusion of momentum between streams of fluid flowing through the bed.

II. Quasi-homogenous, intersecting, non-momentum-diffusion model

In this model, there is no interaction or momentum transport between

fluid streams in the bed. However, the channels do intersect and sideways motion of the fluid from channel to channel may occur.

III. Quasi-homogenous, intersecting, momentum diffusion model

Momentum exchange takes place between fluid streams meeting at an intersection of two channels. In laminar flow, there would be incomplete momentum transport while in turbulent flow almost complete mixing would occur.

IV. Non-homogenous model

Here the properties of the porous medium or packed bed vary from point to point, and the effect of radial porosity become important. This model may incorporate features of the previous ones.

V. Non-isotropic model

Here the effect of direction on the model properties is important. Again, features from previous models may be incorporated into a single model. A very sophisticated model would probably include intersecting channels and momentum diffusion as well as being non isotropic.

In addition to choosing one of the preceding model types, or a variation of one, to describe the porous media, it is necessary to postulate some criterion for the way in which the incoming fluid will distribute itself among the pores or channels of a cross section of the medium. This is equivalent to asking what the fluid velocity in a particular pore will be. Some possible criteria are

1. equalization of total momentum loss over volume
2. minimization of total momentum loss
3. equalization of energy loss over volume

4. minimization of total energy loss
5. equalization of mass flow over volume
6. equalization of pressure

The selection and use of some of these criteria will be discussed later on. Having chosen the general type of model and some particular criterion for flow distribution, the investigator must now make his predictions using the properties of real porous media. In the remainder of this section, some ideas and calculation methods common to both Model 1 and Model 2 are described.

In this work, the models are limited to a description of incompressible laminar flow, although extension to other flow regimes appears possible. In some parts of the calculation, the same nomenclature has been used to mean different things. This is particularly true for subscripts. This practice has been followed to avoid the use of too many cumbersome symbols and has been used only when the immediate meaning of the symbol was obvious.

Before actually considering the physical structure of the models, it would be well to illustrate the method of calculating certain of the model properties from data sampled from the experimental beds. The preparation and sampling of the experimental beds has been described in a previous section. An illustrative section of a packed bed is shown in Figure 3 on page 51. From such a section, the model properties, such as pore diameter and pore length, are to be calculated. Because of the extreme complexity of any real porous media, definitions and descriptions of the properties of the porous media must necessarily be arbitrary and

somewhat incomplete. One simple measure of pore diameter would be the shortest distance between exposed packing faces. While the average value of this distance may have some significance, this definition leads to a distribution of pore size that is too wide and gives unrealistic values of pore size at the tails of the distribution. This would necessitate the use of some completely arbitrary "cut off" values of pore diameter. The difficulty arises from the fact that this definition of pore diameter is a purely geometric one and does not consider any of the dynamic aspects of the flow. As a first step toward defining the model properties used in these calculations, it is assumed that the locus of the maximum velocity within the bed is equidistant from packing surfaces. While this assumption is arbitrary, it is reasonable and certainly is no worse than the usual assumptions made in dealing with packed beds. Such a locus is shown as the dotted line in Figure 3. Since this dotted line is by assumption the locus of maximum velocity, the shear stress is zero at this boundary, and no momentum will be transferred across this boundary either by bulk flow or diffusion. Each separate piece of packing together with its dotted boundary has been given the name "momentum cell." The complete cell is illustrated in Figure 2 on page 51. For each cell sampled, the total cell area S'_m, the area of the exposed packing surface S'_p, and the wetted perimeter of the exposed packing surface Z'_p, are recorded. The areas were measured on the enlarged sections using a Keuffel and Esser planimeter, and the perimeters were measured with a Keuffel and Esser map measure accurate to 1/32 inch. From these sampled quantities, the following quantities can be defined and calculated.

$$S'_i = S'_{mi} = S'_{pi} = \text{momentum cell flow area}$$

$$S_T = \sum_i S'_{mi} = \text{total cross sectional area of the bed}$$

$$\epsilon'_i = (S'_{mi} - S'_{pi})/S'_{mi} = \text{momentum cell porosity} \qquad (37)$$

$$m'_i = (S'_{mi} - S'_{pi})/Z'_{pi} = \text{momentum cell hydraulic radius} \qquad (38)$$

$$\langle v \rangle_i = \frac{\int_{S'_{pi}}^{S'_{mi}} v_i \, dS}{S'_{mi} - S'_{pi}} = \text{average fluid velocity in momentum cell} \qquad (39)$$

$$Q = \sum_i \langle v \rangle_i (S'_{mi} - S'_{pi}) = \text{total volume flow}$$

$$v_o = \sum_i \langle v \rangle_i (S'_{mi} - S'_{pi})/S_T = \text{superficial bed velocity} \qquad (40)$$

The prime indicates that the measured or calculated quantity has a distribution. The calculated quantities ϵ'_i and m'_i are tabulated for each bed and represent a sample from the population of all possible momentum cell porosities and hydraulic radii for a particular type of bed. Illustrative histograms of m' for each type of bed are shown on pages 88 and 90.

As the fluid flows through the bed, each cell contributes a certain fraction to the total momentum loss. The way in which momentum is lost in a cell may be calculated in the following way. Consider an illustrative momentum cell as shown in Figure 3 on page 51, and define the following quantities

$$s^* = \frac{s}{S'_m - S'_p} = \frac{s}{S} \quad \text{and} \quad z^* = \frac{z}{Z'_p}$$

where s = area within the momentum cell with a boundary having some constant shear stress τ

z = perimeter of the area s

These calculations are for a general momentum cell and therefore any

subscripts that would ordinarily be used are dropped. A generalized description is used here (i.e. s and z), rather than a particular coordinate system, to emphasize the fact that the following calculations may, in theory, be applied to any situation. However, a practical calculation cannot be made unless the relationship between s and z is known, as it is for the simplified momentum cell to be treated here. The following boundary conditions apply.

(1) $s^* = S_m^*,\ z^* = Z_m^*;\ \tau = 0$

(2) $s^* = S_p^*,\ z^* = Z_p^*;\ v = 0$

For the momentum cell

$$\int d(\tau z) = \int \frac{\Delta P}{\ell}\, ds + C_1 \tag{41}$$

Applying B.C. (1) gives $C_1 = -\Delta P\, S_m/\ell$, and Equation 41 becomes

$$\tau = \frac{\Delta P\, s}{\ell z} - \frac{\Delta P}{\ell} \tag{42}$$

Newton's law of viscosity is

$$\tau = -\eta\, z \frac{dv}{dn} \tag{43}$$

where n is some general coordinate distance with $dn = ds/z$ so that

$$\tau = -\eta\, z \frac{dv}{ds} \tag{44}$$

Equation 42 now becomes

$$dv = -\frac{\Delta P\, s\, ds}{\eta\, \ell\, z^2} + \frac{\Delta P\, S_m ds}{\eta\, \ell\, z^2} \tag{45}$$

or in terms of dimensionless variables

$$dv = -\frac{\Delta P}{\eta \ell}\left(\frac{S^2 s^* ds^*}{Z_p^2 z^{*2}} - S_m \frac{S\, ds^*}{Z_p^2 z^{*2}}\right)$$

$$dv = -\frac{\Delta P S^2}{\eta \ell Z_p^2}\left(\frac{s^* ds^*}{z^{*2}} - \frac{S_m\, ds^*}{S\, z^{*2}}\right) \tag{46}$$

$$v = -\frac{\Delta P S^2}{\eta \ell Z_p^2}\left(\int_{S_p^*}^{s^*} \frac{t^* dt^*}{z^{*2}} - S_m^* \int_{S_p^*}^{s^*} \frac{dt^*}{z^{*2}} + C_2\right) \tag{47}$$

where t^* is a dummy variable of integration. Applying B.C. (2) gives $C_2 = 0$ and Equation 47 becomes

$$v = -\frac{\Delta P S^2}{\eta \ell Z_p^2}\left(\int_{S_p^*}^{s^*} \frac{t^* dt^*}{z^{*2}} - S_m^* \int_{S_p^*}^{s^*} \frac{dt^*}{z^{*2}}\right) \tag{48}$$

Now by definition

$$\langle v \rangle = \frac{\int v ds}{\int ds} = \frac{\int_{S_p^*}^{S_m^*} v ds^*}{S_m^* - S_p^*} = \int_{S_p^*}^{S_m^*} v ds^* \tag{49}$$

This gives the following expression

$$\langle v \rangle = -\frac{\Delta P S^2}{\eta \ell Z_p^2} \underbrace{\int_{S_p^*}^{S_m^*}\left(\int_{S_p^*}^{s^*} \frac{t^* dt^*}{z^{*2}} - S_m^* \int_{S_p^*}^{s^*} \frac{dt^*}{z^{*2}}\right) ds^*}_{1/k_o} \tag{50}$$

Before any further description of the momentum cell is given, it would be well to discuss the quantity designated as k_o in Equation 50. In order to integrate the expression for k_o rigorously, it is necessary to know how s and z are related for the system being studied. In general,

this is not known and certainly would not be known for something having a complicated cross section, such as a momentum cell. In all cases, k_o will be a function of the system geometry ratios, such as S_p/S_m, and the eccentricity of the packing within the cell. For purposes of calculating k_o for the models, it is assumed that a momentum cell of complex shape may be replaced by an equivalent one having a circular boundary and circular shaped packing. The values for S and Z_p in Equation 50 remain the same. For the idealized circular momentum cell, with the radius measured from the center of the packing, the relationship between s^* and z^* is

$$s^*(k - 1) = z^{*2}$$

where k is defined as S_m/S_p, that is, $k = 1/1-\epsilon$. Performing the first integration indicated by Equation 50 gives

$$\frac{1}{k_o} = \frac{1}{k-1}\int_{S_p^*}^{S_m^*} (s^* - S_p^* - S_m^* \ln s^* + S_m^* \ln S_p^*)\, ds^*$$

The second integration gives, after simplification

$$\frac{1}{k_o} = \frac{1}{k-1}\left[1/2\, S_p^{*2} - 2S_p^*S_m^* + S_m^{*2}(3/2 + \ln \frac{S_p^*}{S_m^*})\right]$$

Substituting for S_p^* and S_m^* in terms of k gives finally

$$\frac{1}{k_o} = \frac{1}{(k-1)^3}\left[1/2 - 2k + k^2(3/2 + \ln \frac{1}{k})\right] \qquad (51)$$

In terms of porosity, k_o becomes

$$k_o = \frac{\epsilon^3}{\epsilon - 1/2\,\epsilon^2 - 1/2\,\epsilon^3 + (1-\epsilon)\ln(1-\epsilon)} \qquad (52)$$

This then is the expression for the momentum cell constant in terms of the cell porosity. It can be shown by an application of L'Hospital's rule that as $\epsilon \longrightarrow 0$, $k_o' \longrightarrow 3$ and as $\epsilon \longrightarrow 1$, $k_o' \longrightarrow \infty$. A plot of k_o' versus ϵ is shown in Figure 50. On this same plot, are shown the k_o' values calculated by Emersleben (67), who used an idealized model of equally spaced cylinders parallel to the direction of flow to obtain his result.

That the assumption of using an equivalent circular momentum cell has some justification, is shown in Figures 52 and 53 on page 119. Figure 52 is a plot, prepared by Schriver (59), of a semi-empirical laminar pressure drop factor versus bed porosity. This factor is used as the laminar constant in Equation 19 of the literature survey. It can be seen that this factor increases with increasing porosity and has a form similar to the calculated curve shown in Figure 50. To compare the two curves, $\left[f_1 L/(f_1 L \text{ at } \epsilon = 0.3) \right]$ is plotted versus $\left[k_o/(k_o \text{ at } \epsilon = 0.3) \right]$ as shown in Figure 53. The agreement is good and shows that the variation of $f_1 L$ with porosity is the same as the variation of k_o' with porosity. The momentum cell constant is further discussed in a later section.

There now remains the problem of calculating k_o' for the special case of the momentum cell that lies between the outermost pieces of packing and the container wall. Note that this type of cell will always have a porosity of 1.0. The boundary conditions for this calculation are $v = 0$ at the container wall and $\tau = 0$ at the appropriate line of maximum velocity within the container. The calculation is very similar to the preceding one and yields the following expression

$$\frac{1}{k_o} = \frac{1}{(1-c)^3}\left[1/2 - 2c + c^2(3/2 + \ln \frac{1}{c})\right] \qquad (53)$$

Here $c = 1 - S'/S_T$. It can be shown, by an application of L'Hospital's rule, that as $c \longrightarrow 0$, $k'_o \longrightarrow 2$ and as $c \longrightarrow 1$, $k'_o \longrightarrow 3$. A plot of k'_o for this type of cell is shown in Figure 51. As mentioned previously, k'_o is a constant that depends on the characteristics of the momentum cell. In flow through ordinary conduits of various shape, this constant is evaluated from the expression for the velocity distribution, if the distribution is known. If the velocity distribution is not known, the flow constant must be evaluated experimentally.

Returning now to Equation 50, which gives the momentum loss per unit volume for a cell, it can be seen that this equation is similar in form to the Hagen-Poiseuille equation for capillary flow. This analogy illustrates an important implicit assumption that has been made in deriving Equation 50. This expression accounts only for viscous drag and neglects any form drag that may be present. This assumption may be valid for true laminar flow, but will not be true for transition or turbulent flow. In addition to the quantities defined by Equation 50, each momentum cell will have a variable length ℓ'_{mi}, an effective length of packing within the cell ℓ'_{pi}, and is orientated at an angle θ'_i to the axis of the bed. In these calculations, momentum loss rather than pressure drop is used because momentum loss is a more fundamental quantity than pressure drop and is somewhat easier to handle during the calculations. Now because the fluid follows a more or less tortuous path through the bed, the effective pressure gradient acting on the fluid in some cell is $\Delta P \cos \theta'_i$ rather than ΔP. Also the fluid must flow through a cell of length ℓ'_{mi} where $\ell'_{mi} =$

$\ell / \cos \theta'_i$ and ℓ is some constant length to be defined. Substituting these quantities into Equation 50 gives the following expression for momentum loss in a cell.

$$p_i = \frac{\eta \ell k'_{oi} \langle v \rangle_i S'_{mi}}{g_c m'^2_i \cos^2 \theta'_i} \qquad (54)$$

where $m'_i = S'_i / Z'_{pi}$ as previously defined. The term $\cos^2 \theta'_i$ is in effect a tortuosity.

Before describing the calculation of θ', it is necessary to describe the general overall structure of the models. The models consist of layers of momentum cell stacked on top of each other to form the bed. The thickness of the layers is a constant distance ℓ and is chosen equal to the diameter of a sphere having the same volume as a piece packing. A typical momentum cell in one of these layers is shown in Figure 2 on page 51. In general, two subscripts are required for each cell, one for the layer and one for the cell position in the layer. However, in both Model 1 and Model 2, the assumption is made that the cells are independent of each other. Thus in the case of a homogenous model, such as Model 1, only one subscript will be required.

It remains now to define the orientation angle of the cell, θ'_i. This angle was calculated using the expression $\theta = \tan^{-1} (y/\ell)$, with the radial distance y calculated in the following way. First, two enlarged cross sections of a particular bed were superimposed. Next two adjacent packing surfaces were chosen at random, with each surface being in a different enlargement. Then the distance, y, between the centroids of these two packing surfaces was measured. The centroid of the exposed packing

Figure 2. Complete view of typical momentum cell

Figure 3. Illustrative cross section of packed bed showing several momentum cells

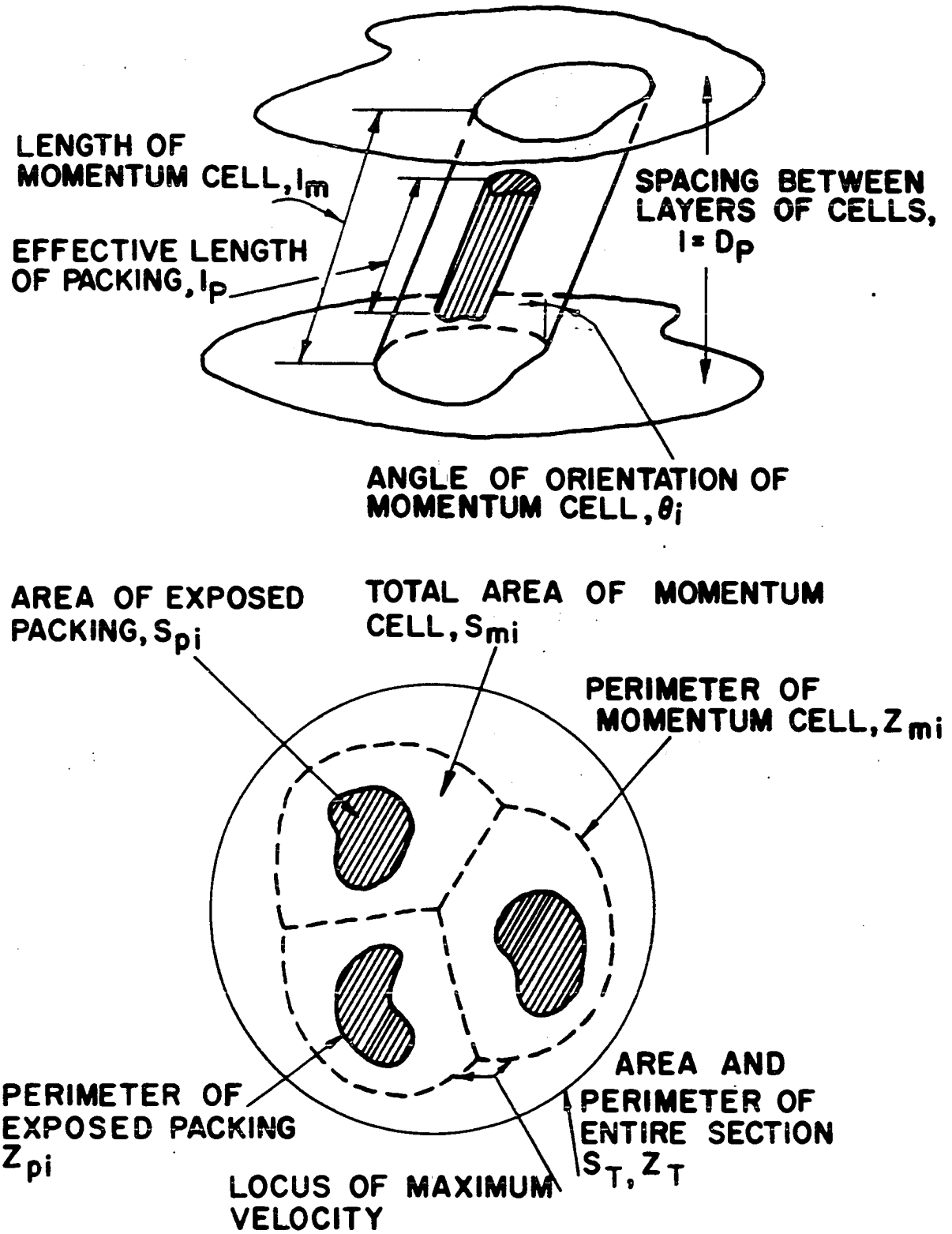
LENGTH OF MOMENTUM CELL, l_m
EFFECTIVE LENGTH OF PACKING, l_p
SPACING BETWEEN LAYERS OF CELLS, $l = D_p$
ANGLE OF ORIENTATION OF MOMENTUM CELL, θ_i
AREA OF EXPOSED PACKING, S_{pi}
TOTAL AREA OF MOMENTUM CELL, S_{mi}
PERIMETER OF MOMENTUM CELL, Z_{mi}
PERIMETER OF EXPOSED PACKING Z_{pi}
AREA AND PERIMETER OF ENTIRE SECTION S_T, Z_T
LOCUS OF MAXIMUM VELOCITY

surface, rather than the centroid of the momentum cell, was used because of the relative ease in locating the centroid of the packing surface. In many cases, the two centroids appeared to be very close together. A line joining two packing centroids was not used if it crossed over another packing face. This is equivalent to assuming that the fluid stream, in going from one layer of cells to another, will choose the closer of two momentum cells. Although not necessarily true for turbulent flow, this assumption seems reasonable for laminar flow. A distance of $2D_p$ was arbitrarily chosen as the maximum y distance. Not crossing an intermediate cell also has the advantage of causing the distribution to tail off naturally at the right tail. The method used to calculate θ'_i has the advantage of giving an approximate distribution of angles in three dimensions, but has the disadvantage of having to use a constant axial length ℓ. An illustrative histogram for θ'_i is shown in Figure 36 on page 90.

With the exception of the momentum cell fluid velocity, $\langle v \rangle_i$, all of the quantities in Equation 54 are now defined and may be calculated using the distributions of the momentum cell properties. The calculation of $\langle v \rangle_i$ is described separately for each model.

Model 1

For Model 1, it is assumed that the bed is homogenous in structure and that the individual momentum cells are independent of each other. This is equivalent to assuming that the way momentum is lost in one cell has no influence on the way in which momentum is lost in any adjacent cell.

Thus, Model 1 is classified under the first group of models described on page 39. Also for this model, the assumption is made that the effective length of packing in the cell is always equal to the cell length, that is $\ell'_{mi} = \ell'_{pi} = \ell/\cos\theta'_i$. The calculation of the fluid velocity in the cell proceeds as follows. First the assumption is made that the average momentum cell fluid velocity for the bed is given by

$$\langle v \rangle_B = V_o/\overline{\epsilon'}_i \tag{55}$$

Here $\overline{\epsilon'}_i$ is the average of the momentum cell porosities for the bed. This is in effect the Dupuit (23) assumption. Now the average velocity for any particular cell will be greater or less than the average cell velocity for the bed, $\langle v \rangle_B$, depending on whether the cell porosity ϵ'_i is greater or less than the average bed porosity $\overline{\epsilon'}_i$. Thus

$$\langle v \rangle_i = \langle v \rangle_B \frac{\overline{\epsilon'}_i}{\epsilon'_i} = \left(\frac{V_o}{\overline{\epsilon'}_i}\right)\left(\frac{\overline{\epsilon'}_i}{\epsilon'_i}\right) = \frac{V_o}{\epsilon'_i} \tag{56}$$

If all the momentum cells had the same area $\overline{S'}_{mi}$, this postulate for cell fluid velocity can be shown to be the same as criterion number five on page 41, that is, the criteria of equal mass flow in each cell. Equation 54 now becomes

$$p_i = \frac{\eta\, \ell\, V_o\, k'_{oi}\, S'_{mi}}{g_c\, \epsilon'_i\, m'^2_i \cos^2\theta'_i} = C_o \frac{k'_{oi}\, S'_{mi}}{\epsilon'_i\, m'^2_i \cos^2\theta'_i} \tag{57}$$

Here C_o represents those quantities that will remain fixed during a calculation for any particular bed.

Before continuing with a description of the main calculations, the

calculation of certain momentum cell properties for two special cases of Raschig ring orientation should be discussed. In the first case, the ring is lying completely on its side. Unless there is a substantial pressure difference between the ends of the ring, there will be little flow and the fluid will not actually "see" the interior of the ring. For this case, both the hydraulic radius and porosity of the cell are calculated as though the ring were solid. In the second case, the ring is orientated so that the entire hole is visible. For this case, the hydraulic radius and porosity of the cell are calculated as usual. However, the cell constant k_o' will be a combination of k_o' for a conduit with solid boundaries and k_o' for a channel with one solid boundary and one boundary where the shear stress is zero. In this case, the composite k_o' was calculated by weighting the two types of k_o' according to their flow areas.

Returning to the momentum loss calculations, the calculation and utilization of the P_{ij} are as follows. Consider an illustrative two dimensional array as shown in Figure 4.

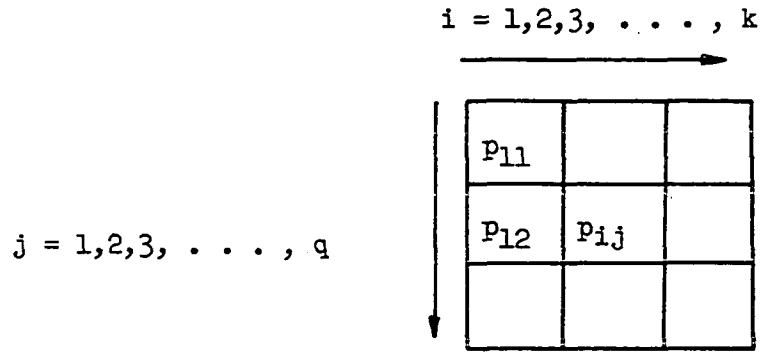

Figure 4. Illustrative Array of Momentum Cells

Note that kq is equivalent to the bed volume. Now consider a group of beds having the same gross properties such as porosity, volume, size and type of packing. Each of these beds will be composed of the same number of cells. The momentum loss, per unit length, is given by

$$\sum_{i}^{k} \sum_{j}^{q} \frac{p_{ij}}{L} \tag{58}$$

There will, however, be a difference in pressure drop (momentum loss) between these beds. Thus, we are interested in the mean and variance of the group

$$\left(\sum_{i} \sum_{j} \frac{p_{ij}}{L}\right)^{(1)}, \left(\sum_{i} \sum_{j} \frac{p_{ij}}{L}\right)^{(2)}, \ldots\ldots, \left(\sum_{i} \sum_{j} \frac{p_{ij}}{L}\right)^{(s)}$$

Here the superscript 1,2,3, . . . , s designates a particular bed. Under the assumption that the momentum cells are independent of each other, the mean and variance for this group of beds is given by

$$\text{Mean}\left[\left(\sum_{i} \sum_{j} \frac{p_{ij}}{L}\right)^{(s)}\right] = \frac{kq}{L} \mu(p_{ij}) \tag{59}$$

$$\text{Variance}\left[\left(\sum_{i} \sum_{j} \frac{p_{ij}}{L}\right)^{(s)}\right] = \frac{kq}{L^2} \sigma^2(p_{ij}) \tag{60}$$

where $\mu(p_{ij})$ = mean of the population of p_{ij}

$\sigma^2(p_{ij})$ = variance of the population of p_{ij}

For this particular model, k and q are estimated as follows

q = number of layers of momentum cells in bed = L/ℓ

$$= L/D_p \tag{61}$$

k = number of independent channels = $S_T/\bar{S}'_{mi}$

In an actual calculation, the distributions of k'_{oi}, ϵ'_i, θ'_i, m_i, and S'_{mi}, which have been previously punched on cards, are input to the computer (IBM 7074), and a population of p_{ij} is synthesized by having the computer repeatedly draw from distributions of the primed quantities and calculate the p_{ij}. As noted previously, because of the assumption that the momentum cells are independent of each other. a single subscript may be used during the actual calculations. The sample mean, $\bar{x}(p_{ij})$, and the sample variance, $s^2(p_{ij})$, of the resulting population of p_{ij} will depend on the number of p_{ij} calculated. It is important to note here that the computer may sample from these distributions in two different ways. In the first method, referred to as uncorrelated sampling, the sampling is purely random, and the hydraulic radius that was tabulated experimentally for one cell might be used with the porosity that was tabulated for another cell. In the second method, referred to as correlated sampling, the hydraulic radius of a cell is used with the porosity that was tabulated for that cell. Both of these sampling methods were investigated. Scatter plots showed that ϵ'_i and m'_i were strongly correlated as expected, while S'_{mi} showed little correlation with anything. Because of the somewhat arbitrary manner in which the orientation angle, θ'_i, was calculated, it was assumed to be uncorrelated with any of the other variables.

While the cell properties are truly only samples from infinite populations, certain simplifications may be made if the sample is regarded as the population itself. This assumption is equivalent to saying that no new information on the distribution of a particular cell property may be

gained by further sampling. With this assumption, the mean $\mu(p_{ij})$, for the correlated case, may be calculated

$$\mu(p_{ij}) = E(p_{ij}) = C_o\left[E\left(\frac{k_o'}{\epsilon' m'^2}\right) E(S_m') E\left(\frac{1}{\cos^2\theta'}\right)\right] \qquad (62)$$

Here E denotes "expected value," and C_o contains those quantities that are constant during any particular calculation, i.e. η , ℓ , V_o, and g_c. Note that $\mu(p_{ij})$ is now regarded not as a sample mean but as the true mean of the population of p_{ij}. With the samples of the primed quantities now regarded as populations, calculation of the expected values is a straight forward but tedious procedure and is best done on the computer. The population variance $\sigma^2(p_{ij})$ may also be calculated.

$$\sigma^2(p_{ij}) = C_o^2\left[E\left(\frac{k_o'}{\epsilon' m'^2}\right)^2 E(S_m')^2 E\left(\frac{1}{\cos^2\theta'}\right)^2 - \left(E\left(\frac{k_o'}{\epsilon' m'^2}\right) E(S_m') E\left(\frac{1}{\cos^2\theta'}\right)\right)^2\right] \qquad (63)$$

Equations 62 and 63 allow $\mu(p_{ij})$ and $\sigma^2(p_{ij})$ to be calculated without the need for repeated random sampling. As the number of p_{ij} becomes large, $\bar{x}(p_{ij})$ should approach $\mu(p_{ij})$ and $s^2(p_{ij})$ should approach $\sigma^2(p_{ij})$. The rate at which this occurs is dependent on the distributions of cell properties. This calculation was performed for a bed of spheres (bed C3), and the results are shown in Figures 5 and 6. These plots show that $\bar{x}$ and s^2 do approach μ and σ^2.

A convenient method for expressing the results of a calculation is to give the standard deviation, σ , of the pressure drop or momentum loss between the beds, as some sort of percentage of the mean of the beds. Here this percentage is taken equal to 1.96 times the coefficient of variation. Using Equations 59 and 60, gives

Figure 5. Stabilization of $\bar{x}(p_{ij})$ to $\mu(p_{ij})$ for Model 1

Figure 6. Stabilization of $s^2(p_{ij})$ to $\sigma^2(p_{ij})$ for Model 1

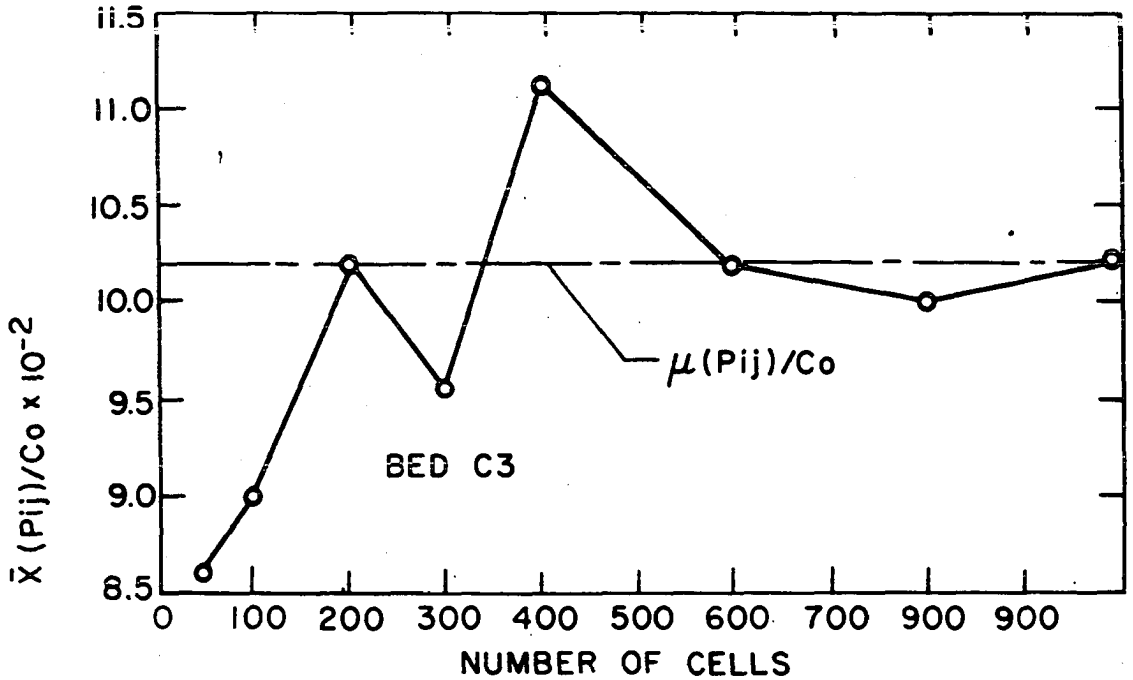
11.5
11.0
10.5
10.0
9.5
9.0
8.5
$\bar{X}$ (Pij)/Co x 10^{-2}
μ(Pij)/Co
BED C3
0 100 200 300 400 500 600 700 900 900
NUMBER OF CELLS

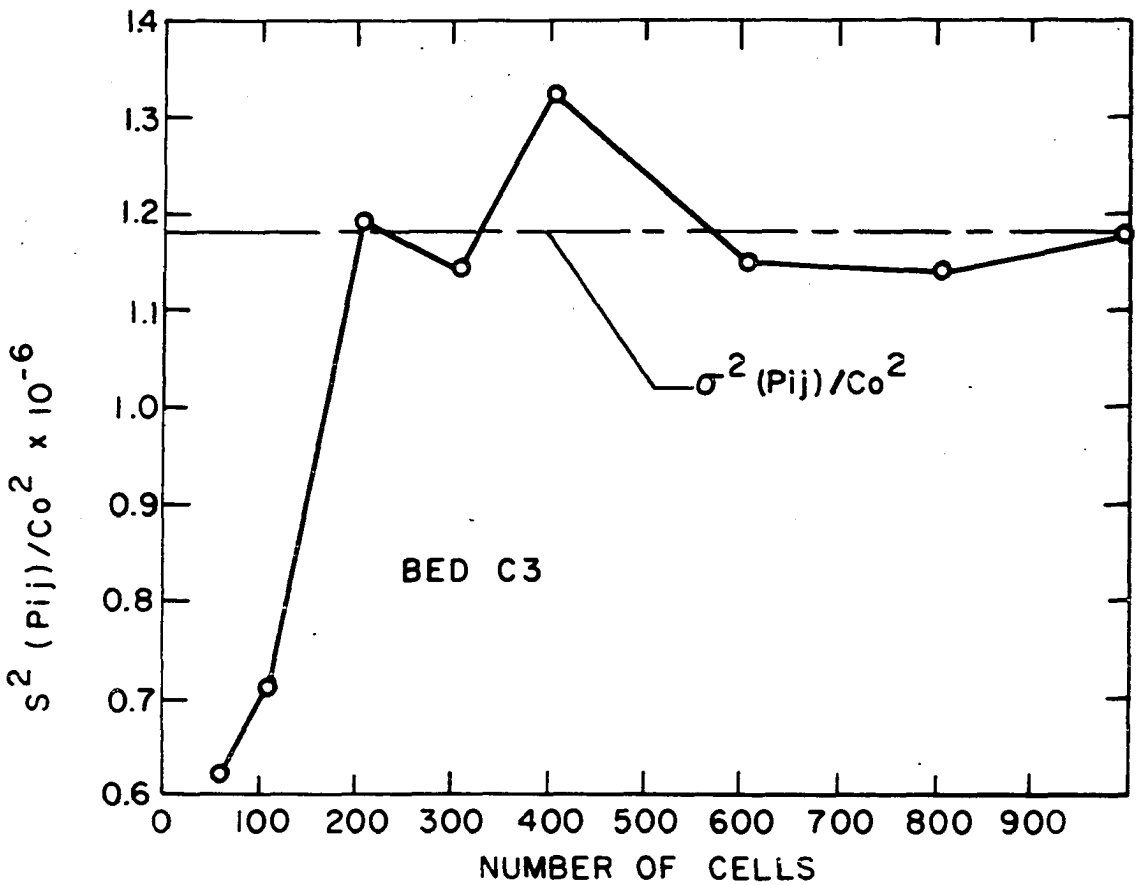
1.4
1.3
1.2
1.1
1.0
0.9
0.8
0.7
0.6
s^2 (Pij)/Co^2 x 10^{-6}
σ^2 (Pij)/Co^2
BED C3
0 100 200 300 400 500 600 700 800 900
NUMBER OF CELLS

$$\text{Percent-mean variation} = \frac{1.96\sqrt{\frac{kq}{L^2}\sigma^2(p_{ij})}}{\frac{kq}{L}\mu(p_{ij})}(100) \qquad (64)$$

or

$$\text{Percent-mean variation} = \frac{196\,\sigma(p_{ij})}{\sqrt{kq}\,\mu(p_{ij})} \qquad (65)$$

The numerator of Equation 64 is the 95% tolerance limit for the population of $\sum_i \sum_j p_{ij}/L$. Note that this expression does not contain any terms involving the fluid, since C_o cancels out of the expression, but only terms involving the physical properties of a particular packed bed. Equation 65 shows that the percent-mean variation should decrease as $\sqrt{kq}$. Thus for large beds, the percent-mean variation will be small, and a designer need not be concerned with the variation in momentum loss between beds.

Model 2

Many of the calculation procedures outlined in Model 1 are also used for Model 2. The main differences are the physical structure of the models and the methods of obtaining the cell fluid velocity.

The physical concept of a model composed of layers of momentum cells remains the same as before. In this model, however, the bed is divided into a number of annular regions. Although any number of regions are possible, only two are used in this calculation. Model 2 is then classified under the general model type IV as listed on page 40. It is now

assumed that the momentum loss for any cell in a given layer may be written as the product of a quantity that is a function only of the physical properties of the cell and the superficial fluid velocity of the cell. The following equations may be written for a layer of cells in a two-region model.

$$M_{ci} = K_{ci} V_{ci} \qquad i = 1,2,3, \ldots, n \tag{66}$$

$$M_{wj} = K_{wj} V_{wj} \qquad j = 1,2,3, \ldots, m \tag{67}$$

There are then n + m cells in a given layer of the model.

Mass balance: $$\sum_i S'_{mci} V_{ci} + \sum_j S'_{mwj} V_{wj} = Q = S_T V_o \tag{68}$$

Momentum balance: $$\sum_i S'_{mci} M_{ci} + \sum_j S'_{mwj} M_{wj} = S_T M \tag{69}$$

Energy balance: $$\sum_i S'_{mci} V_{ci} M_{ci} + \sum_j S'_{mwj} V_{wj} M_{wj} = S_T V_o M \tag{70}$$

To obtain the fluid velocities in a layer of cells in the present model, it is assumed or hypothesized that minimization of the energy loss, criteria number four on page 41 is the proper one. In the following calculations, it will be simpler to use a single subscript k, where k = 1,2, 3, . . . , n + m. The notation for the core and wall region will be used again later on. The method of Lagrange multipliers will be used to minimize the energy loss. On substituting Equations 66 and 67 into Equations 69 and 70, there results

$$\sum_k K_k S'_{mk} V_k^2 = M S_T V_o = \text{total energy loss} \tag{71}$$

First constraint equation $$\sum_k K_k S'_{mk} V_k = M S_T \tag{72}$$

Second constraint equation $$\sum_k S'_{mk} V_k = S_T V_o \tag{73}$$

In terms of the Lagrange multipliers λ_1 and λ_2,

$$f = \sum_k K_k S'_{mk} V_k^2 + \lambda_1 \sum_k K_k S'_{mk} V_k + \lambda_2 \sum_k S'_{mk} V_k \tag{74}$$

The following equations must then be solved

$$\frac{\partial f}{\partial V_k} = 2 K_k V_k + \lambda_1 K_k + \lambda_2 = 0 \qquad k = 1,2,3, \ldots, n + m \tag{75}$$

along with the equations of constraint, Equations 72 and 73. A solution to this system can be found by choosing $K_1 V_1 = \ldots = K_k V_k = M$ = a constant. Then Equations 72 and 75 will be satisfied if $\lambda_1 = 0$ and $\lambda_2 = -2 K_k V_k = -2M$. It can be seen that this applies to any number of cells. The physical meaning of the assumption that $K_k V_k = M$ is that the superficial velocity of each cell adjusts itself so that the momentum loss for each cell in a given layer will be the same. This is certainly not an unreasonable assumption in itself. There will, however, be a variation in momentum loss from layer to layer in the bed. Note that choosing $K_k V_k = M$ means that criteria one and four on page 41 are the same. It now remains to satisfy Equation 73, that is, Equation 68. This can be done by first calculating M. Returning to a two-region model, we have

$$V_{ci} = M/K_{ci} \qquad \text{and} \qquad V_{wj} = M/K_{wj} \tag{76}$$

Equation 68 now becomes

$$M \sum_i S'_{mci}/K_{ci} + M \sum_j S'_{mwj}/K_{wj} = S_t V_o$$

or

$$M = \frac{V_o S_T}{\left(\sum_i \frac{S'_{mci}}{K_{ci}} + \sum_j \frac{S'_{mwj}}{K_{wj}} \right)} \tag{77}$$

Once M is known, individual V_i and V_j may be calculated if desired. To illustrate this method, imagine a layer of cells in a bed that consists of just two momentum cells, a core cell and a wall cell. Then Equations 66, 67, 68, 69, and 70 give

$$S_c V_c + S_w V_w = S_T V_o \tag{78}$$

$$S_c K_c V_c + S_w K_w V_w = M S_T \tag{79}$$

$$S_c K_c V_c^2 + S_w K_w V_w^2 = M S_T V_o \tag{80}$$

Substituting Equation 78 into Equation 80 and minimizing the energy loss, by differentiating with respect to V_w, gives

$$V_w = \frac{V_o}{(S_w + \frac{S_c}{K_c} K_w)}$$

V_c may now be calculated from Equation 78. Suppose the following illustrative values are assumed: $S_c/S_T = 0.6$, $S_w/S_T = 0.4$, $K_c = 5$, and $K_w = 3$. K_w will be less than K_c since the porosity of the wall region is higher. Then $V_c = 0.79V_o$ and $V_w = 1.32V_o$. Exactly the same result is obtained by assuming equal momentum loss for each region, that is, $K_cV_c = K_wV_w$.

The details of calculating the momentum loss for the entire bed are as follows. The bed is divided into a core region and a wall region with cross sectional areas S_c and S_w respectively. As before, there are q layers of independent momentum cells in the model with $q = L/D_p$. The flow equation is the same as before

$$M = \frac{\eta\, k'_{oi}\, \ell'_{pi}\, \langle v \rangle_i\, S'_{mi}}{g_c\, m'^2_i \cos^2 \theta'_i} \qquad (81)$$

This equation is similar to Equation 54, for the homogenous model, except that $\langle v \rangle_i$ and ℓ'_{pi} are determined differently. The assumption is now made that the volume porosity of each momentum cell, in a given region, is constant. That is, a cell in the core region will have a volume porosity ϵ_c, and a cell in the wall region will have a volume porosity ϵ_w. The values for ϵ_c and ϵ_w were calculated in the following way. The width of the wall section was arbitrarily chosen equal to one pellet diameter, and it was assumed that most of the variation in bed properties occurred within this zone. This fixes the area of both the core and wall regions. Values of porosity, obtained from the plots of porosity versus radial position (shown on pages 81 and 83), were weighted according to area to give the values for ϵ_c and ϵ_w. In all cases except Raschig rings, the average bed porosity, calculated from ϵ_c and ϵ_w, was made to match the average bed porosity calculated from the momentum cell porosities, $\overline{\epsilon'_i}$.
A sample calculation of ϵ_c and ϵ_w is given in the Appendix. Because of the special method of calculating ϵ'_i for certain Raschig ring orientations, given in the description of Model 1, $\overline{\epsilon}_r$ is a better indication of the average volume porosity of the bed than $\overline{\epsilon'_i}$. Therefore the average

bed porosity for Raschig rings, calculated from ϵ_c and ϵ_w, was made to match $\bar{\epsilon}_r$.

Once ϵ_c and ϵ_w have been calculated, they are used in the following way.

$S'_{pi}\, \ell'_{pi}$ = volume of packing in momentum cell

$S'_{mi}\, \ell'_{mi}$ = volume of momentum cell

Then

$$\frac{S'_{pi}\, \ell'_{pi}}{S'_{mi}\, \ell'_{mi}} = 1 - \epsilon_v; \qquad \epsilon_v = \epsilon_c \text{ or } \epsilon_w$$

but $$(1 - \epsilon'_i)\, S'_{mi} = S'_{pi}$$

so that $$\frac{(1-\epsilon'_i)\, S'_{mi}\, \ell'_{pi}}{S'_{mi}\, \ell'_{mi}} = 1 - \epsilon_v$$

or $$\ell'_{pi} = \left(\frac{1-\epsilon_v}{1-\epsilon'_i}\right)\ell'_{mi} = \left(\frac{1-\epsilon_v}{1-\epsilon'_i}\right)\frac{\ell}{\cos\theta'_i} \qquad (82)$$

This says that

a. $\epsilon_v = \epsilon'_i$ $\qquad \ell'_{mi} = \ell'_{pi}$

b. $\epsilon_v > \epsilon'_i$ $\qquad \ell'_{mi} > \ell'_{pi}$

c. $\epsilon_v < \epsilon'_i$ $\qquad \ell'_{mi} < \ell'_{pi}$

Now for each cell

$$\langle v \rangle_i = V_i / \epsilon'_i \qquad (83)$$

That is, the average flow velocity in the cell is equal to the superficial velocity divided by the cell porosity. Substituting Equations 82 and 83

into Equation 81, gives

$$M = \underbrace{\frac{\eta \ell}{g_c} \frac{k'_{oi} (1-\epsilon_v) S'_{mi}}{m'^2_i \epsilon'_i (1-\epsilon'_i) \cos^2 \theta'_i}}_{K_i} V_i \qquad (84)$$

i.e. $M = K_i V_i$

Each distribution of a cell property, such as hydraulic radius, is divided into two separate distributions depending on whether or not the radial position of a cell places it in the core or wall region. Sample plots of ϵ'_i and m'_i versus radial position are shown in Figures 47 and 48 on page 103. The quantity $\sum_i S'_{mci}/K_{ci}$ is calculated for the core region, with K_{ci} calculated according to Equation 84, and the cell properties being randomly picked from the core distributions. The process is repeated until $\sum_i S_{mci} = S_c$. This gives the number of cells in the core region. A similar procedure is now repeated for the wall region. If one of the momentum cells adjacent to the wall is selected, then θ' is assumed to be 0°, that is $\ell'_{mi} = \ell$. Since V_o and S_T are known for any particular calculation, M may now be calculated from Equation 77. The V_i and V_j may also be calculated if desired. Since there are n + m cells in a given layer, the total momentum loss for the t th layer is

$$\mathfrak{M}_t = \frac{(n+m) V_o S_T}{\left(\sum_i^n \frac{S'_{mci}}{K_{ci}} + \sum_j^m \frac{S'_{mwj}}{K_{wj}} \right)} \qquad (85)$$

$\mathfrak{M}_t$ may be written in terms of C_o, where C_o contains the quantities that remain constant during any particular calculation. A block diagram outlining the computer calculations is shown on page 68. The momentum loss

Figure 7. Block diagram of computer calculations for Model 2

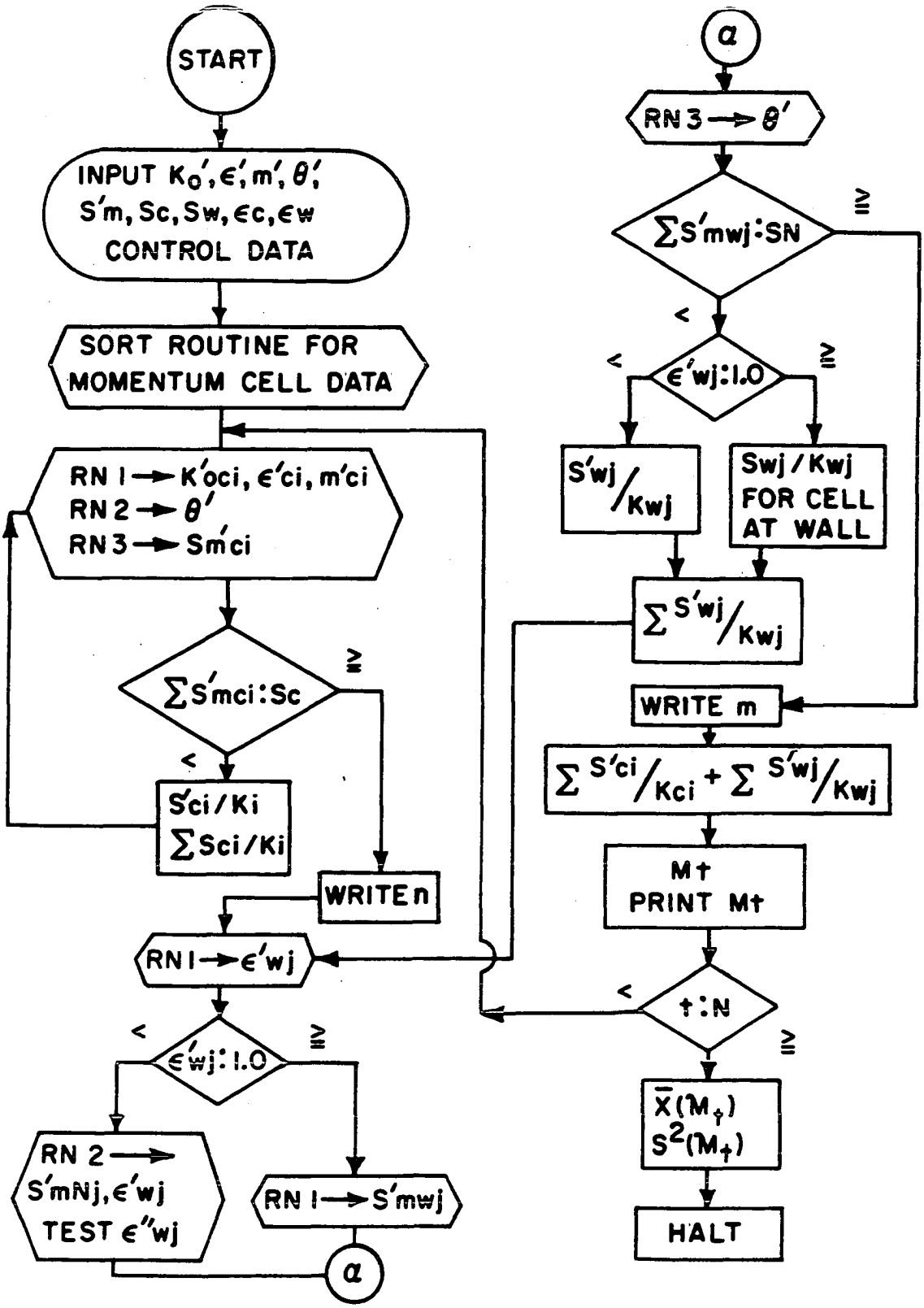
START
INPUT K_0', ϵ', m', θ', S'm, Sc, Sw, ϵc, ϵw CONTROL DATA
SORT ROUTINE FOR MOMENTUM CELL DATA
RN 1 → K'oci, ϵ'ci, m'ci
RN 2 → θ'
RN 3 → Sm'ci
$\sum$S'mci : Sc
<
≧
S'ci / Ki
$\sum$Sci / Ki
WRITE n
RN 1 → ϵ'wj
ϵ'wj : 1.0
<
≧
RN 2 → S'mNj, ϵ'wj TEST ϵ''wj
RN 1 → S'mwj
α
α
RN 3 → θ'
$\sum$S'mwj : SN
≧
<
ϵ'wj : 1.0
<
≧
S'wj / Kwj
Swj / Kwj FOR CELL AT WALL
$\sum S'_{wj}/K_{wj}$
WRITE m
$\sum S'_{ci}/K_{ci} + \sum S'_{wj}/K_{wj}$
Mt
PRINT Mt
t : N
<
≧
$\bar{X}(M_t)$
$S^2(M_t)$
HALT

per unit length for an entire bed is given by

$$\sum_{t}^{p} \frac{m_t}{L} \tag{86}$$

As before, we are interested in the mean and variance of the group

$$\left(\sum_t \frac{m_t}{L}\right)^{(1)}, \left(\sum_t \frac{m_t}{L}\right)^{(2)}, \ldots, \left(\sum_t \frac{m_t}{L}\right)^{(s)}$$

The mean and variance are given by

$$\text{Mean}\left[\left(\sum_t \frac{m_t}{L}\right)^{(s)}\right] = \frac{q}{L}\mu(m_t) \tag{87}$$

$$\text{Variance}\left[\left(\sum_t \frac{m_t}{L}\right)^{(s)}\right] = \frac{q}{L}\sigma^2(m_t) \tag{88}$$

In this model, $\bar{x}(m_t)$ and $s^2(m_t)$ were obtained by calculating a large number ($q = 500$) of m_t. It was then assumed that $\bar{x}(m_t)$ was very close to $\mu(m_t)$ and that $s^2(m_t)$ was very close to $\sigma^2(m_t)$. Plots of $\bar{x}$ and s^2, not including the quantities contained in C_o, are shown in Figures 8 and 9 on page 71. These figures show that the $\bar{x}$ and s^2 do stabilize as they did in Model 1. The percent-mean variation is calculated exactly as before.

Figure 8. Stabilization of $\bar{x}$ ($\mathfrak{m}_t$) for Model 2

Figure 9. Stabilization of $s^2(\mathfrak{m}_t)$ for Model 2

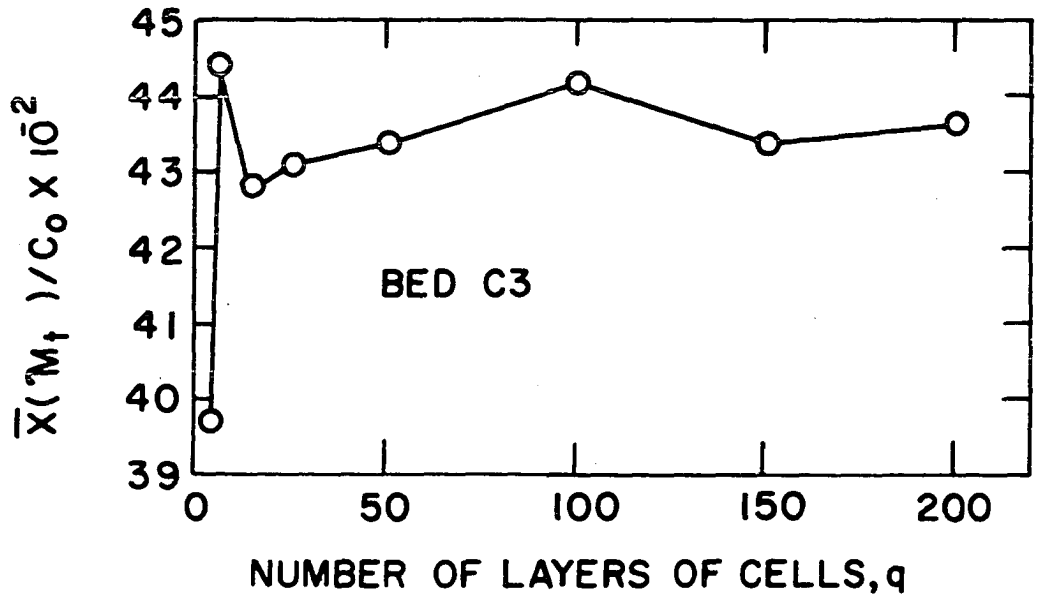
45
44
43
42
41
40
39
$\bar{X}(M_t)/C_o \times 10^2$
BED C3
0
50
100
150
200
NUMBER OF LAYERS OF CELLS, q

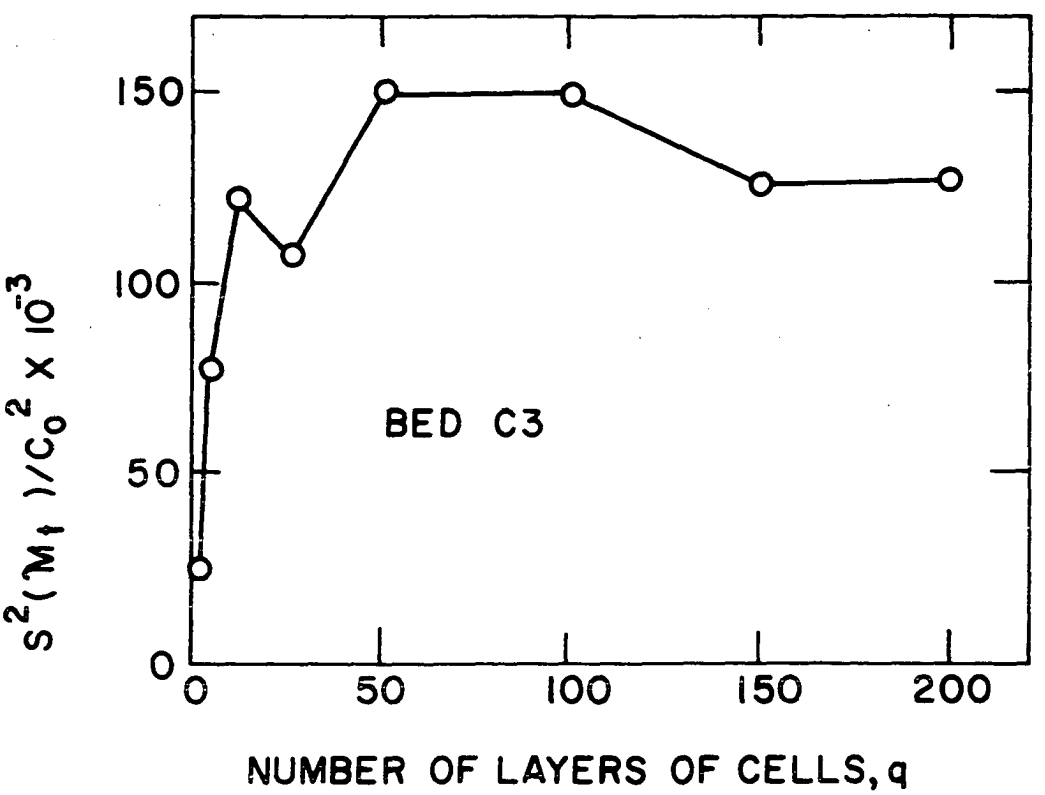
150
100
50
0
$S^2(M_t)/C_o^2 \times 10^{-3}$
BED C3
0
50
100
150
200
NUMBER OF LAYERS OF CELLS, q

RESULTS AND DISCUSSION

Physical Properties of the Experimental Beds

The results and discussion dealing with the physical properties of the experimental beds can best be introduced by considering the photographs of typical sections from these beds shown on pages 75 and 77. Tables summarizing the characteristics of the packing and physical characteristics of the beds sampled for momentum cell properties are given in the Appendix. It is at once evident from these photographs that a variety of exposed packing shapes and distributions of packing within the container are obtained, especially for a packing such as Raschig rings. Figure 10 shows a section from bed B1. Note that although the majority of the spheres do not appear to be orientated in any particular way, the spheres closest to the wall are partially orientated by the presence of the container wall. This is because the spheres at the wall will have one less degree of freedom in their movements, during the formation of the bed, than the rest of the spheres in the container. This effect will be more apparent in later pictures. Note also that the porosity appears higher in the region close to the wall. Figure 11 for bed C1 is similar in appearance to Figure 10 except that the effects mentioned for bed B1 are now more noticable. There is also some evidence of channeling or the formation of regions with high porosity. Figure 12 shows a longititudinal section from bed C2. This picture illustrates the definite tendency of the wall to orientate the packing closest to it. It also shows that a packed bed may not necessarily be uniform throughout even when the individual pieces

are hand dropped, as in this case. A section from bed C3 is shown in Figure 13. This section is similar in appearance to the others except that the packing has a fairly even distribution due to the larger D_T/D_p ratio and the hand-drop method of packing. Figure 14 shows a section from bed C4 which was formed by randomly dumping the packing into the container. While this photograph shows features common to the others, it also shows a very uneven distribution of packing with channels or areas of large void fraction. This would be expected since the pieces of packing have not as yet come to equilibrium positions during the formation of the bed, and spaces having a high porosity are created. This is especially true for packing having rough surfaces such as cork or unglazed clay. Note that the larger channels appear near the wall. Figure 15 shows a section from bed D1 for Raschig rings. A wide variety of shapes is obtained for the exposed packing faces, with the influence of the holes being very evident. Although the packing tends to be oriented near the wall, the odd shape of the packing makes this effect less pronounced than with spheres. Note here the special case of a ring lying on its side. Unless there is an appreciable pressure difference between the ends of the hole, there will be little flow through the ring, and the fluid will not actually "see" the interior of the ring as it passes in an exial direction through the bed. There is another special case where the ring is orientated so that the entire hole may be seen. The calculation of the momentum cell porosity, ϵ', and momentum cell constant, k_o', for these special cases has been discussed previously in the description of the models. A section from a bed of randomly dumped Raschig rings, bed D2, is shown in Figure 16.

Figure 10. Typical section from bed B1, spheres, packing hand dropped

Figure 11. Typical section from bed C1, spheres, packing hand dropped

Figure 12. Longitudinal section from bed C2, spheres, packing hand dropped

Figure 13. Typical section from bed C3, spheres, packing hand dropped

Figure 14. Typical section from bed C4, spheres, packing randomly dropped

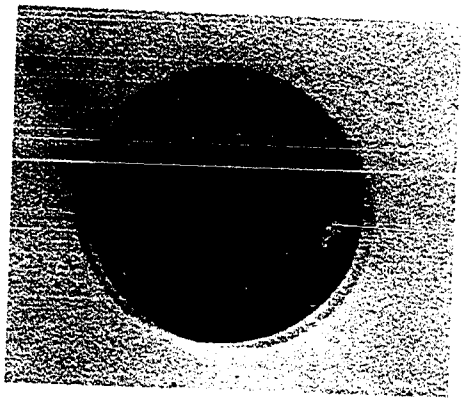

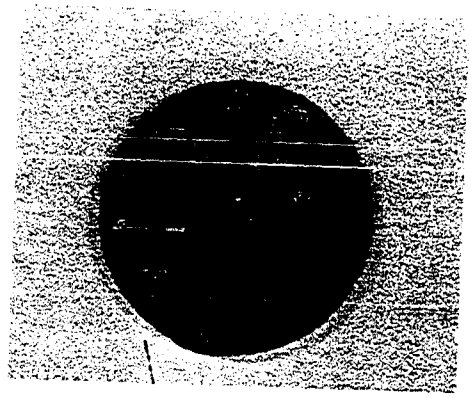

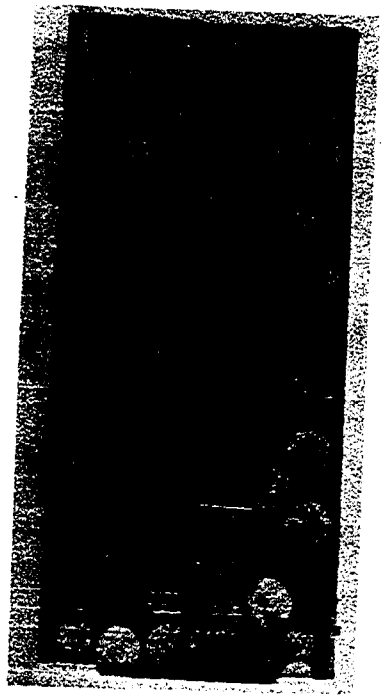

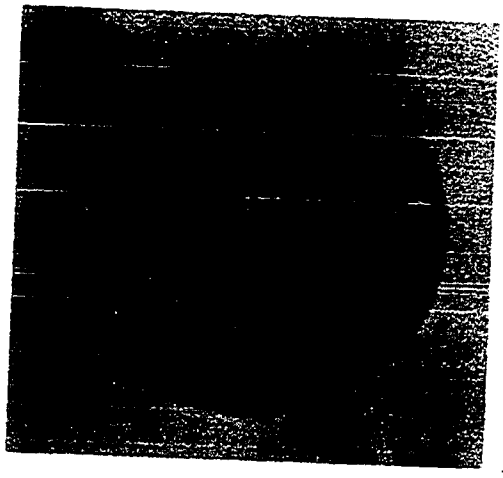

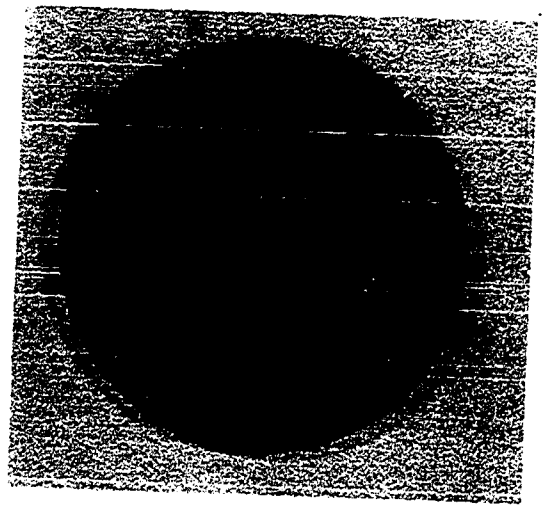

Figure 15. Typical section from bed D1, Raschig rings, packing hand dropped

Figure 16. Typical section from bed D2, Rashig rings, packing randomly dumped

Figure 17. Typical section from bed E1, cylinders, packing hand dropped

Figure 18. Typical section from bed E2, cylinders, packing hand dropped

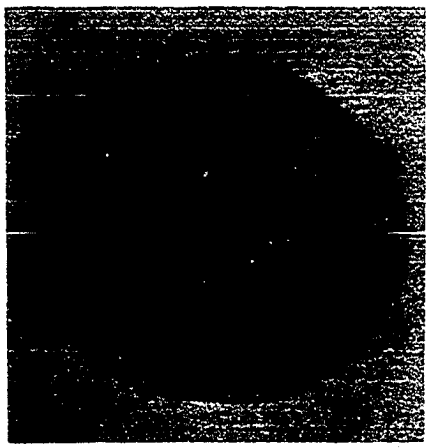

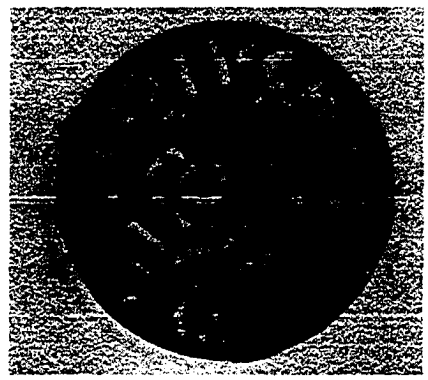

Although the porosity here is higher than in the section from bed D1, the packing distribution is fairly even, and only slightly more channeling is evident. Figure 17 shows a section from a bed of cylinders, bed E1. Again, the packing appears densest in the center region and loosest in the region near the wall. The packing is not quite so ordered in the wall region as it was for the beds of spheres because the packing shape allows a greater variety of orientations than was possible with spheres. It should be noted that it is possible for packing with flat surfaces to mate some of these surfaces and thus reduce the effective specific surface of the bed, S. Very little of this was seen in any of the sections for beds of cylinders. Figure 18 shows a section from bed E2. Again the porosity is higher in the wall region than the center of the bed, and the packing is not ordered in the wall region as much as might be the case with spheres.

The plots given on pages 81 and 83 show how the porosity of the experimental beds varies with radial position. In constructing these plots, four or five enlarged cross sections were randomly selected from a particular bed, and the area of each cross section was arbitrarily divided into equal annular sub areas. The porosity of each annular section, ϵ_r, was then determined from planimeter measurements. Although a section may be divided into more than five annular sub areas, too many divisions lead to large errors in area measurements. The radial position of the plotted points is the midpoint of a particular annular section. Since the individual points represent area porosities and not point porosities, a dotted line instead of a solid line is drawn through the average of each group

of points to indicate a trend rather than a completely determined experimental curve. The average bed porosity based on the annular sub areas, $\bar{\epsilon}_r$, is also given for each bed. These plots show the characteristic increase in porosity near the container wall, with the porosity considered as 1.0 right at the wall. The plots also exhibit a sudden decrease in porosity as one moves away from the container wall. This sudden decrease in porosity has been observed by Roblee, Baird, and Tierney (52) who found that it was part of a decreasing periodic variation as one moved toward the center of the bed. When the width of the annular sub areas is on the order of one pellet radius, as for bed C4, the complete details of this periodic variation cannot be uncovered. However, the periodic nature of the variation is well illustrated by these plots and indicates that the wall may continue to have an effect beyond one packing diameter from the wall.

This periodic variation can be explained in the following way. Consider a packed column containing say, spheres. Now the effect of the wall is to orient a layer of spheres at the wall and to cause more spheres than usual to be located adjacent to the wall. This effect was visible in the photographs of the cross sections of the experimental beds. Each sphere that touches the wall is uniquely oriented and will have its center located at a distance of one pellet radius from the wall. Consequently there will be a minimum porosity at this distance from the wall. Also, there will be a maximum porosity approximately one pellet diameter from the wall, since this is the point of maximum porosity for a sphere located at the wall. The porosity at one pellet diameter is a rough measure of the

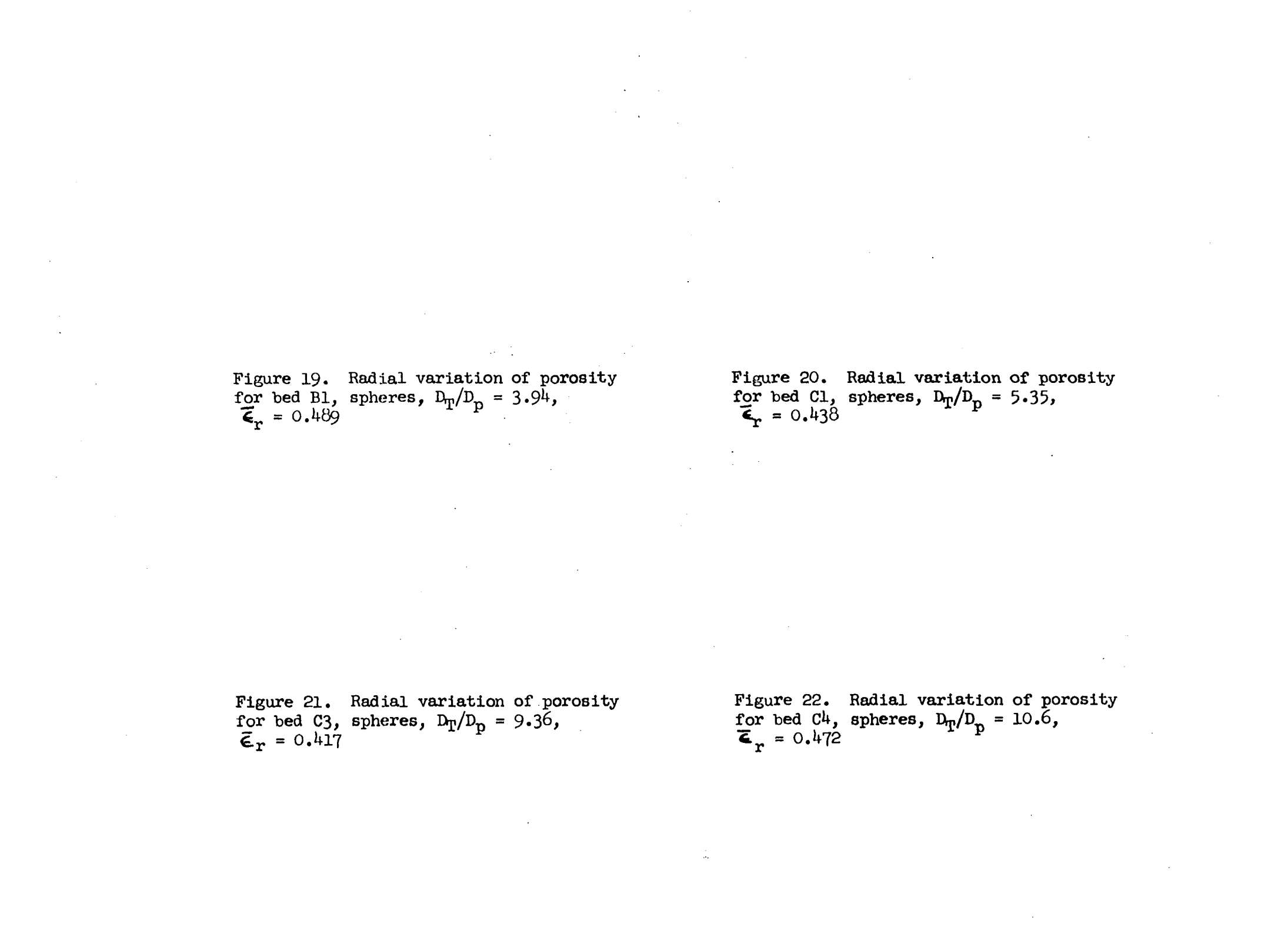

Figure 19. Radial variation of porosity for bed B1, spheres, $D_T/D_p = 3.94$, $\bar{\epsilon}_r = 0.489$

Figure 20. Radial variation of porosity for bed C1, spheres, $D_T/D_p = 5.35$, $\bar{\epsilon}_r = 0.438$

Figure 21. Radial variation of porosity for bed C3, spheres, $D_T/D_p = 9.36$, $\bar{\epsilon}_r = 0.417$

Figure 22. Radial variation of porosity for bed C4, spheres, $D_T/D_p = 10.6$, $\bar{\epsilon}_r = 0.472$

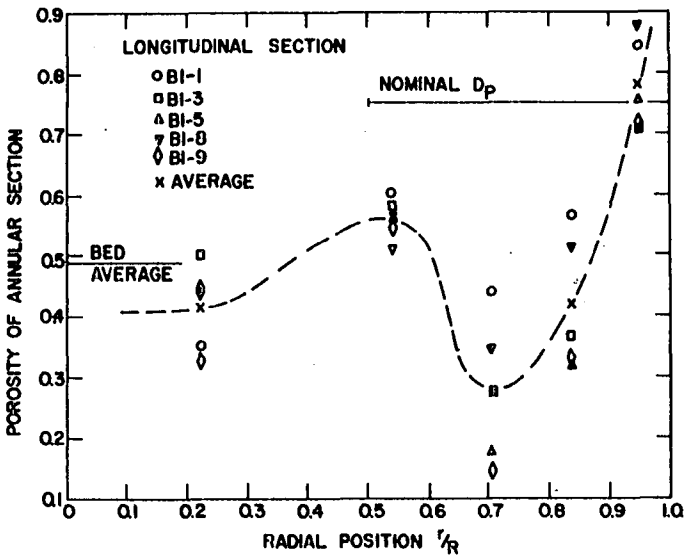
LONGITUDINAL SECTION
BI-1
BI-3
BI-5
BI-8
BI-9
AVERAGE
NOMINAL D_P
BED AVERAGE
POROSITY OF ANNULAR SECTION
RADIAL POSITION r/R

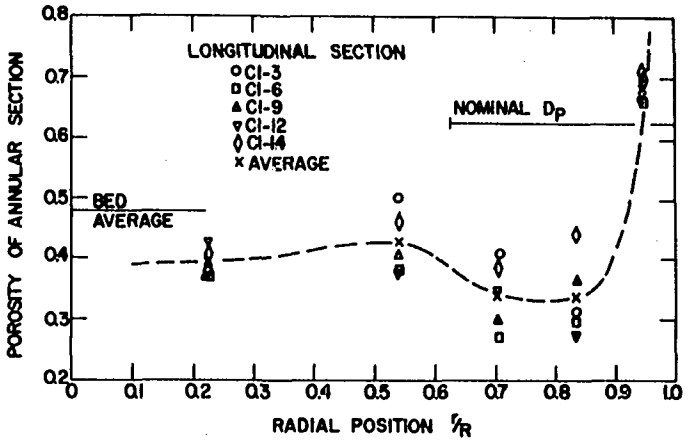
LONGITUDINAL SECTION
CI-3
CI-6
CI-9
CI-12
CI-14
AVERAGE
NOMINAL D_P
BED AVERAGE
POROSITY OF ANNULAR SECTION
RADIAL POSITION r/R

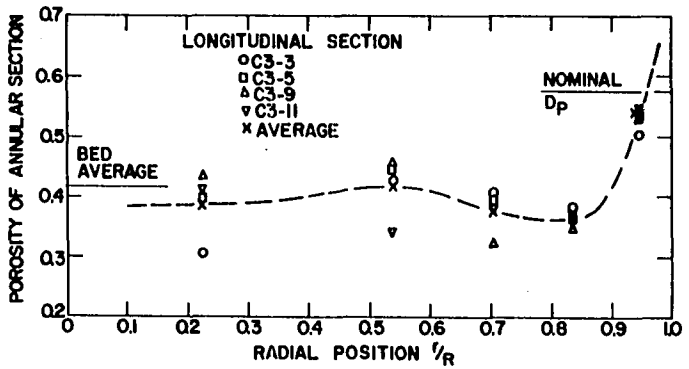
LONGITUDINAL SECTION
C3-3
C3-5
C3-9
C3-11
AVERAGE
NOMINAL D_P
BED AVERAGE
POROSITY OF ANNULAR SECTION
RADIAL POSITION r/R

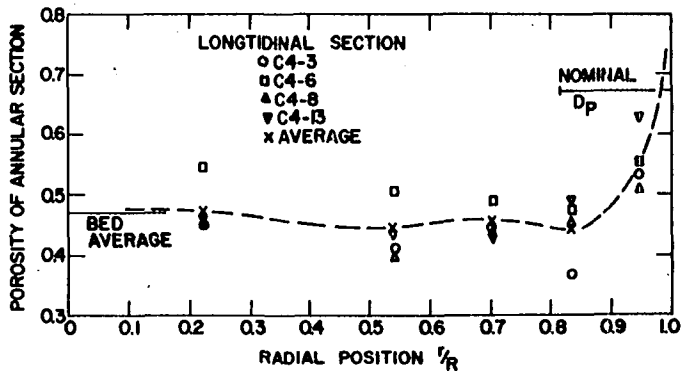
LONGTIDINAL SECTION
C4-3
C4-6
C4-8
C4-13
AVERAGE
NOMINAL D_P
BED AVERAGE
POROSITY OF ANNULAR SECTION
RADIAL POSITION r/R

Figure 23. Radial variation of porosity for bed D1, Raschig rings, $D_T/D_p = 5.51$, $\bar{\epsilon}_r = 0.574$

Figure 24. Radial variation of porosity for bed D2, Raschig rings, $D_T/D_p = 5.50$, $\bar{\epsilon}_r = 0.641$

Figure 25. Radial variation of porosity for the bed E1, cylinders, $D_T/D_p = 7.10$, $\bar{\epsilon}_r = 0.438$

Figure 26. Radial variation of porosity for bed E2, cylinders, $D_T/D_p = 4.53$, $\bar{\epsilon}_r = 0.470$

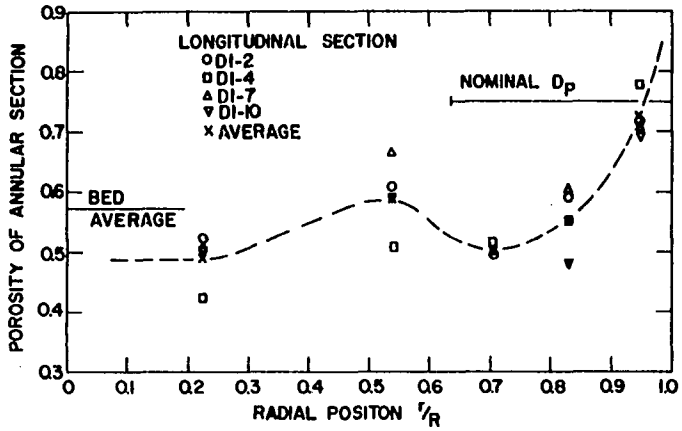
LONGITUDINAL SECTION
D1-2
D1-4
D1-7
D1-10
AVERAGE
NOMINAL D_P
BED AVERAGE
POROSITY OF ANNULAR SECTION
RADIAL POSITON r/R

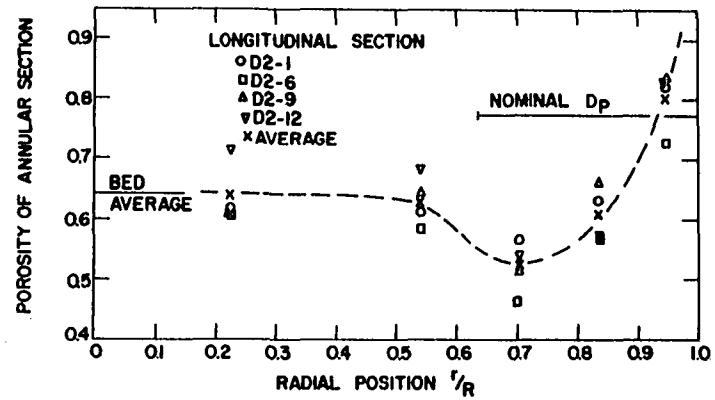
LONGITUDINAL SECTION
D2-1
D2-6
D2-9
D2-12
AVERAGE
NOMINAL D_P
BED AVERAGE
POROSITY OF ANNULAR SECTION
RADIAL POSITION r/R

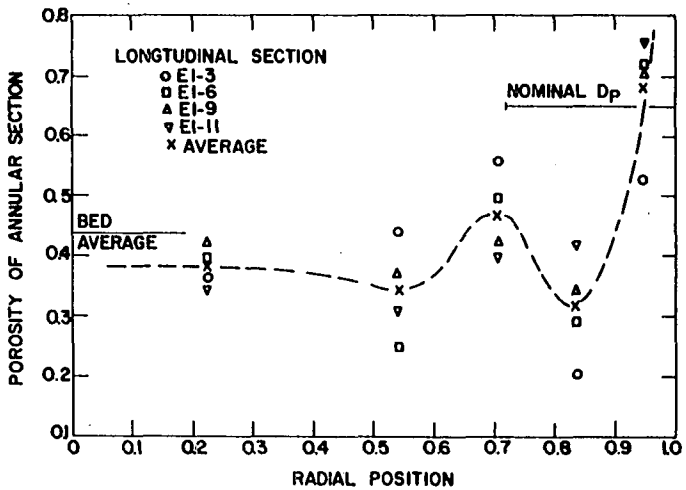
LONGTUDINAL SECTION
E1-3
E1-6
E1-9
E1-11
AVERAGE
NOMINAL D_P
BED AVERAGE
POROSITY OF ANNULAR SECTION
RADIAL POSITION

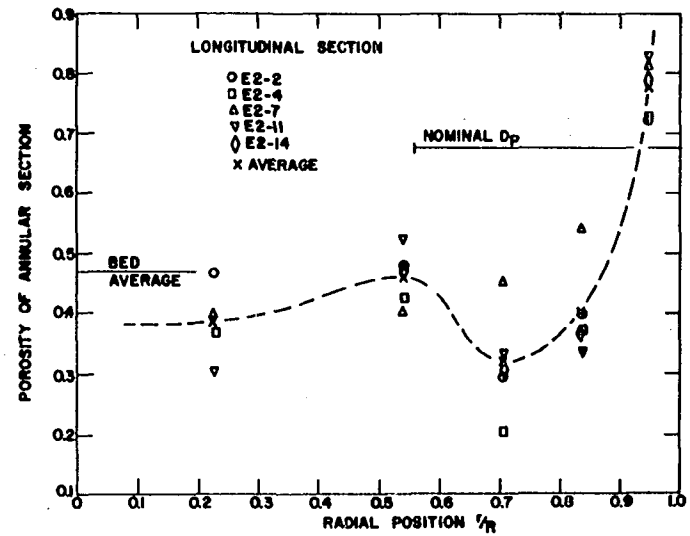
LONGITUDINAL SECTION
E2-2
E2-4
E2-7
E2-11
E2-14
AVERAGE
NOMINAL D_P
BED AVERAGE
POROSITY OF ANNULAR SECTION
RADIAL POSITION r/R

separation of the first two radial layers of packing. These effects are well illustrated by Figure 19, which shows the porosity going from a minimum at one pellet radius from the wall to a maximum at one pellet diameter from the wall. Examination of the curves shows that these maximum and minimum points occur at or near fixed multiples of the particle radius. This cycling would be expected to die out as one moves toward the center of the bed due to increased mixing of the radial layers of packing. With the exception of the beds of Raschig rings, the same is true for the other beds of spheres and cylinders. For Raschig rings, the presence of the hole in the ring causes the porosity to be higher at one pellet radius than it would ordinarily be if the ring were actually a solid cylinder. As would be expected, the minimum porosity for these Raschig rings occurs at approximately 0.75 pellet radius from the wall.

The scatter among the individual points for a given radial section seems greatest for beds having the smallest D_T/D_p ratio (beds B1 and E2). This is possibly due to the fact that in a given annular section for one of these beds, fewer packing surfaces are available for measurement than for beds having a larger D_T/D_p ratio thus giving rise to a greater variation between the individual points for the annular section. The use of these plots to obtain the porosities for the core and wall regions of Model 2 was described in a previous section.

Given below is a table showing the porosities of the experimental beds as calculated by three different methods. The porosities for each bed, calculated by the three different methods, agree to within one or two percent of each other, except in the case of Raschig rings. One would

Table 1. Experimental bed porosities calculated by various methods

	B1	C1	C3	C4	D1	D2	E1	E2
Porosity based on bed measurements, ϵ	0.479	0.452	0.425	0.486	0.575	0.626	0.429	0.467
Porosity based on annular sections, $\bar{\epsilon}_r$	0.489	0.438	0.417	0.472	0.574	0.641	0.438	0.470
Porosity based on momentum cells, $\bar{\epsilon}'$	0.481	0.450	0.408	0.474	0.515	0.588	0.419	0.422

expect $\bar{\epsilon}'$ for the Raschig rings to be lower than ϵ or $\bar{\epsilon}_r$, due to the way in which $\bar{\epsilon}'$ was calculated for the rings. This method of calculation was described in the section dealing with the packed bed models. The agreement of the porosity values, calculated by the different methods, indicates that neglecting the top and bottom 1/2 inch of the beds during the sampling apparently has little effect on the average bed porosity. The reasons for neglecting the ends of the beds during the sampling were described in the section on bed preparation and sampling. In all cases where comparison was made with the work of other investigators, the comparison was made on the basis of $\bar{\epsilon}'$ unless otherwise noted.

The momentum cell hydraulic radius m' is a particularly important quantity since it combines several other momentum cell properties in its calculation. It also enters in to the calculation of momentum loss as a squared quantity. Illustrative histograms of hydraulic radius for the eight experimental beds samples for momentum cell properties are shown

on pages 88 and 90 . The population mean and variance for each distribution are given on the facing pages. It should be realized that these are only illustrative histograms with an arbitrary class width. The histograms are not symmetric but show a definite tendency to tail to the right. This might be expected since portions of the bed may be densely packed and will give close to the minimum momentum cell hydraulic radius available for the particular packing used. Other portions of the bed, which are loosely packed, may give rise to very large values of hydraulic radius. The scatter for the beds having a low D_T/D_p ratio (B1 and E2) and those in which the packing was randomly dumped (C4 and D2) is evident. Also for these beds, the histograms seem to present a more ragged appearance than the histograms for the beds having a larger D_T/D_p ratio or hand dropped packing. The spread in the histograms for Raschig rings is explained by the odd shape of the packing which can give rise to a variety of exposed packing faces (see Figure 15 page 77) and hence a large range of values for the momentum cell hydraulic radius. The effect of this increased spread is to increase the variation in pressure drop or momentum loss for a group of beds having the same superficial properties. If the populations, represented by the histograms, are now thought of as samples from infinite populations of hydraulic radius, then the variances may be thought of as mean squares and may be used to construct F tests on the true population variances. Although many variance F tests could be made, those that compare different methods of bed formation and different values of D_T/D_p ratio for the same type of packing seem the most important. The F ratios for beds in which the packing was randomly dumped versus beds in which the

Figure 27. Illustrative histogram of m' for bed B1, spheres,

$\mu(m') = 7.79 \times 10^{-2}$ inches
$\sigma^2(m') = 7.22 \times 10^{-4}$ inches^2

Figure 28. Illustrative histogram of m' for bed C1, spheres,

$\mu(m') = 5.48 \times 10^{-2}$ inches
$\sigma^2(m') = 3.22 \times 10^{-4}$ inches^2

Figure 29. Illustrative histogram of m' for bed C3, spheres,

$\mu(m') = 5.55 \times 10^{-2}$ inches
$\sigma^2(m') = 3.06 \times 10^{-4}$ inches^2

Figure 30. Illustrative histogram of m' for bed C4, spheres,

$\mu(m') = 7.21 \times 10^{-2}$ inches
$\sigma^2(m') = 5.05 \times 10^{-4}$ inches^2

Figure 31. Illustrative histogram of m' for bed D1, Raschig rings,

$\mu(m') = 7.27 \times 10^{-2}$ inches
$\sigma^2(m') = 4.84 \times 10^{-4}$ inches^2

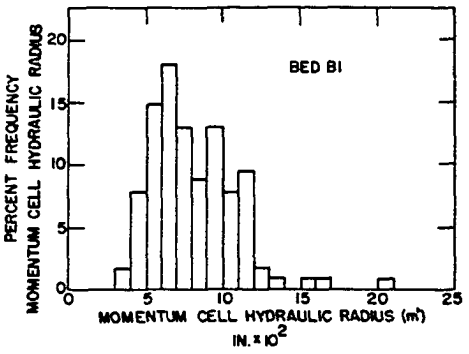
BED B1
PERCENT FREQUENCY
MOMENTUM CELL HYDRAULIC RADIUS
MOMENTUM CELL HYDRAULIC RADIUS (m')
IN. x 10²

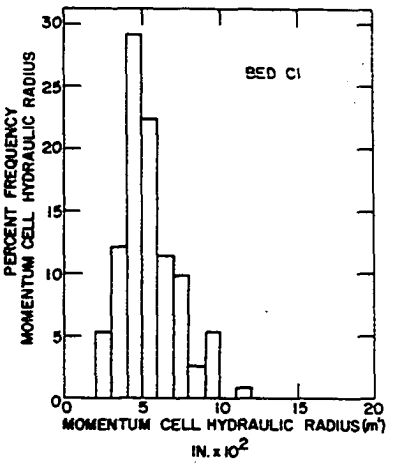
BED C1
PERCENT FREQUENCY
MOMENTUM CELL HYDRAULIC RADIUS
MOMENTUM CELL HYDRAULIC RADIUS (m')
IN. x 10²

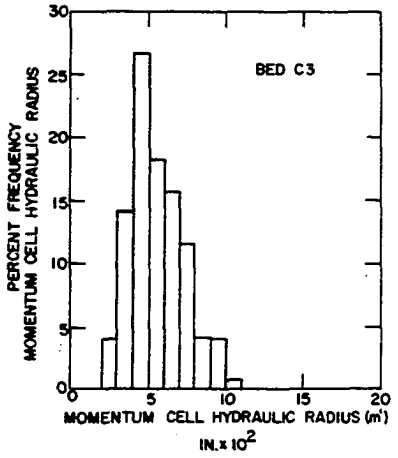
BED C3
PERCENT FREQUENCY
MOMENTUM CELL HYDRAULIC RADIUS
MOMENTUM CELL HYDRAULIC RADIUS (m')
IN. x 10²

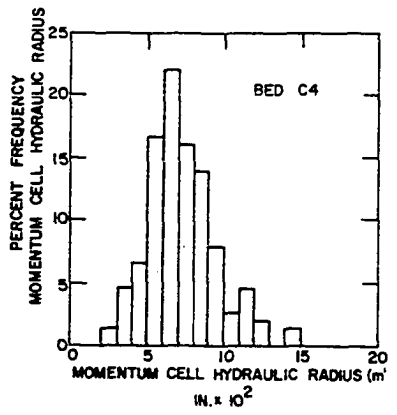
BED C4
PERCENT FREQUENCY
MOMENTUM CELL HYDRAULIC RADIUS
MOMENTUM CELL HYDRAULIC RADIUS (m')
IN. x 10²

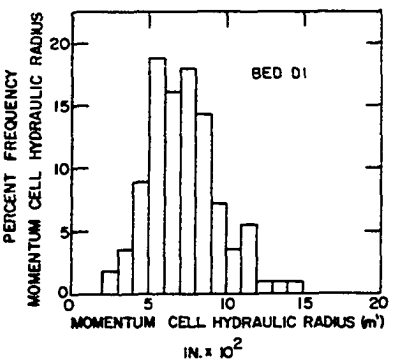
BED D1
PERCENT FREQUENCY
MOMENTUM CELL HYDRAULIC RADIUS
MOMENTUM CELL HYDRAULIC RADIUS (m')
IN. x 10²

Figure 32. Illustrative histogram of m' for bed D2, Raschig rings,

$$\mu(m') = 9.55 \times 10^{-2} \text{ inches}$$
$$\sigma^2(m') = 9.09 \times 10^{-4} \text{ inches}^2$$

Figure 33. Illustrative histogram of m' for bed E1, cylinders,

$$\mu(m') = 5.57 \times 10^{-2} \text{ inches}$$
$$\sigma^2(m') = 2.49 \times 10^{-4} \text{ inches}^2$$

Figure 34. Illustrative histogram of m' for bed E2, cylinders,

$$\mu(m') = 5.80 \times 10^{-2} \text{ inches}$$
$$\sigma^2(m') = 4.02 \times 10^{-4} \text{ inches}^2$$

Figure 35. Illustrative histogram of ϵ' for bed C3, spheres,

$$\mu(\epsilon') = 0.408$$
$$\sigma^2(\epsilon') = 9.85 \times 10^{-3}$$

Figure 36. Illustrative histogram of θ' for bed E1, cylinders

$$\mu(\theta') = 0.625 \text{ radians}$$
$$\sigma^2(\theta') = 5.23 \times 10^{-2} \text{ radians}^2$$

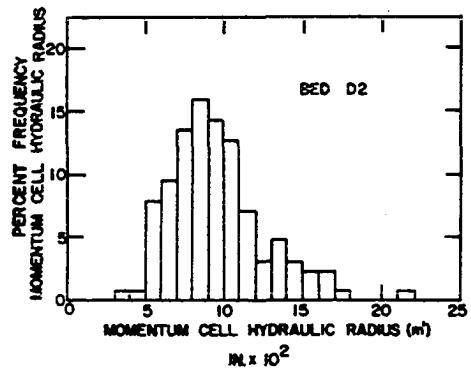
BED D2
PERCENT FREQUENCY
MOMENTUM CELL HYDRAULIC RADIUS
MOMENTUM CELL HYDRAULIC RADIUS (m')
IN. x 10²

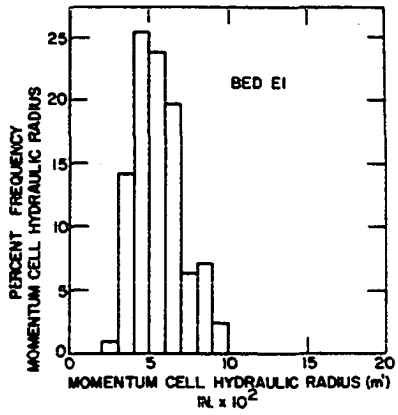
BED E1
PERCENT FREQUENCY
MOMENTUM CELL HYDRAULIC RADIUS
MOMENTUM CELL HYDRAULIC RADIUS (m')
IN. x 10²

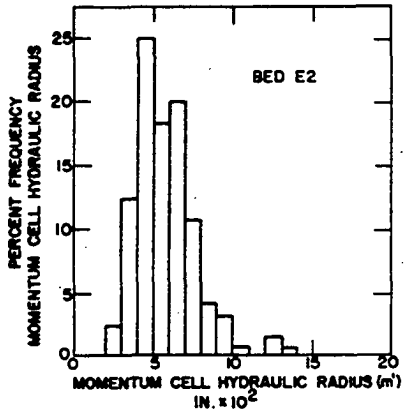
BED E2
PERCENT FREQUENCY
MOMENTUM CELL HYDRAULIC RADIUS
MOMENTUM CELL HYDRAULIC RADIUS (m')
IN. x 10²

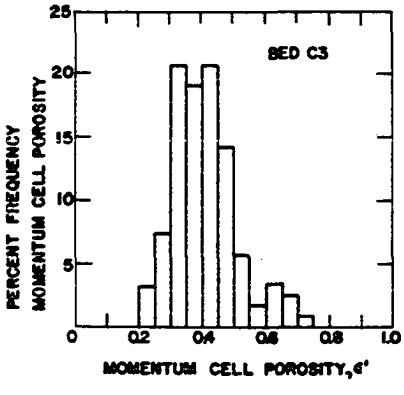
BED C3
PERCENT FREQUENCY
MOMENTUM CELL POROSITY
MOMENTUM CELL POROSITY, ε'

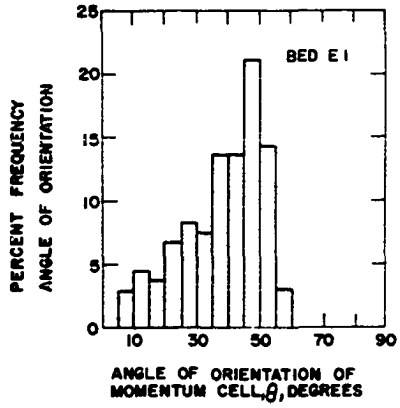
BED E1
PERCENT FREQUENCY
ANGLE OF ORIENTATION
ANGLE OF ORIENTATION OF
MOMENTUM CELL, β, DEGREES

packing was hand dropped (C4/C3, C4/C1, C4/B1, and D2/D1) were all found significant at the one percent level except for the test C4/B1 which was not significant. These tests indicate that the method of packing may cause a large variation in momentum cell hydraulic radius, even for a bed with a reasonably large D_T/D_p ratio such as bed C4. F tests for beds having a low D_T/D_p ratio versus beds with a higher D_T/D_p ratio were also made. The tests B1/C1, B1/C3, and E2/E1 were found significant at the one percent level while the test B1/C4 was found significant at the five percent level. These last tests show the importance of the D_T/D_p ratio, especially low values of D_T/D_p, to the variation of the momentum cell hydraulic radius and therefore to the variation in momentum loss between packed beds.

On page 90 are shown typical illustrative histograms of the momentum cell porosity ϵ' and momentum cell angle of orientation θ'. As expected, the porosity histogram shows a similarity in form to the hydraulic radius histogram since the two quantities are highly correlated. The histogram for θ' tails to the left because in the method of calculation for θ' very large angles are not at all probable while the smaller angles will appear often. This histogram seems more representative of the angular path taken by the fluid than of the actual angles between all pieces of packing.

The table below gives the population means and variances for the momentum cell properties. This table should be used along with Table 7 in the Appendix which lists the characteristics of each bed. For beds of spheres, the means and variances decrease with decreasing porosity (i.e. increasing D_T/D_p) except in the case of bed C4, in which the packing was

Table 2. Population mean and variance for samples of momentum cell properties

Population Mean

Bed	Type	k'_o	$\overline{\epsilon'}$	$\overline{m'}$ inches	$\overline{\theta'}$ radians	$\overline{S'_m}$ inches^2
B1	spheres	3.56	0.481	0.0779	0.663	0.252
C1	spheres	3.54	0.450	0.548	0.678	0.139
C3	spheres	3.53	0.408	0.0555	0.625	0.135
C4	spheres	3.67	0.474	0.0721	0.703	0.150
D1	R. rings	3.61	0.515	0.0727	0.647	0.263
D2	R. rings	3.80	0.588	0.0955	0.701	0.319
E1	cylinders	3.54	0.419	0.0557	0.667	0.166
E2	cylinders	3.61	0.422	0.0580	0.658	0.172

Population Variance

Bed	Type	k'_o x10	ϵ' x10^2	m' inches^2 x10^4	θ' radians^2 x10^2	S'_m inches^4 x10^3
B1	spheres	1.81	3.74	7.22	6.54	8.76
C1	spheres	1.12	2.99	3.22	5.90	2.78
C3	spheres	0.580	0.985	3.06	5.23	1.42
C4	spheres	0.790	1.04	5.05	4.61	2.64
D1	R. rings	1.79	1.13	4.84	5.04	11.69
D2	R. rings	3.27	1.45	9.09	4.07	25.66
E1	cylinders	0.596	1.19	2.49	4.87	3.39
E2	cylinders	1.88	2.48	4.02	4.55	4.88

randomly dumped causing an increase in bed porosity. This may be explained by the fact that in order for the bed to reach these lower porosities, the packing will tend to form more uniform and stable configurations, and this tendency will decrease both the means and the variances of the populations of momentum cell properties. The means and variances for θ' show only a partial correlation with the average bed properties such as $\overline{\epsilon'}$. This is possibly due to the fact that the somewhat arbitrary method used to calculate θ' may not be entirely adequate to describe the angular distribution of packing within the bed. This would be especially true for packing having a complex shape such as Raschig rings. As expected, the values for the cell properties of bed D2 are greater than those for D1 since bed D2 has randomly dumped packing. Although bed D2 has the highest average bed porosity of any of the beds, it is not high enough to give a good illustration of how k_o' varies with ϵ'. Again, the values for bed E2 are greater than those for E1 since E2 has a smaller D_T/D_p ratio than E1. Table 2 cannot be used as a complete description of the variation of bed properties since it does not describe the important correlation between ϵ' and m'.

The correlation between ϵ' and m' is illustrated by the plots shown on pages 97 and 99. These plots show a definite non-linear correlation that decreases with increasing porosity. The hydraulic radius given by Carman (13) is also shown on these plots. While other expressions giving hydraulic radius as a function of porosity are available, the one given by Carman is by far the most commonly used, and therefore it is given here for comparison. The spreading of the points with increasing porosity

can be partially explained in the following way: In order to achieve areas of low porosity in the bed, the pieces of packing will tend to orient themselves in a way that will allow them to move closer together. This will produce a more or less uniform orientation of the packing in these areas. A section or slice through such an area will show momentum cells having roughly the same flow area, S', and porosity, ϵ'. The cells will also have roughly the same packing area, S'_p, and perimeter, Z'_p, of the exposed packing face. The condition of low porosity then, will create cells having nearly the same hydraulic radius. At higher porosities, the pieces of packing have more freedom to orient themselves in various ways and directions. Therefore a section through a region of high porosity will show cells having widely varying flow areas, porosities, and size and shape of the exposed packing faces. These conditions create momentum cells with widely varying hydraulic radii. This effect is noticable for every bed except those for Raschig rings. Since the spreading of the hydraulic radius with porosity occurs for cylinders, it can be concluded that the presence of the hole in the Raschig ring allows the rings to present packing face areas of widely varying size and shape even at the lower porosities. It was noticed that certain groups of points on the Raschig ring plots seemed to indicate that a separate curve could be drawn through them parallel to the Kozeny-Carman curve. Such a group is illustrated by the string of points farthest to the left in the plot for bed D1. Examination of the momentum cells for these points, on the enlarged sections, showed that each cell in a particular group had roughly the same shape for the exposed packing face (for example, a semi-circular shape). This is the

shape that the fluid would "see" as it travels through the bed according to the models previously described. The same is true to a more limited extent for the beds of cylinders.

Comparison of the data points with the Kozeny-Carman curve suggests that the variation of momentum cell hydraulic radius m' with porosity should be the same as that given by the Kozeny-Carman curve. That this is so may be easily shown. Since

$$m' = \frac{S'_m - S'_p}{Z'_p} \qquad \text{and} \qquad \epsilon' = \frac{S'_m - S'_p}{S'_m}$$

then

$$m' = \frac{S'_p}{Z'_p}\left(\frac{\epsilon'}{1-\epsilon'}\right) \tag{89}$$

This is compared with the Kozeny-Carman expression

$$\text{average bed hydraulic radius} = \frac{\epsilon}{S} = \frac{\epsilon}{S_o(1-\epsilon)} \tag{90}$$

It can be seen that Equations 89 and 90 have the same porosity function. There are, however, other considerations. Equation 89 shows that the individual hydraulic radii will vary depending on the ratio of S'_p to Z'_p. This means that more than one hydraulic radius is possible at the same porosity. This ratio in turn depends on the shape of the particle, its angle of orientation, and where it is cut. This method of calculating the cell hydraulic radius automatically takes into account the shape of the packing no matter how complex it may be. Equation 90 is an average bed hydraulic radius based on the surface to volume ratio of the packing and does not allow any such variation since S_o is constant for any one type of regular packing. Also, the hydraulic radius according to Equation

Figure 37. m' versus ϵ' for bed B1, spheres, $D_T/D_p = 3.94$, sample size = 115

Kozeny (37)
Carman (13)

Figure 38. m' versus ϵ' for bed C1, spheres, $D_T/D_p = 5.35$, sample size = 112

Figure 39. m' versus ϵ' for bed C3, spheres, $D_T/D_p = 9.36$, sample size = 120

Figure 40. m' versus ϵ' for bed C4, spheres, $D_T/D_p = 10.6$, sample size = 150

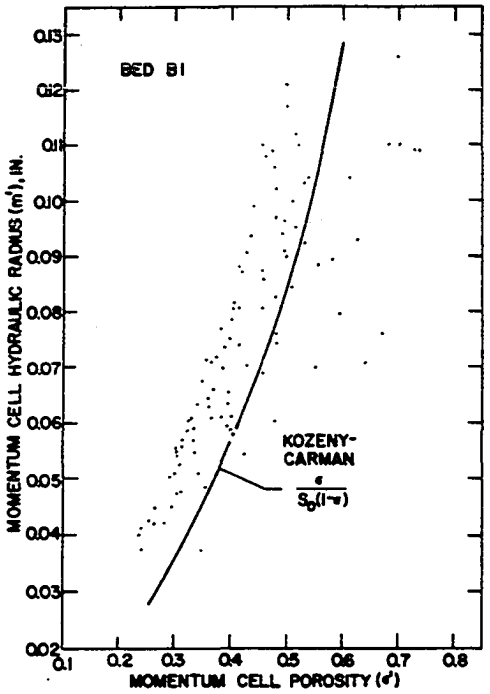
BED B1
MOMENTUM CELL HYDRAULIC RADIUS (m'), IN.
MOMENTUM CELL POROSITY (ε')
KOZENY-CARMAN
ε / S₀(1-ε)

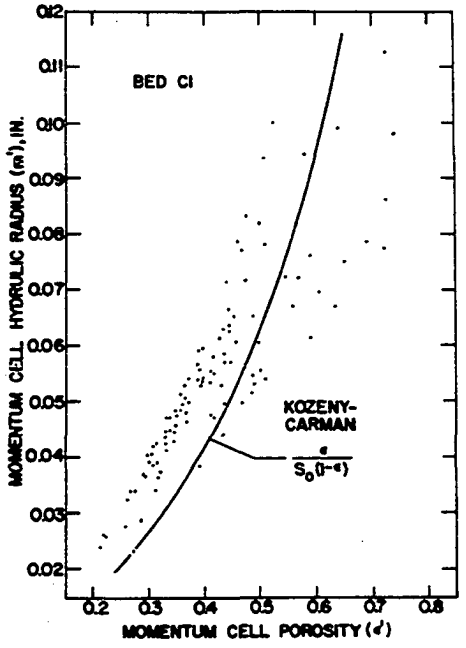
BED C1
MOMENTUM CELL HYDRAULIC RADIUS (m'), IN.
MOMENTUM CELL POROSITY (ε')
KOZENY-CARMAN
ε / S₀(1-ε)

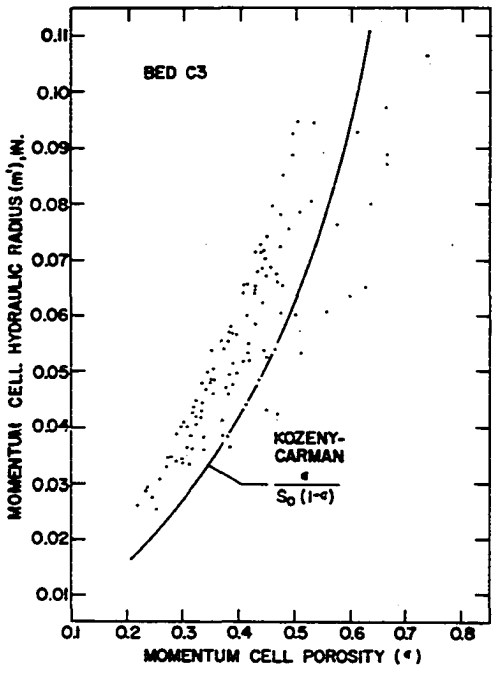
BED C3
MOMENTUM CELL HYDRAULIC RADIUS (m'), IN.
MOMENTUM CELL POROSITY (ε')
KOZENY-CARMAN
ε / S₀ (1-ε)

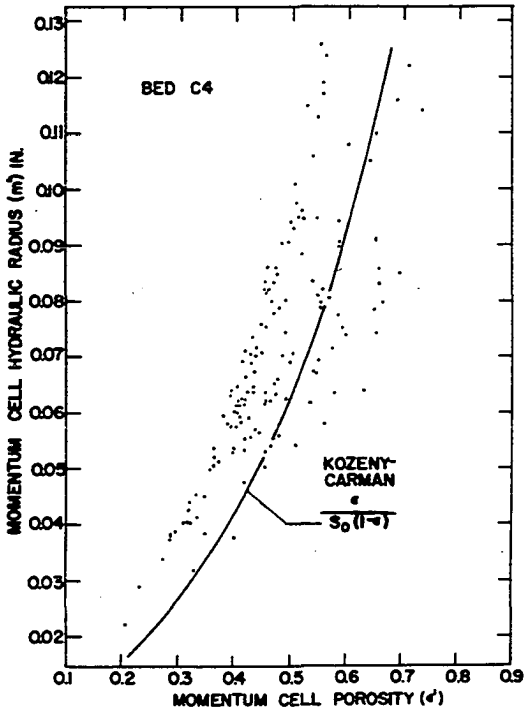
BED C4
MOMENTUM CELL HYDRAULIC RADIUS (m') IN.
MOMENTUM CELL POROSITY (ε')
KOZENY-CARMAN
ε / S₀ (1-ε)

Figure 41. m' versus ϵ' for bed D1, Raschig rings, $D_T/D_p = 5.51$, sample size = 112

Figure 42. m' versus ϵ' for bed D2, Raschig rings, $D_T/D_p = 5.50$, sample size = 126

Figure 43. m' versus ϵ' for bed E1, cylinders, $D_T/D_p = 7.10$, sample size = 126

Figure 44. m' versus ϵ' for bed E2, cylinders, $D_T/D_p = 4.53$, sample size = 120

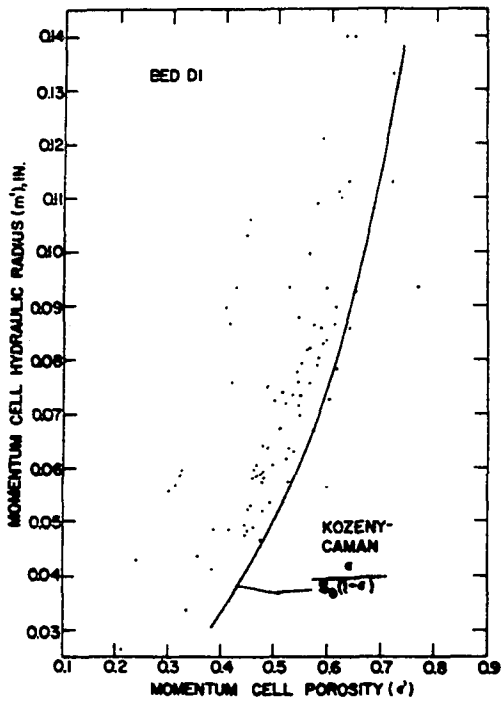
BED D1
MOMENTUM CELL HYDRAULIC RADIUS (m'), IN.
MOMENTUM CELL POROSITY (ε')
KOZENY-CAMAN
ε / S₀(1-ε)

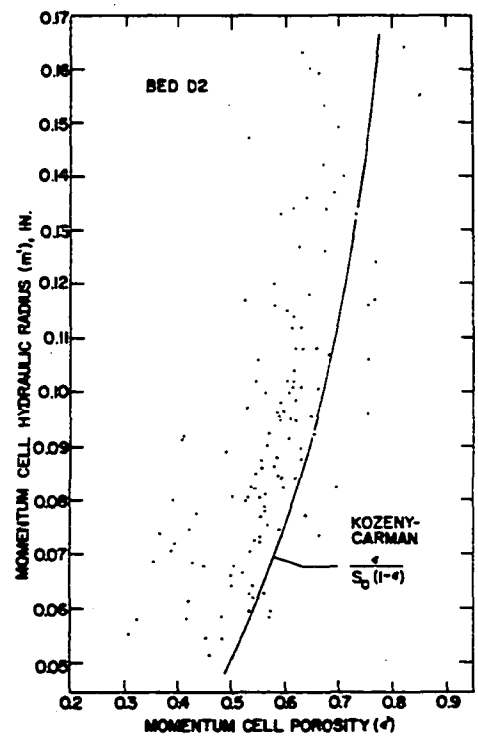
BED D2
MOMENTUM CELL HYDRAULIC RADIUS (m'), IN.
MOMENTUM CELL POROSITY (ε')
KOZENY-CARMAN
ε / S₀(1-ε)

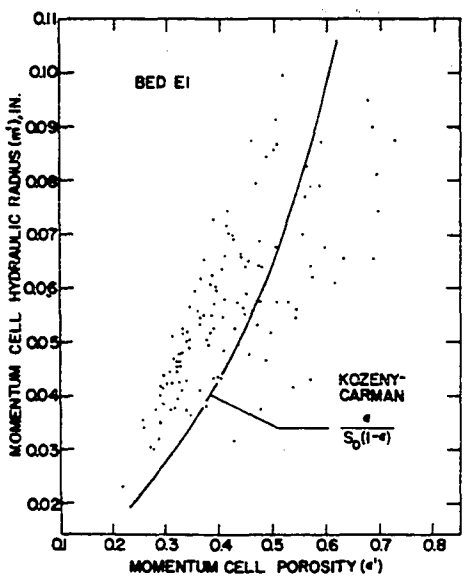
BED E1
MOMENTUM CELL HYDRAULIC RADIUS (m'), IN.
MOMENTUM CELL POROSITY (ε')
KOZENY-CARMAN
ε / S₀(1-ε)

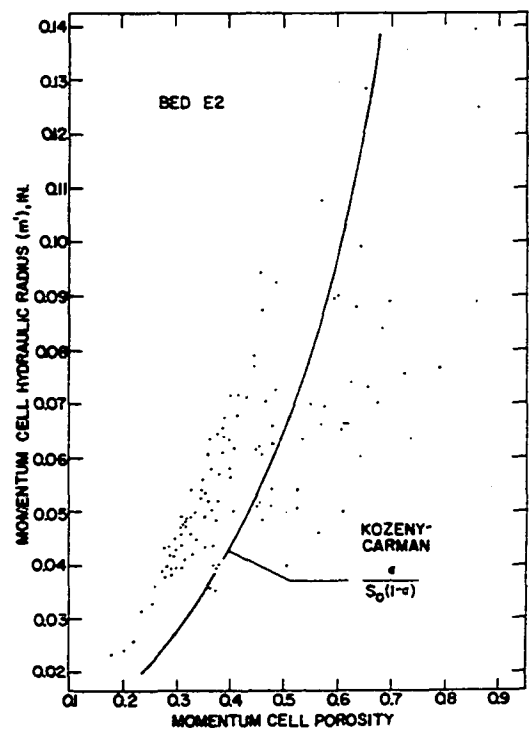
BED E2
MOMENTUM CELL HYDRAULIC RADIUS (m'), IN.
MOMENTUM CELL POROSITY
KOZENY-CARMAN
ε / S₀(1-ε)

90 may be in error when $S_o(1-\epsilon)$ fails to accurately represent the specific surface of the bed, S. This would be the case if the packing consisted of plates. Then S_o would remain the same, but many of the packing surfaces would mate and reduce the effective surface area of the bed. The hydraulic radius calculated according to Equation 89 would take this into account, since two particles having mated surfaces may be treated as one when measuring the cell area and perimeter.

Examination of these plots of m' versus ϵ' shows that the Kozeny-Carman hydraulic radius falls below the majority of the data points. The reason for this is that the hydraulic radius, m', calculated according to Equation 89, is based on an area concept while the hydraulic radius, m, calculated according to Equation 90, is based on a volume concept. This idea was partially discussed in the literature survey section where the two definitions for hydraulic radius, Equations 26 and 27, were presented. The two definitions are equivalent for circular capillaries, but may not be for packed beds. Harmson (32) considers a homogenous bed of equal size particles whose dimensions are small compared to those of the container. These particles have arbitrary shape but are orientated completely at random. For these conditions, Harmson has shown that the ratio between the hydraulic radii, calculated by the two different definitions, is $m/m' = \pi/4$. Therefore any comparison between models based on these two definitions should involve this ratio. Looking at the plots, one can see that multiplication of the expression for the Kozeny-Carman hydraulic radius by $4/\pi$ brings the line into approximate agreement with the bulk of the data points. More will be said on this later during the discussion of the

model predictions.

Also of interest, is the relative scatter of the plots. The plot for bed B1 shows a slight increase in scatter over the plots for beds C1 and C3 since B1 has a very low D_T/D_p ratio. Also, the scatter for bed C4 is higher than either bed C1 or C3 since bed C4 was formed from randomly dumped packing while C1 and C3 were formed from hand-dropped packing. The plots for Raschig rings show high scatter, for reasons previously given, with the plot for bed D2, with randomly dumped packing, showing slightly more scatter than the D1 plot. The magnitude of the scatter for cylinders is considerably greater than that for spheres and was somewhat of a surprise. Evidently at the higher porosities, where the pieces of packing have more freedom of orientation, cylinders, because of their shape, are able to present more of a variety of exposed packing shapes than spheres and therefore a larger range of momentum cell hydraulic radius. Again, the scatter for bed E2 is greater than that for bed E1 since E2 has the smaller D_T/D_p ratio.

Shown on page 103 are some typical plots illustrating the variation of bed properties with axial and radial directions. Figures 45 and 46 for bed D1 are based on section averages of the momentum cell properties ϵ' and m'. Less scatter about the means could probably be obtained by using the porosities and hydraulic radii for all the momentum cells in each section. The random scatter of the points, however, seems to indicate that there is no definite variation of bed properties with axial length, so that the effects of bed length are not very important except perhaps for very short beds. Similar plots were obtained for the other

Figure 45. Example plot of average section porosity (based on ϵ') versus axial distance for bed D1, Raschig rings, $\overline{\epsilon'} = 0.515$

Figure 46. Example plot of average section hydraulic radius (based on m') versus axial distance for bed D1, Raschig rings, $\overline{m'} = 7.27 \times 10^{-2}$ inches

Figure 47. Example plot of momentum cell porosity ϵ' versus radial position for bed C1, spheres

Figure 48. Example plot of momentum cell hydraulic radius m' versus radial position for bed C1, spheres

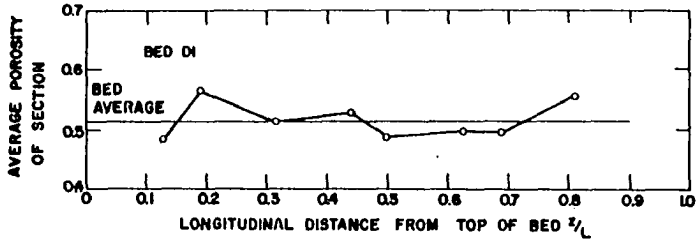
AVERAGE POROSITY OF SECTION
BED DI
BED AVERAGE
0.7
0.6
0.5
0.4
0 0.1 0.2 0.3 0.4 0.5 0.6 0.7 0.8 0.9 1.0
LONGITUDINAL DISTANCE FROM TOP OF BED z/L

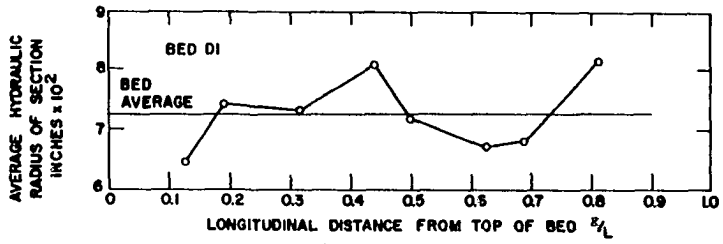
AVERAGE HYDRAULIC RADIUS OF SECTION INCHES x 10²
BED DI
BED AVERAGE
9
8
7
6
0 0.1 0.2 0.3 0.4 0.5 0.6 0.7 0.8 0.9 1.0
LONGITUDINAL DISTANCE FROM TOP OF BED z/L

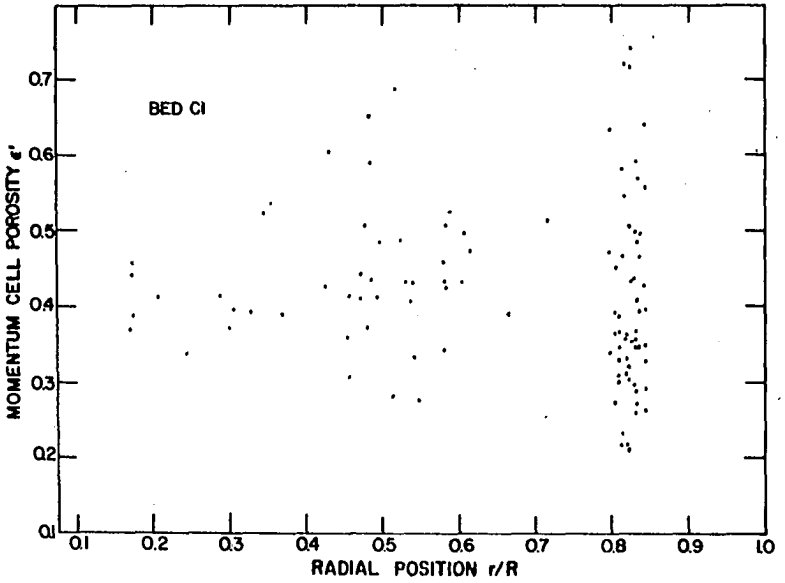
MOMENTUM CELL POROSITY e'
BED CI
0.7
0.6
0.5
0.4
0.3
0.2
0.1
0.1 0.2 0.3 0.4 0.5 0.6 0.7 0.8 0.9 1.0
RADIAL POSITION r/R

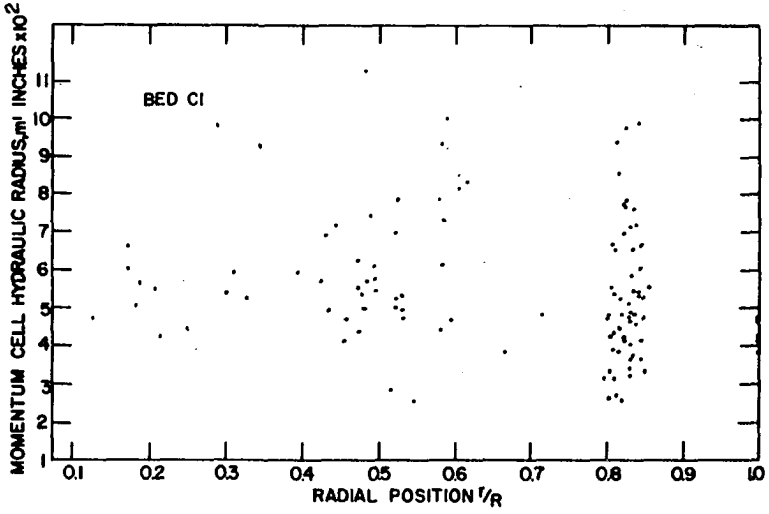
MOMENTUM CELL HYDRAULIC RADIUS,m' INCHES x10²
BED CI
11
10
9
8
7
6
5
4
3
2
1
0.1 0.2 0.3 0.4 0.5 0.6 0.7 0.8 0.9 1.0
RADIAL POSITION r/R

experimental beds. Figures 47 and 48 show the variation of ϵ' and m' with radial position for bed C1. The gaps in the groups of points are areas of the bed where few packing centers are found, resulting in fewer momentum cells. Although the scatter is relatively large, there does seem to be some indication that it is less near the center of the bed than near the wall. A larger sample of momentum cells would be needed to completely determine the extent of the scatter. As expected, plots for beds with hand-dropped packing and the higher D_T/D_p ratios showed the least scatter.

Results for Models

The predictions of the models for mean momentum loss or pressure drop are compared with the predictions of Carman (13) and Rose (53). The models are then discussed in the light of these comparisons. The model predictions for the variation in momentum loss between beds are also given, and a partial comparison is made with the work of Rose. It should be realized that the model predictions are for the specific experimental beds constructed. The exploratory nature of this work and the stochastic method of calculation does make absolute comparisons with experimental data possible unless these data happen to be taken for beds having exactly the same gross properties as the experimental beds. However, relative comparisons of the model predictions for each bed, with the predictions of other investigators, are possible.

The equation of Carman (13) is representative of a large number of similar expressions that have the same porosity function and differ slightly

in the value of the constants used. The equation of Rose (53) is interesting in that it has a different porosity function than that of Carman. While other investigators have given correlation equations, the porosity functions are usually grossly in error or meant only for specific situations. For these reasons, the equations of Carman and Rose are selected for comparison with the models. The comparisons of course are only for the laminar flow regime, with a Reynolds number < 1.0. The comparisons for mean momentum loss are discussed first and the variation between beds of the same type discussed later.

Since the machine calculations are for a specific D_T/D_p ratio, the comparisons are best made on the basis of momentum loss per unit length. For purposes of comparison the Carman equation may be written

$$\frac{lb_f}{L} = \frac{\eta V_o S_T}{g_c} \underbrace{5.0\, S_o^2 \frac{(1-\epsilon)^2}{\epsilon^3}}_{\text{Carman}} \tag{91}$$

The equation of Rose may be written

$$\frac{lb_f}{L} = \frac{\eta V_o S_T}{g_c} \underbrace{27.78\, S_o^2 \frac{1.115(1-\epsilon)\left[(1-\epsilon)^2 + 0.018\right]}{\epsilon^{1.5}}}_{\text{Rose}} \tag{92}$$

Model 1 may be written

$$\frac{lb_f}{L} = \frac{\eta V_o S_T}{g_c} \underbrace{\frac{k \mu (p_{i,j})}{S_T}}_{\text{Model 1}} \tag{93}$$

Model 2 may be written

$$\frac{lb_f}{L} = \frac{\eta V_o S_T}{g_c} \underbrace{\bar{x}(m_t)}_{\text{Model 2}} \tag{94}$$

The $\mu(p_{ij})$ and $\bar{x}(\dot{m}_t)$ contain only those quantities that vary during a particular calculation. To compare the above equations, it is necessary to compare only the quantities labeled Carman, Rose, Model 1, and Model 2. Both Carman and Rose found that wall correction factors were needed to bring their predictions into agreement with experimental data. Carman reasoned that the added area of the wall was the important quantity and corrected for this added area by the following empirical correction factor.

$$\text{Carman correction for wall effect} = A_c = \left[\frac{S + 1/2\, S_c}{S}\right] \qquad (95)$$

Rose realized that the wall effect actually consisted of two effects. The first effect was due to the added area of the wall, and the second effect was due to the change in flow distribution because of the higher porosity near the container wall. Rose thought that the first effect would be the controlling one in laminar flow while the second effect would be more important in turbulent flow where impact and inertia effects are dominant. Rose gave his wall-correction factors, A_R, in graphical form. Whenever wall-correction factors are used with Equations 91 and 92, they will be indicated.

As mentioned previously, the Carman hydraulic radius, m (see Equation 90), is based on a volume concept, as is the measure of pore diameter employed by Rose, while the momentum cell hydraulic radius, m' (see Equation 89), is based on an area concept. Harmson (32) has shown that for a homogenous porous medium the ratio m/m' is $\pi/4$. The use of this ratio was shown to bring the Carman hydraulic radius into better agreement with the experimental m' given on the plots of m' versus ϵ'. Therefore in comparing

Models 1 and 2 with the predictions of Carman and Rose, it will be necessary to multiply Equations 93 and 94 by $(4/\pi)^2$. The calculated results for Model 1 and Model 2 are shown in Tables 3 and 4 respectively.

Table 3. Calculated results for Model 1

Bed	$\mu(p_{ij})$ Correlated	$\mu(p_{ij})$ Uncorrelated	$\sigma^2(p_{ij})$ Correlated $\times 10^{-4}$	$\sigma^2(p_{ij})$ Uncorrelated $\times 10^{-4}$
B1	971.3	892.2	123.8	78.62
C1	1181	1062	226.7	122.8
C3	1021	930.3	118.3	69.41
C4	711.4	634.1	125.8	53.13
D1	958.9	894.6	208.9	115.3
D2	618.6	602.6	52.27	43.85
E1	1206	1128	164.3	105.5
E2	1264	1141	290.5	148.0

Table 4. Calculated results for Model 2

Bed	$\bar{x}(m_t)$ Correlated inches^2	$\bar{x}(m_t)$ Uncorrelated inches^2	$s^2(m_t)$ Correlated $\times 10^{-3}$ inches^4	$s^2(m_t)$ Uncorrelated $\times 10^{-3}$ inches^4
B1	1897	1792	209.5	327.4
C1	4114	3989	516.5	710.1
C3	4296	4268	121.6	146.8
C4	2518	2491	37.89	43.09
D1	1828	1743	48.27	59.80
D2	1055	997.6	23.91	32.25
E1	4406	4364	204.7	205.1
E2	3979	3832	549.1	780.3

The comparisons of the predictions of Carman and Rose with those of the models are best given in table form and are shown in Table 5. Since the comparisons are relative, the mean momentum loss for Models 1 and 2 is chosen as the base, and therefore the predictions of Carman and Rose are given as a percent deviation from the model predictions. The columns are labeled with capital letters for ease of reference during the discussion.

Table 5. Comparison of model predictions

Bed	Porosity	Carman $inches^{-2}$	A_c	A (Carman)A_c $inches^{-2}$	Rose $inches^{-2}$	B (Rose)A_B $inches^{-2}$	C $\left(\frac{4}{\pi}\right)^2$(Model 1 Correlated $inches^{-2}$)
B1	0.481	1684	1.353	2278	1919	2782	6,255
C1	0.450	4258	1.239	5276	4642	6267	13,731
C3	0.408	6618	1.129	7452	6656	7989	12,225
C4	0.474	3348	1.124	3763	3774	4491	7,693
D1	0.574	1955	1.153	2254	2453	3262	5,905
D2	0.641	997	1.184	1180	1299	1728	3,143
E1	0.438	5513	1.151	6345	4846	5960	11,760
E2	0.470	4345	1.257	5462	3676	5147	11,889

Bed	D $\left(\frac{4}{\pi}\right)^2$ x (Model 2 Correlated $inches^{-2}$)	E $\left(\frac{4}{\pi}\right)^2$ x (Model 2 Uncorrelated $inches^{-2}$)	F % Deviation A and C	G % Deviation A and D	H % Deviation B and D	I % Deviation A and E	J % Deviation B and E
B1	3073	2903	-63.6	-25.9	-9.5	-21.5	-4.17
C1	6665	6462	-61.6	-20.6	-6.0	-18.4	-3.02
C3	6960	6914	-39.1	+7.5	+14.8	+16.0	+15.5
C4	4079	4035	-51.1	-7.4	+10.1	-7.4	+11.3
D1	2961	2824	-61.8	-23.7	+10.1	-12.5	+15.5
D2	1709	1616	-62.4	-31.0	+1.1	-27.0	+6.93
E1	7138	7070	-46.0	-10.7	-16.5	-10.3	-15.7
E2	6446	6208	-54.0	-15.3	-20.1	-12.0	-17.1
Avg. Percent Deviation			55.0	17.8	11.0	15.6	11.2

Column F shows the comparison of Carman (column A) with Model 1 (column C). From a prediction standpoint, the results are somewhat disappointing. The results for Model 1 are as much as 2.5 times those for Carman. Although the Carman predictions may be in error, it seems obvious that the predictions of Model 1 are too high. The reason for this lies in the manner in which the momentum cell fluid velocities were calculated for Model 1. In this model, the assumption was made that the mass flow velocity, for each momentum cell in a given layer, was approximately equal. This assumption leads to the following expression

$$\Delta P \propto \frac{k_o'}{\epsilon' m'^2}$$

Examination of the individual values of $k_o'/\epsilon' m'^2$, showed that often a low value of ϵ' was used with a low value of m', especially in the case where ϵ' and m' were correlated, giving rise to high values of ΔP. These high values occurred often enough to dominate the mean and give high prediction values. It may be concluded that the criterion of approximately equal mass velocity in each momentum cell is an unrealistic one. Because of the abnormally high prediction values, Model 1 was not considered in the remainder of the comparisons for momentum loss.

The comparison of correlated and uncorrelated Model 2 with the predictions of Carman and Rose is shown in columns G, H, I, and J respectively, with the average percent deviation shown below each column. For reasons previously mentioned, the comparisons are made with a wall-effect correction for Carman and Rose and the factor $(4/\pi)^2$ for Model 2. The comparisons show that Model 2 predicts reasonable values for momentum loss and

that the predictions of Rose agree remarkably well with those of the model. The predictions of Chilton and Colburn (18) were also compared with those of Model 2, but their values were as much as 1000 percent in excess of those of the model and were not considered further. This is probably due to the fact that they did not include a porosity function in their correlation. In any real physical situation, m' and ϵ' are strongly correlated, as the plots of m' versus ϵ' show, and therefore the correlated model would probably be more applicable than the uncorrelated model. A graphical comparison of correlated Model 2 witn the predictions of Carman and Rose is shown in Figure 49. For Model 2, the predictions for the correlated and uncorrelated cases are fairly close. Therefore the points in Figure 49, plotted for the correlated case, are also an approximate indication of the results for the uncorrelated case.

The reasonable agreement of the model with Carman and Rose indicates the apparent importance of the $\pi/4$ term. However, Harmson (32), in showing that the ratio m/m' was $\pi/4$, assumed that the porous medium was completely homogenous and that the dimensions of the particle were small compared to the dimensions of the container. Model 2 is a non-homogenous two-region model, and a factor slightly different than $\pi/4$ may be more applicable for comparison purposes, although it would be hard to predict just what this would be. Also, a number of the experimental beds had relatively low values of the D_T/D_p ratio, and this would have an effect on the $\pi/4$ factor. It seems, however, that in many cases, such as capillary rise phenomena, a definition of hydraulic radius based on area would be more applicable than a definition based on volume.

Figure 49. Comparison of mean momentum loss for correlated Model 2 with the predictions of Carman (13) and Rose (53)

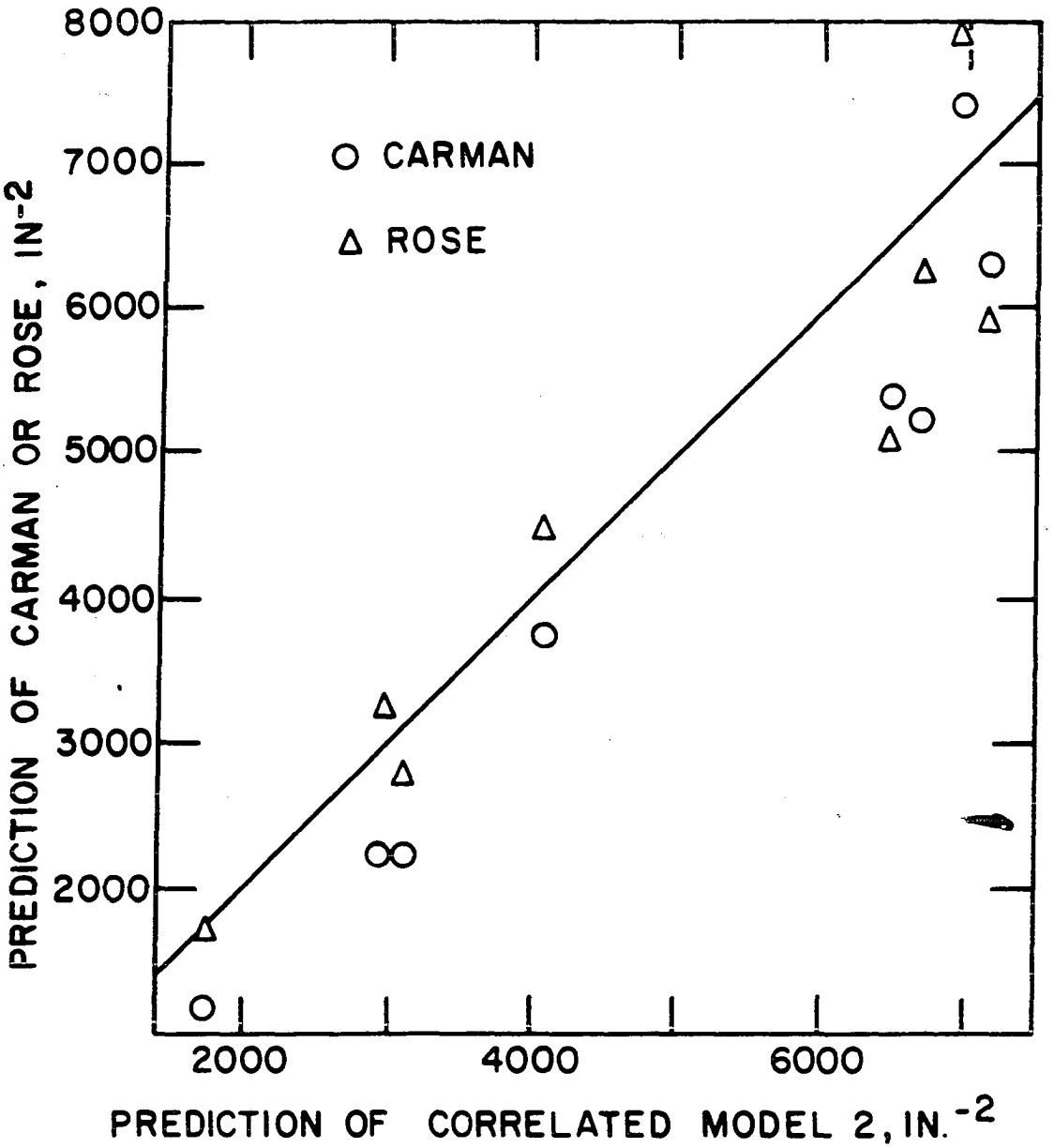
8000
7000
6000
5000
4000
3000
2000
O CARMAN
Δ ROSE
PREDICTION OF CARMAN OR ROSE, IN.-2
2000
4000
6000
PREDICTION OF CORRELATED MODEL 2, IN.-2

As mentioned earlier, both Carman and Rose found that a wall-effect correction factor was needed to bring their predictions into better agreement with the experimental data. The agreement of the correlated Model 2 with Carman and Rose indicates that the model apparently accounts for this wall effect. The percent deviation between Carman and Model 2 appears to decrease with increasing D_T/D_p ratio (i.e. decreasing wall effect), although no such trend is evident for the comparisons with Rose. The two-region model, with each region having its own volume porosity and distributions of momentum cell properties, seems to account for the wall effect. Since a good deal of the variation in bed properties, for a non-homogenous bed, occur within one or one and a half pellet diameters from the wall, a two-region model should be fairly reliable. A homogenous model, using actual measured properties for a bed with a low D_T/D_p ratio, could also account for the wall effect but not to the extent that a two-region could do so.

It is difficult to estimate the contribution of θ' to the model. Although it seems reasonable that any moderate change in porosity would produce some change in bed tortuosity, the means and variances for the distributions show only a partial correlation with the average bed properties such as $\bar{\epsilon}'$. This is probably due to the somewhat arbitrary manner in which the θ' were calculated. It is probably best to think of the distributions as supplying a mean value of the tortuosity (i.e. $1/\cos^2\theta'$) and a contribution to the variance that is very roughly the same for each type of experimental bed studied here. The method of calculating the may not be entirely adequate to describe the actual angular distribution of the packing, especially for complex shapes such as Raschig rings. It

may, however, give average θ' values (approximately 35° to 40°) that are more indicative of the actual fluid path than the constant value of 45° assumed by Carman. Carman based his value of 45° on a consideration of the packing geometry and some visual observations of dye flow through a bed of glass beads. Other investigators, such as Bartell and Osterhof (5), have proposed values as high as 50°. In laminar flow, however, the fluid, in moving from particle to particle, will tend to move to the particle closest in line to its present direction of travel, and the length of flow path may be somewhat less than that dictated by the actual geometrical distribution of the packing. The question of tortuosity is a very difficult one, and investigators have not agreed on a uniform method of determining this factor. It may be that the use of average values for the mean and variance of the tortuosity is the best that can be done.

The results for the momentum cell constant, k_o', are interesting and important. Figures 50 and 51 on page 117 show the way in which the calculated momentum cell constant changes with porosity, and Figures 52 and 53 compare the calculated k_o' with some experimental data. The data in Figure 52 are from Schriver (59) and show how the experimentally determined laminar constant, f_{1L}, increases with increasing porosity. This laminar constant is the same as 72α in Equation 19 of the literature survey. The values taken from the curve in Figure 52 are compared with the calculated k_o' values by means of a relative plot, using f_{1L} and k_o' at a porosity of 0.3 as the basis. This plot is shown in Figure 53. The agreement is quite good and shows that f_{1L} varies with porosity in the same manner as the calculated k_o'. The agreement is even more remarkable when one

considers that the simple model used to calculate k_o' was that of a cylinder in an infinite extent of fluid, with porosity considered as the only variable. Such an agreement indicates that although the system geometry is a factor in determining k_o', porosity is the most important variable. The calculated k_o' is compared with the value given by Emersleben (67) in Figure 50. Emersleben used a more complicated model but intended his calculations to be valid in the range $0.9 < \epsilon < 1.0$. Figure 50 shows that Emersleben's values do approach the calculated values at the higher porosities. At these higher porosities, the fluid flow conditions become more and more like the simple model used so that k_o' would be expected to be more accurate at the higher porosities. The reason that flL or k_o' increases with increasing porosity is the following: At lower porosities, flow through the bed is similar to flow through a group of channels, hence the use of channel theory models such as Carman's. At higher porosities, the bed approaches conditions where the particles have less influence on each other, and the channel concept of a packed bed has less and less meaning. Finally at very high porosities, the pressure drop or drag on the bed should be given as a function of Stoke's law for drag on an individual particle. However, the porosity function used in the channel models, as a description of channel width, causes the expression to approach 0, instead of satisfying Stoke's law, as the porosity approaches 1.0. Therefore the constant k_o' rises in value to satisfy Stoke's law for free fall conditions. Note that the concept of the porous medium being equivalent to a group of circular channels gives a k_o' value of 2.0 and does not allow this value to rise as it should. Figure 51 shows how k_o' for a momentum

Figure 50. k_o' for a momentum cell with packing compared with k_o given by Emersleben (67)

Figure 51. k_o' for a momentum cell at the container wall

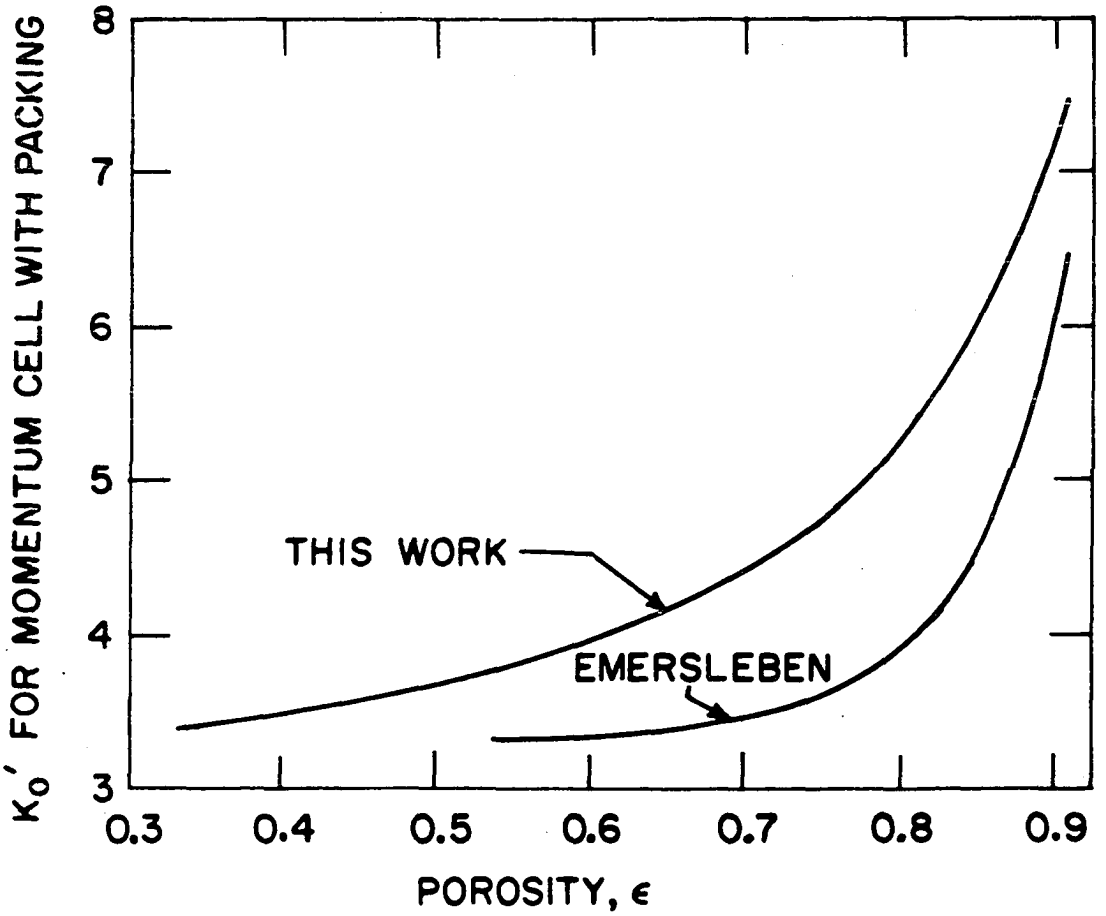
K_0' FOR MOMENTUM CELL WITH PACKING
8
7
6
5
4
3
THIS WORK
EMERSLEBEN
0.3
0.4
0.5
0.6
0.7
0.8
0.9
POROSITY, ϵ

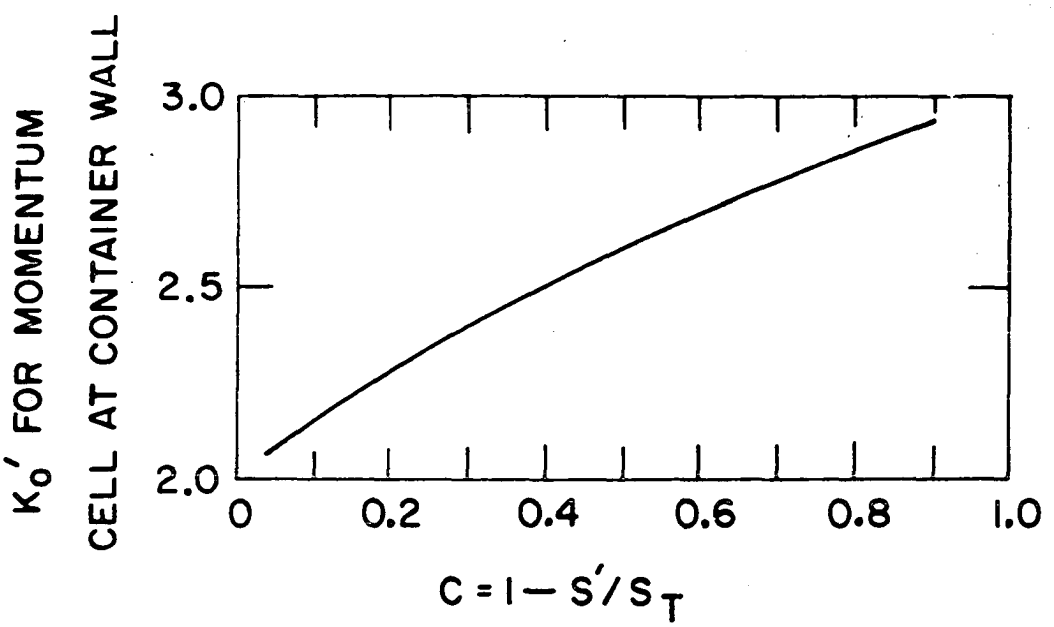
K_0' FOR MOMENTUM CELL AT CONTAINER WALL
3.0
2.5
2.0
0
0.2
0.4
0.6
0.8
1.0
$C = 1 - S'/S_T$

Figure 52. Laminar porosity constant f_{1L} versus bed porosity

- ○ spheres, $\epsilon = 0.412$
- ▲ crushed Galena, $\epsilon = 0.483$
- △ Raschig rings, $\epsilon = 0.707$
- ◇ Berl saddles, $\epsilon = 0.725$
- □ nickel saddles, $\epsilon = 0.931$

Figure 53. Comparison of f1L with k_o'

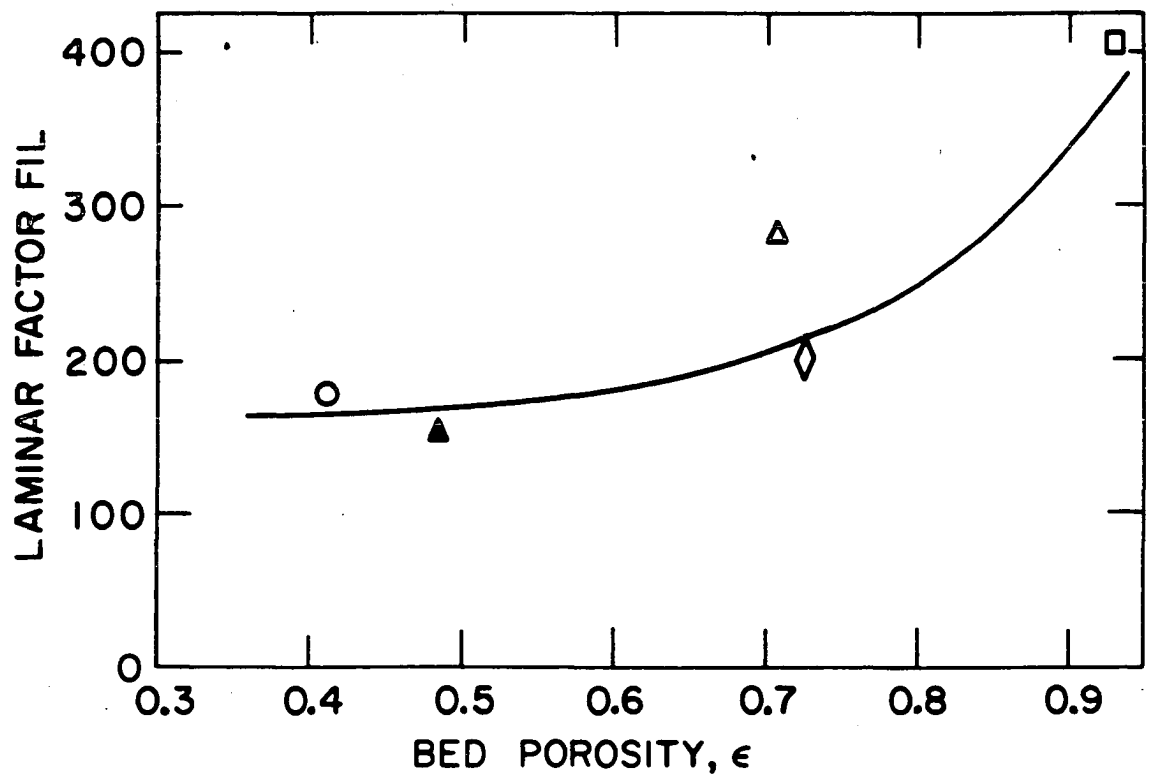
LAMINAR FACTOR FIL
400
300
200
100
0
0.3
0.4
0.5
0.6
0.7
0.8
0.9
BED POROSITY, ε

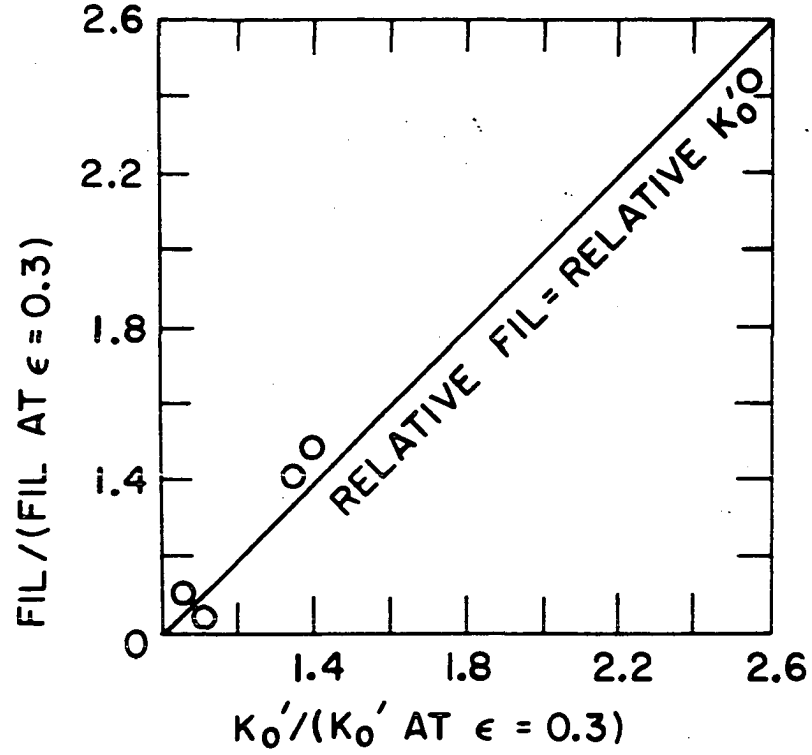
FIL/(FIL AT ε=0.3)
2.6
2.2
1.8
1.4
0
1.4
1.8
2.2
2.6
K₀′/(K₀′ AT ε = 0.3)
RELATIVE FIL = RELATIVE K₀′

cell at the wall varies with the fraction of the cross sectional area of the bed. It rises from a value of 2.0, which is the value for a circular tube with no packing, to a value of 3.0, which is the value for a rectangular conduit with infinite length. It is fortunate that the majority of packed and granular beds have porosities ranging from 0.3 to 0.6 so that the channel concept is more or less applicable. At porosities found in fluidized beds or in settling suspensions, the value of k_o' would be extremely important. Usually any simple model for the laminar constant must be modified by experimental data, as has been done by Fan (27), to take into account the particle shape and the fact that the simple models do not actually converge on Stoke's law at the highest porosities. The simplified method of calculating k_o' used in this model appears adequate for the complexity of the situation.

As has been previously pointed out in the section on theory, the models used in this work are essentially friction drag models that neglect any form drag that may be present. If one can assume that the predictions of Carman and Rose are in approximate agreement with experimental data, then the agreement of Model 2 with Carman and Rose indicates that friction drag is the major factor contributing to pressure drop in laminar flow. This appears reasonable for true laminar flow, where the amount of packing surface is the controlling factor, but may not be true for any other type of flow. More than likely, the contribution of form drag is roughly constant for laminar flow and the type of packings and orientations usually found in packed beds. This may also explain why a group of channels, which experience only friction drag, are a fair representation of porous media

for intermediate values of porosity.

The variances $\sigma^2(p_{ij})$ and $s^2(m_t)$ are also listed in Table 3 with the values for mean momentum loss. Again, the unrealistically high values predicted by Model 1 would seem to exclude it from consideration when comparing with other investigators. Also since m' and ϵ' are correlated, only the predictions of bed variance, $s^2(m_t)$, for correlated Model 2 will be considered. A standard method of presenting results such as these is to give the confidence limit as a percentage of the mean (i.e. the percent-mean variation). Since the sample variance, $s^2(m_t)$, is thought of as closely approximating the population variance $\sigma^2(m_t)$ in these calculations, the confidence limit is best thought of as a population tolerance limit. The method of calculating the percent mean variation (PMV) was described in the section on theory. For comparison purposes, the PMV can best be given as a function of bed length. Now

$$\text{Percent-mean variation} = \frac{196 \;\; s(m_t)}{\sqrt{q} \;\; \bar{x}(m_t)}$$

Since $q = L/D_p$, this may be rewritten as

$$\text{PMV} = \frac{196 \;\; s(m_t) \sqrt{D_p}}{\bar{x}(m_t) \;\; \sqrt{L}} \tag{96}$$

For any bed, D_p is a constant so that the PMV may be plotted versus L as a straight line on log-log paper. The results for the eight experimental beds are plotted in this manner and are shown in Figure 54. Suppose for example one had a group of beds the same as bed E2 (cylinders) and that each bed was six inches long. One could then expect the momentum loss for

Figure 54. Percent-mean variation versus length for the experimental beds studied

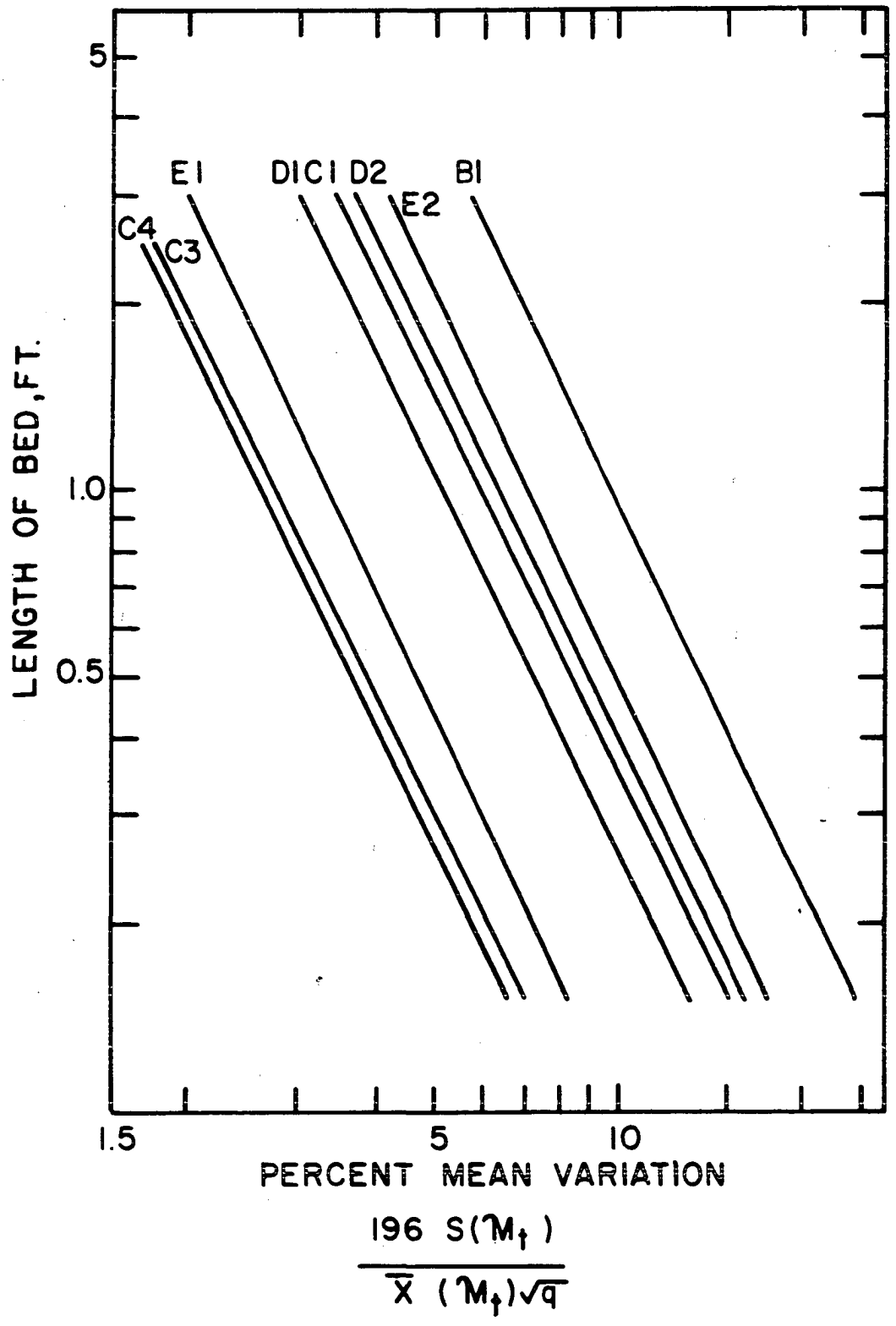
5
1.0
0.5
LENGTH OF BED, FT.
E1
D1
C1
D2
B1
E2
C4
C3
1.5
5
10
PERCENT MEAN VARIATION
196 S(M_t)
X̄ (M_t)√q

95 percent of these beds to be within ± 10 percent of the mean momentum loss for the entire group. The curves show that, for beds having the same packing and same length, the percent-mean variation increases with decreasing D_T/D_p ratio. Thus, beds B1 and E2, having the lowest D_T/D_p ratio, have the highest variation. Bed D2 for Raschig rings shows a higher variation than bed D1 since the packing for bed D2 was randomly dumped. Although the packing in bed C4 was randomly dumped, it shows less variation than bed C3 with hand-dropped packing. This may be because bed C4 had a somewhat higher D_T/D_p ratio than bed C3. Comparison of these results with those of other workers is extremely difficult if not impossible. Although many workers have mentioned this problem of variation, only one investigator, Rose (53), has made any pressure drop measurements on repeatedly packed beds at the same conditions. Smith and Roper (61), in their work on transition and turbulent flow, reported very large variations in pressure drop at the same porosity. However, their data are suspect since they found that an increase in porosity gave an increase in pressure drop. Rose made his measurements on a bed of spheres, but it is not at all clear just what bed conditions were used to obtain the percent-mean variation, which was about eight percent. If one can assume a D_T/D_p ratio of seven and a bed length of eight or nine inches, then for these conditions, Figure 54 gives approximately a five percent variation. This value of five percent is in fair agreement with Rose's value of eight percent. It should be remembered, however, that this value of five percent contains only the intrinsic variation due to statistical fluctuations and does not include any experimental error. Thus, the value of five percent should probably

be increased by a few percent to obtain a total variation. Although no absolute comparison with experimental data is possible, the results for the variation between beds seem entirely reasonable and can be used as a rough prediction of the true variation.

An interesting point is the comparison of the magnitude of the means and variances for the correlated case with the uncorrelated case. These results are listed in Tables 3 and 4. For Model 1, the table shows that correlated $\mu(p_{ij}) >$ uncorrelated $\mu(p_{ij})$ and correlated $\sigma^2(p_{ij}) >$ uncorrelated $\sigma^2(p_{ij})$. In this case, the relevant calculation form is

$$\Delta P \propto \frac{1}{\epsilon' m'^2}$$

In the correlated case, a low value of ϵ' will be used with a low value of m', and a high value of ϵ' will be used with a high value of m'. This gives rise to widely varying values of ΔP, and gives undue weight to the high values when the average momentum loss is calculated. In the uncorrelated case, the computer will tend to pick the most probable values of ϵ' and m', independent of each other, and will avoid choosing too many values from the ends of the distributions. This results in a lower mean, due to the absence of low ϵ' correlated with a low m', and a lower variance, due to the more limited values of ϵ' and m' chosen. Model 2 uses the following calculation form

$$\Delta P \propto \frac{(1-\epsilon_v)}{m'^2 \epsilon' (1-\epsilon')}$$

where ϵ_v is the volume porosity of the momentum cell and has the value ϵ_c or ϵ_w. In this case correlated $\bar{x}(m_t) \cong$ uncorrelated $\bar{x}(m_t)$ and

correlated $\hat{s}^2(\bar{m}_t)$ < uncorrelated $\hat{s}^2(\bar{m}_t)$. It is difficult to say exactly why the correlated variance should be less than the uncorrelated variance for this model. One possible explanation is that the term $(1-\epsilon')$, which is in effect a compensating factor for the term $m'^2\epsilon'$, has less stabilizing effect when ϵ' and m' are uncorrelated than when correlated. The variances between beds for Model 2 are in all cases lower than those for Model 1. This is due to the fact that the greatest variation in momentum cell properties occurs in the area adjacent to the wall. Separation of the momentum cells into a core and a wall region, as is done in Model 2, gives less weight to those cells having widely varying properties and results in a lower variance than was obtained for the homogenous model. The variances for the correlated case are the most important and are the ones considered.

For purposes of prediction, it is recommended that the equation of Rose, including a wall-effect correction, be used with the plot of percent-mean variation versus bed length given on page 123. Part of the data used by Rose to obtain his porosity function were for suspensions and other conditions of high porosity. For this reason, his porosity function may be somewhat more accurate than Carman's, especially at high porosities. In dealing with porous media having a widely varying pore size distribution, it is almost mandatory that some statistical method of calculation, involving this pore size distribution, be used.

CONCLUSIONS AND RECOMMENDATIONS

Conclusions

The following conclusions may be reached as a result of this investigation.

1. A packed bed may be satisfactorily represented by a simple stochastic model whose structure consists of layers of independent momentum sinks called momentum cells. The boundary of each cell is determined by the locus of maximum velocity within the packed bed. The locus of maximum velocity is unknown but can be approximated by assuming it to be equidistant from packing surfaces.

2. The expression that determines the momentum loss for a cell may be derived by a momentum balance over the cell and the use of the proper boundary conditions. This method yields an expression similar to the Hagen-Poiseuille equation for capillary flow except that the derived expression is more applicable to porous media and correctly predicts that the laminar constant, k'_o, will increase with increasing porosity.

3. The defined quantities appearing in the expression for the cell momentum loss may be obtained by direct measurements on experimental beds constructed for this purpose of wax and cork. A method is described that is believed to adequately sample the entire experimental bed and give a representative picture of the defined momentum cell properties.

4. The momentum cell hydraulic radius, m', is strongly correlated with the momentum cell porosity, ϵ', with the porosity dependence given by $(1-\epsilon')^2/\epsilon'^3$. This expression is approximately correct, for the over-all

effect of porosity, at intermediate values of porosity. The method used for calculating the momentum cell hydraulic radius allows different values of m to be obtained at the same porosity. The range of values obtained for m', at a given porosity, increases with increasing porosity because the individual pieces of packing have more freedom of orientation at the higher porosities.

5. The variances of the distributions of momentum cell properties, obtained by sampling the experimental beds, were found to decrease with an increasing D_T/D_p ratio. Hand dropping the packing into the container, instead of randomly dumping it, was also found to decrease the variance of the resulting distributions. In many cases, the decrease amounted to 50 percent of the original variance.

6. The radial porosity variation in the experimental beds was found to be periodic in nature, although the method of calculation used did not allow the complete details of such a variation to be uncovered. This periodic variation was explained by the orientation of the packing at the container wall.

7. The laminar constant, k_o', is not constant but increases with increasing porosity to satisfy Stoke's law for free fall conditions. The simplified method of calculating k_o' for the momentum cells correctly predicts that k_o' will increase with increasing porosity. The reasonable agreement between the calculated values of k_o' and values based on experimental indicate that although particle shape is a factor, porosity is the most important variable in determining k_o'.

8. The flow criterion of equal momentum loss for each cell in a

given layer of the model (minimization of energy loss) gives reasonable values of average momentum loss and appears to be the correct criterion for this model. The use of approximately equal mass flow velocities for each momentum cell in a given layer is a poor flow criterion and yields values of average momentum loss for the model that are too high.

9. A non-homogenous two-region model, with each region having its own volume porosity and distribution of momentum cell properties, is a satisfactory representation for beds having a low D_T/D_p ratio. This two-region model accounts for the wall effect, indicating that most of the radial variation in bed properties occurs within a distance of one or one and one-half pellet diameters from the wall.

10. The predictions of the two-region model, for the beds studied, compare favorably with the predictions of Carman (13) and Rose (53), and the predictions of Rose differ by an average of only 11 percent from the model predictions.

11. The results of the stochastic calculations for the experimental beds studied may be used as a rough prediction of the momentum loss between beds having the same superficial or gross properties. This variation decreases with increasing D_T/D_p ratio but may be as high as 15 or 20 percent of the mean for short beds with a low D_T/D_p ratio.

Recommendations

Part of the value of any exploratory project, such as this, is to indicate the directions that future research should take. Therefore the

following recommendations are made as a result of this investigation.

1. More experimental beds should be constructed for various D_T/D_p ratios, porosities, types of packing, and methods of packing. The information obtained from such beds would be useful in projects involving heat, mass, and momentum transfer. It would also provide a better understanding of the geometrical nature of porous media and packed beds.

2. Improved methods for sampling the experimental beds need to be devised that will provide a more realistic picture of the packed bed properties. This is a difficult problem and is made more difficult by the fact that the bed properties sampled are usually dictated by the particular model chosen by the investigator and may not necessarily be an accurate picture of the true nature of the bed.

3. The calculation methods and physical models used in this work should be refined and extended to cover such important areas as turbulent flow, compressible flow, displacement phenomena, and two-phase flow in porous media.

4. The present models and methods of calculation could be extended to cover prediction of the velocity profile in packed beds. This would require a more complete sampling of the experimental beds than was done in this work.

5. An investigation of the nature of tortuosity in packed beds is indicated as needed research. The values of tortuosity used in the models must be a realistic indication of the fluid path and yet must be simple enough to be calculated from the experimental beds. The nature of the wall effect is another area that deserves attention. This effect is

probably related to the radial variation of porosity within the packed bed.

6. An experimental investigation of the variation in momentum loss for repeatedly packed beds having the same superficial bed properties is badly needed. Such an investigation would include the effect of D_T/D_p ratio, bed length, type of flow, and experimental error. It would be invaluable to the designer who is interested in comparing two different correlations.

NOMENCLATURE

A_C	wall correction factor due to Carman (13)
A_R	wall correction factor due to Rose (53)
c	a dimensionless variable defined as $1 - S'/S_T$
C_o	a constant
D_T	diameter of the packed bed
D_p	packing diameter; for non-spherical packing, D_p is the diameter of an equivalent volume sphere
E	expected value
flL	laminar flow constant
g_c	gravitational constant
k	a dimensionless number defined as S'_m/S'_p; the number of independent channels in Model 1
k'_o	momentum cell constant that depends on the shape and porosity of the cell
K	factor containing the geometrical properties of a momentum cell, see Equation 84
ℓ	constant axial distance between layers of momentum cells, $\ell = D_p$
lb_f	pounds force
ℓ'_m	actual length of a momentum cell
ℓ'_p	length of packing within the momentum cell
L	length of bed
m	number of momentum cells in the wall region of Model 2; the average bed hydraulic radius, $m = \epsilon/S = \epsilon/S_o(1-\epsilon)$

m'	hydraulic radius of momentum cell, $m' = (S'_m - S'_p)/Z'_p$
M	momentum loss per unit volume for a momentum cell in Model 2
$\mathfrak{M}$	momentum loss per unit volume for a layer of momentum cells in Model 2
n	number of momentum cells in the core region of Model 2
p	momentum loss for a momentum cell in Model 1
P	pressure
ΔP	pressure drop across bed or momentum cell
PMV	percentage-mean variation, see Equation 96
q	number of layers of momentum cells in the models
Q	volume flow rate through the bed
r	radial distance
R	radius of bed
s	area within momentum cell having a boundary with a constant shear stress τ ; sample standard deviation
s^*	dimensionless s, $s^* = s/(S'_m - S'_p)$
s^2	sample variance
S	surface per unit volume of packed bed
S'	flow area of momentum cell, $S' = S'_m - S'_p$
S_c	cross sectional area of the core region of Model 2; surface per unit volume of empty column
S'_m	total cross sectional area of momentum cell
S_o	surface per unit volume of packing
S'_p	cross sectional area of packing in momentum cell
S_T	total cross sectional area of bed

S_w	cross sectional area of the wall region in Model 2
v	point velocity of fluid in momentum cell
$\langle v \rangle$	average fluid velocity in momentum cell
$\langle v \rangle_B$	average momentum cell fluid velocity for the bed
V	superficial velocity of fluid in momentum cell
V_o	superficial bed velocity, $V_o = Q/S_T$
$\bar{x}$	sample mean
z	perimeter of the area s; axial distance
z^*	dimensionless z, $z^* = z/Z_p'$
Z_p'	perimeter of packing in momentum cell
α	proportional to
ϵ	overall bed porosity
ϵ'	area porosity of momentum cell, $\epsilon' = (S_m' - S_p')/S_m'$
$\bar{\epsilon}'$	average bed porosity based on ϵ'
ϵ_r	porosity of annular section
$\bar{\epsilon}_r$	average bed porosity based on ϵ_r
ϵ_c	porosity of core region in Model 2
ϵ_w	porosity of wall region in Model 2
η	fluid viscosity
θ'	momentum cell angle of orientation
μ	population mean
ρ	fluid density
σ^2	population variance
τ	shear stress

BIBLIOGRAPHY

1. Adamson, J. E. Application of the Kozeny equation to consolidated porous media. Nature. 166: 314-315. 1950.

2. Andersson, K. E. B. Pressure drop in packed beds. Royal Institute of Technology (Stockholm) Transactions. No. 201. 1963.

3. Arthur, J. R., Linnett, J. W., Raynor, E. J., and Sington, E. P. C. The flow of an air stream through a layer of granules. Faraday Society Transactions. 46: 270-281. 1950.

4. Bakhmeteff, B. A. and Feodoroff, N. V. Flow through granular media. American Society of Mechanical Engineers Transactions. 59: 97-104. 1937.

5. Bartell, F. E. and Osterhof, H. J. The pore size of compressed carbon and silica membranes. Journal of Physical Chemistry. 32: 1553-1571. 1928.

6. Blake, F. C. The resistance of packing to fluid flow. American Institute of Chemical Engineers Transactions. 14: 415-421. 1922.

7. Brinkman, H. C. A calculation of the viscous force exerted by a flowing fluid on a dense swarm of particles. Applied Scientific Research. A1: 27-34. 1947.

8. _____. On the permeability of media consisting of closely packed porous particles. Applied Scientific Research. A1: 81-86. 1948.

9. Brownell, L. E., Dombrowski, H. S., and Dickey, C. A. Pressure drop through porous media. IV. New data and revised correlation. Chemical Engineering Progress. 46: 415-422. 1950.

10. Burke, S. P. and Plummer, W. B. Gas flow through packed columns. Industrial Engineering Chemistry. 20: 1196-1200. 1928.

11. Carman, P. C. The determination of the specific surface of powders. I. The Society of Chemical Industry Journal. 57: 225-234. 1938.

12. _____. The flow of gases through porous media. New York, Academic Press. 1956.

13. _____. Fluid flow through granular beds. Institution of Chemical Engineers (London) Transactions. 15: 150-166. 1937.

14. _____. Some physical aspects of water flow in porous media. Faraday Society Discussions. 3: 72-77. 1948.

15. Chalkey, J. W., Cornfield, J., and Park, H. A method for estimating surface to volume ratios. Science. 110: 295-297. 1949.

16. Chalmers, J., Taliaferro, D. B., and Rawlins, E. L. Flow of air and gas through porous media. American Institute of Mining, Metallurgical, and Petroleum Engineers Transactions. 98: 375-400. 1932.

17. Childs, E. C. and Collis-George, N. The permeability of porous materials. Royal Society Proceedings. Series A, 201: 392-405. 1950.

18. Chilton, T. H. and Colburn, A. P. Pressure drop in packed tubes. Industrial and Engineering Chemistry. 23: 913-919. 1931.

19. Collins, R. E. Flow of fluids through porous materials. New York, Reinhold Publishing Company. 1961.

20. Coppage, J. E. and London, A. L. Heat transfer and flow friction characteristics of porous media. Chemical Engineering Progress. 52: 57-63. 1956.

21. Coulson, M. A. The flow of fluids through granular beds: effect of particle shape and voids in streamline flow. Institution of Chemical Engineers (London) Transactions. 27: 237-257. 1949.

22. D'Arcy, H. P. G. Les fontaines publiques de la ville de Dijon. Paris, Victor Dalmont. 1856. (Original not available; cited in Carman, P. C. Fluid flow through granular beds. Institution of Chemical Engineers (London) Transactions. 15: 150. 1937.)

23. Dupuit, A. J. Etudes theoriques et pratiques sur le movement des eaux dans les canaux decouverts et a travers les terrains permeables. Paris, Victor Dalmont. 1863. (Original not available; cited in Carman, P. C. Fluid flow through granular beds. Institution of Chemical Engineers (London) Transactions. 15: 150. 1937.)

24. Ergun, S. Fluid flow through packed columns. Chemical Engineering Progress. 48: 89-94. 1952.

25. _____ and Orning, A. A. Fluid flow through randomly packed columns and fluidized beds. Industrial and Engineering Chemistry. 41: 1179-1184. 1949.

26. Fair, G. M. and Hatch, L. P. Fundamental factors governing the streamline flow of water through sands. American Water Works Association Journal. 25: 1551-1565. 1933.

27. Fan, L. T. Pressure drop of single phase flow in packed columns. Kansas State University Bulletin. 43, No. 4: 1-43. 1959.

28. Fancher, G. H. and Lewis, J. A. Flow of simple fluids through porous materials. Industrial and Engineering Chemistry. 25: 1139-1147. 1933.

29. Furnas, C. C. The flow of gases through beds of broken solids. U. S. Bureau of Mines Bulletin 307. 1929.

30. Gamson, B. W., Thodos, G., and Hougen, O. A. Heat, mass, and momentum transfer in the flow of gases through granular solids. American Institution of Chemical Engineers Transactions. 39: 1-35. 1943.

31. Givan, C. V. Flow of water through granular materials: initial experiments with lead shot. American Geophysical Union Transactions. 15: 572-579. 1934.

32. Harmson, G. J. The concept of hydraulic radius in porous media. American Institute of Mining, Metallurgical, and Petroleum Engineers Transactions. 204: 274-277. 1955.

33. Hatfield, M. R. Fluid flow through porous carbon. Industrial and Engineering Chemistry. 31: 1419-1424. 1939.

34. Hickox, G. H. Flow through granular materials. American Geophysical Union Transactions. 15: 567-572. 1934.

35. Hubbert, M. K. D'Arcy's law and the field equations of the flow of underground fluids. American Institute of Mining, Metallurgical, and Petroleum Engineers Transactions. 207: 222-239. 1956.

36. Iberall, A. S. Permeability of glass wool and other highly porous media. United States National Bureau of Standards Journal of Research. 45: 398-406. 1950.

37. Kozeny, J. Kapillare Leitung des Wassers in Boden. Akademie der Wissenschaften in Wien Sitzungsberichte. 136a: 271-306. 1927.

38. Leva, M. Pressure drop through packed tubes. I. General correlation. Chemical Engineering Progress. 43: 549-554. 1947.

39. _____ and Grummer, M. Pressure drop through packed tubes. II. Effect of surface roughness. Chemical Engineering Progress. 43: 633-638. 1947.

40. _____ and _____. Pressure drop through packed tubes. III. Prediction of voids in packed tubes. Chemical Engineering Progress. 43: 713-718. 1947.

41. Lorenz, P. M. Tortuosity in porous media. Nature. 189: 386-387. 1961.

42. Macmullin, R. B. and Muccini, G. A. Characteristics of porous beds and structures. A.I.Ch.E.J. (American Institute of Chemical Engineers Journal). 2: 393-403. 1956.

43. Marshall, T. J. Permeability and the size distribution of pores. Nature. 180: 664-665. 1957.

44. Martin, J. J., McCabe, W. L., and Monrad, C. C. Pressure drop through stacked spheres: effect of orientation. Chemical Engineering Progress. 47: 91-94. 1951.

45. Millington, R. J. and Quirk, J. P. Permeability of porous solids. Faraday Society Transactions. 57: 1-8. 1961.

46. Morcom, A. R. Fluid flow through granular materials. Institution of Chemical Engineers (London) Transactions. 24: 30-43. 1946.

47. Muskat, M. The flow of homogenous fluids through porous media. Ann Arbor, Edwards Publishing Company. 1946.

48. _____ and Botset, H. G. Flow of gas through porous materials. Physics. 1: 27-47. 1931.

49. Oman, A. O. and Watson, K. M. Pressure drops in granular beds. National Petroleum News. 36: R795-R802. 1944.

50. Prager, S. Viscous flow through porous media. The Physics of Fluids. 4: 1477-1482. 1961.

51. Ranz, W. E. Friction and transfer coefficients for single particles and packed beds. Chemical Engineering Progress. 48: 247-253. 1952.

52. Roblee, L. H. S., Baird, R. M., and Tierney, J. W. Radial porosity variations in packed beds. A.I.Ch.E.J. (American Institute of Chemical Engineers Journal). 4: 460-464. 1958.

53. Rose, H. E. Fluid flow through beds of granular materials. In Conference by the Institute of Physics, Leamington Spa, Oct. 25-28, 1950. pp. 136-163. London, Edward Arnold and Company. 1951.

54. _____. An investigation into the laws of flow of fluids through beds of granular materials. Institution of Mechanical Engineers (London) Proceedings. 153: 141-168. 1945.

55. Scheidegger, A. E. General statistical hydrodynamics in porous media. Geofis. e Pura E Applicata. 30: 17-26. 1955.

56. _____. The physics of flow through porous media. Revised edition. Toronto, University of Toronto Press. 1960.

57. _____. Statistical approach to miscible displacement in porous media. Canadian Mining and Metallurgical Bulletin. 52: 26-30. 1959.

58. Schriever, W. Law of flow for the passage of a gas-free liquid through a spherical-grain sand. American Institute of Mining, Metallurgical, and Petroleum Engineers Transactions. 86: 329-336. 1930.

59. Schriver, C. B. The effect of porosity on pressure drop in packed tubes. Unpublished M.S. thesis. Ames, Iowa, Library, Iowa State University of Science and Technology. 1960.

60. Slichter, C. S. Theoretical investigation of the motion of ground waters. 19th Annual Report of the U. S. Geological Survey. Part 2: 295-384. 1897.

61. Smith, K. L. and Roper, G. H. Flow through porous media. Australian Journal for Chemical Engineers. 1: 5-15. 1960.

62. Stanton, T. E. and Pannel, J. R. Study of the relationships for dimensionless groups for flow through smooth circular pipes. Teddington, England. National Physical Laboratory. Collected Researches. Vol. 11. 1914. (Original not available; cited in Carman, P. C. Fluid flow through granular beds. Institution of Chemical Engineers (London) Transactions. 15: 150. 1937.

63. Stepochkin, B. F. A two-term equation for the resistance of porous media. International Chemical Engineering. 3: 64-67. 1963.

64. Sullivan, R. R. and Hertel, K. L. Specific surface of fibers and powders. Advances in Colloid Science. 1: 37-80. 1942.

65. Terzaghi, C. Determination of permeability of clay. Engineering News Record. 95: 832-836. 1925.

66. Verschoor, H. Experimental data on the viscous force exerted by a flowing fluid on a dense swarm of particles. Applied Scientific Research. A2: 155-161. 1950.

67. Von Emersleben, O. Das D'Arcysche Filtergesetz. Physikalische Zeitschrift. 26: 601-610. 1925.

68. Wagstaff, J. B. and Nirmaier, E. A. Air flow in beds of granular solids. Industrial Engineering Chemistry. 47: 1129-1135. 1955.

69. Wentz, C. A. and Thodos, G. Pressure drops in flow of gases through packed and distended beds of spherical particles. American Institute of Chemical Engineers Journal. 9: 81-84. 1963.

70. Wiggins, E. J., Campbell, W. B., and Maass, O. Determination of the specific surface of fiberous materials. Canadian Journal of Research. Section B, 17: 318-324. 1939.

71. Syllie, M. R. J. and Gardner, G. H. F. Permeability and the size distribution of pores. Nature. 181: 477. 1958.

72. Wyllie, M. R. J. and Gregory, A. R. Fluid flow through unconsolidated porous aggregates. Industrial and Engineering Chemistry. 47: 1379-1388. 1955.

ACKNOWLEDGEMENTS

The author wishes to express his appreciation to the following for their services.

To Dr. Raymond Fahien for his suggestion of the problem and his many hours of guidance and helpful criticism during the investigation.

To Dr. Herbert David for his patience and time in discussing various aspects of the problem.

To his colleagues among the graduate students who often provided needed ideas and assistance.

Special thanks is due John Foster for his many hours of careful work spent in making the necessary measurements.

APPENDIX

Sample Calculation of Porosities for the Core and Wall Regions

Bed C3

All distances are given in dimensionless form with the tube radius, R, as the base. All areas are given in dimensionless form, unless otherwise noted, with the cross sectional area of the tube as the base. The area of each annular section is 0.2.

Porosities of annular sections	Cumulative radii of annular sections
$\epsilon_1 = 0.388$	$r_1 = 0.447$
$\epsilon_2 = 0.420$	$r_2 = 0.632$
$\epsilon_3 = 0.377$	$r_3 = 0.775$
$\epsilon_4 = 0.368$	$r_4 = 0.895$
$\epsilon_5 = 0.532$	$r_5 = 1.000$
$\overline{\epsilon}_r = 0.417$	

Bed porosity based on momentum cells, $\overline{\epsilon'} = 0.408$

$D_p = 0.215$ and $S_T = 9.665$ inches^2 therefore $S_c = 5.956$ inches^2 and $S_w = 3.709$ inches^2.

Using the radial distances given above, we have

fraction of annular section in core region $= (1.000 - 0.215)^2 - (0.775)^2$

$= 0.0162$

fraction of annular section in wall region $= 0.2 - 0.0162 = 0.1838$

Then

$$\epsilon_c = \left[\frac{(0.2)(0.388) + (0.2)(0.420) + (0.2)(0.377) + (0.0162)(0.368)}{0.2 + 0.2 + 0.2 + 0.0162}\right]\left(\frac{0.408}{0.417}\right)$$

$$\epsilon_c = 0.385$$

$$\epsilon_w = \left[\frac{(0.1838)(0.368) + (0.2)(0.532)}{0.1838 + 0.2}\right]\left(\frac{0.408}{0.417}\right) = 0.445$$

Characteristics of Packing Used

Table 6. Characteristics of packing used

	spheres	spheres	Raschig rings	cylinders
Designation	B	C	D	E
Nominal dimensions, in.	1/2	3/8	1/2 x 1/4 x 1/2	3/8 x 3/8
Actual dimensions, in.	0.509	0.375	0.497 x 0.250 x 0.506	0.370 x 0.425
Specific surface S_o, $in.^{-1}$	11.79	16.01	20.17	15.51
Diameter of equivalent volume sphere, in. [a]	0.509	0.375	0.572	0.444

[a] D_p for Raschig rings calculated on the basis of the outside dimensions of the ring.

Physical Characteristics of Beds Sampled for Hydraulic Radius

Table 7. Physical characteristics of beds sampled for momentum cell properties

	B1	C1	C3	C4	D1	D2	E1	E2
Type of packing	spheres	spheres	spheres	spheres	Raschig rings	Raschig rings	cylinders	cylinders
Bed height, in.	5.36	6.36	7.69	9.50	8.05	8.52	8.02	5.38
Bed diameter, in.	2.01	2.01	3.51	3.99	3.15	3.14	3.15	2.01
Average measured bed porosity	0.479	0.452	0.425	0.486	0.575	0.626	0.429	0.467
Method of packing	hand dropped	hand dropped	hand dropped	randomly dumped	hand dropped	randomly dumped	hand dropped	hand dropped
D_T/D_p [a]	3.94	5.35	9.36	10.6	5.51	5.50	7.10	4.53
Number of pieces of packing	127	335	1549	2212	364	338	778	198
Number of sections cut	16	16	12	16	12	13	12	16
Number of sections used	9	8	6	5	8	7	6	8
Sample size	115	112	120	150	112	126	126	120

[a] D_p for Raschig rings calculated on the basis of the outside dimensions of the ring.

Computer Program Listing

```
      MOMENTUM LOSS IN POROUS MEDIA, MODEL 2,HETEROGENOUS
      DIMENSION AMOM(3000),FUNCTC(3000),FUNCTW(3000),CONST(300),
     1PORS(300),HYDR(300),THETA(300),AREAM(300),R(300),CONSTA(300),
     1PORSA(300),HYDRA(300),AREAMA(300),RA(300),CONSTB(300),PORSB(300),
     1HYDRB(300),AREAMB(300),RB(300)
      COMMON AMOM,FUNCTC,FUNCTW,CONST,PORS,HYDR,THETA,AREAM,R,CONSTA,
     1PORSA,HYDRA,AREAMA,RA,CONSTB,PORSB,HYDRB,AREAMB,RB
    1 FORMAT(42H1   SCHRIVER,MOMENTUM LOSS IN POROUS MEDIA)
    3 FORMAT(55H                                                        )
    4 FORMAT(55H                                                        )
    5 FORMAT(14,I12,I4,I4,I2,I2,I2)
    7 FORMAT(E10.4,E10.4,E10.4,E10.4,E10.4,E10.4)
    9 FORMAT(I4,I4,I4,I4,I4,I4)
   11 FORMAT(12HJ       I = I4)
   13 FORMAT(12HJ       K = I4)
   15 FORMAT(12HJ      KA = I4)
   17 FORMAT(12HJ      KB = I4)
   19 FORMAT(12HJ   SMEAN = E12.4)
   21 FORMAT(12HJ    SVAR = E12.4)
   23 FORMAT(5HJAMOMI4,3H = E12.4)
   25 FORMAT(7E10.4)
   31 READ INPUT TAPE 5,3
      READ INPUT TAPE 5,4
      READ INPUT TAPE 5,5,N,M,IMAX,KMAX,JTYPE,JRPT,JDUMP
      READ INPUT TAPE 5,7,C,REF,AREAC,AREAW,PORSC,PORSW
      READ INPUT TAPE 5,9,L1,L2,L3,L4,L5,L6
      READ INPUT TAPE 5,25,(CONST(II),II = 1,L1)
      READ INPUT TAPE 5,25,(PORS(II),II = 1,L2)
      READ INPUT TAPE 5,25,(HYDR(II),II = 1,L3)
      READ INPUT TAPE 5,25,(THETA(II),II = 1,L4)
      READ INPUT TAPE 5,25,(AREAM(II),II = 1,L5)
      READ INPUT TAPE 5,25,(R(II),II = 1,L6)
      AL4 = L4
      KA = 0
      KB = 0
      DO 41 II = 1,L1
      IF(R(II)- REF)43,45,45
   43 KA = KA + 1
      RA(KA) = R(II)
      CONSTA(KA) = CONST(II)
      PORSA(KA) = PORS(II)
      HYDRA(KA) = HYDR(II)
      AREAMA(KA) = AREAM(II)
      GO TO 41
   45 KB = KB + 1
```

```
      RB(KB) = R(II)
      CONSTB(KB)=CONST(II)
      PORSB(KB) = PORS(II)
      HYDRB(KB) = HYDR(II)
      AREAMB(KB) = AREAM(II)
   41 CONTINUE
      WRITE OUTPUT TAPE 10,1
      WRITE OUTPUT TAPE 10,3
      WRITE OUTPUT TAPE 10,4
      WRITE OUTPUT TAPE 10,15,KA
      WRITE OUTPUT TAPE 10,17,KB
      AKA = KA
      AKB = KB
      GO TO(51,91),JTYPE
   51 DO 81 J = 1,N

      SUM1 = 0
      SUM2 = 0
   53 DO 61 I =1,IMAX
      CALL RANDOM(M,X)
      I1 = (AKA*X)
      CALL RANDOM(M,X)
      I2 = (AKA*X)
      CALL RANDOM(M,X)
      I3 = (AKA*X)
      CALL RANDOM(M,X)
      I4 = (AL4*X)
      THET = THETA(I4+1)
      CALL RANDOM(M,X)
      I5 = (AKA*X)
      SUM1 = SUM1 + AREAMA(I5+1)
      IF(SUM1 - AREAC)55,55,57
   55 FUNCTC(I)=(HYDRA(I3+1)*HYDRA(I3+1)*PORSA(I2+1)*(1.0-PORSA(I2=1))*
     1COSF(THET)**2)/(C*CONSTA(I1+1)*(1.0-PORSC))
   61 SUM2 = SUM2 + FUNCTC(I)
   57 I = I - 1
      WRITE OUTPUT TAPE 10,11,I
      SUM3 = 0
      SUM4 = 0
      DO 71 K=1,KMAX
      CALL RANDOM(M,X)
      K1 = (AKB*X)
      CALL RANDOM(M,X)
      K2 = (AKB*X)
      CALL RANDOM(M,X)
      K3 = (AKB*X)
      CALL RANDOM(M,X)
      K4 = (AL4*X)
```

```
      THET = THETA(K4+1)
      CALL RANDOM(M,X)
      K5 = (AKB*X)
      SUM3 = SUM3 + AREAMB(K5+1)
      IF(SUM3 - AREAW)59,59,73
   59 IF(PORSB(K2+1) - 1.0)63,65,65
   63 FUNCTW(K)=(HYDRB(K3+1)*HYDRB(K3+1)*PORSB(K2+1)*(1.0-PORSB(K2+1))*
     1COSF(THET)**2)/(C*CONSTB(K1+1)*(1.0-PORSW))
      GO TO 71
   65 FUNCTW(K)=(HYDRB(K3+1)*HYDRB(K3+1)*PORSB(K2=1))/(C*CONSTB(k1+1))
   71 SUM4 = SUM4 + FUNCTW(K)
   73 K = K - 1
      WRITE OUTPUT TAPE 10,13,K
      AI=I
      BK=K
      SUM5 = SUM2 + SUM4
      AMOM(J) =(AI + BK)/(SUMS)
   81 WRITE OUTPUT TAPE 10,23,J,AMOM(J)
      GO TO 161
   91 DO 151 J=1,N
      SUM6 = 0
      SUM7 = 0
      DO 97 I=1,IMAX
      CALL RANDOM(M,X)
      I1 = (AKA*X)
      CALL RANDOM(M,X)
      I4 = (AL4*X)
      THET = THETA(I4+1)

      CALL RANDOM(M,X)
      I5 = (AKA*X)
      SUM6 = SUM6 +AREAMA(I5+1)
      IF(SUM6 - AREAC)93,93,99
   93 FUNCTC(I)=(HYDRA(I1+1)*HYDRA(I1+1)*PORSA(I1+1)*(1.0-PORSA(I1+1))*
     1COSF(THET)**2)/(C*CONSTA(I1+1)*(1.0-PORSC))
   97 SUM7 = SUM7 + FUNCTC(I)
   99 I = I - 1
      WRITE OUTPUT TAPE 10,11,I
      SUM8 = 0
      SUM10 = 0
      DO 121 K=1,KMAX
      CALL RANDOM(M,X)
      K2 = (AKB*X)
      IF(PORSB(K2+1) - 1.0)101,107,107
  101 CALL RANDOM(M,X)
      K5 = (AKB*X)
      IF(PORSB(K5+1) - 1.0)103,101,101
  103 CALL RANDOM(M,X)
```

```
      K4 = (AL4*X)
      THET = THETA(K4+1)
      SUM8 = SUM8 + AREAMB(K5+1)
      GO TO 111
  107 CALL RANDOM(M,X)
      K4 = (AL4*X)
      THET = THETA(K4+1)
      SUM8 = SUM8 + AREAMB(K2+1)
  111 IF(SUM8 - AREAW)113,113,131
  113 IF(PORSB(K2+1) - 1.0)115,119,119
  115 FUNCTW(K)=(HYDRB(K2+1)*HYDRB(K2+1)*PORSB(K2+1)*(1.0-PORSB(K2+1))*
     1COSF(THET**2)/(C*CONSTB(K2+1)*(1.0-PORSW))
      GO TO 121
  119 FUNCTW(K)=(HYDRB(K2+1)*HYDRB(K2+1)=PORSB(K2+1))/(C*CONSTB(K2+1))
  121 SUM10 = SUM10 + FUNCTW(K)
  131 K = K - 1
      WRITE OUTPUT TAPE 10,13,K
      AI=I
      BK=K
      SUM11 = SUM7 + SUM10
      AMOM(J) = (AI + BK)/(SUM11)
  151 WRITE OUTPUT TAPE 10,23,J,AMOM(J)
  161 Y=0
      Z=0
      DO 163 J = 1,N
      Y = Y + (AMOM(J)**2)
  163 Z = Z + AMOM(J)
      AN = N
      P = (Z**2)/AN
      SMEAN = Z/AN
      SVAR = (Y-P)/(AN - 1.0)
      WRITE OUTPUT TAPE 10,19,SMEAN
      WRITE OUTPUT TAPE 10,21,SVAR
      GO TO(31,165),JRPT
  165 GO TO(167,169),JDUMP
  167 STOP 89
  169 STOP
      END
```

Data Tables

Table 8. Measured data for momentum cells

Section Cell Number	S_p' in.^{2}	S_m' in.^{2}	Z_p' in.	r/R	Section Cell Number	S_p' in.^{2}	S_m' in.^{2}	Z_p' in.	r/R
I. Bed B1, spheres									
B1-1	**Magnification: 3.370**								
1	2.24	4.15	5.28	0.747	7	2.22	4.42	5.38	0.296
2	1.05	2.45	3.75	0.764	8	1.64	2.69	4.75	0.290
3	0.43	1.06	2.34	0.342	9	1.79	2.91	4.75	0.695
4	0.95	1.83	3.50	0.237	10	1.61	3.33	4.53	0.758
5	0.24	0.89	1.78	0.579	11	2.11	3.55	5.22	0.753
6	1.65	3.02	4.66	0.764	12	-	6.71	21.5	1.000
B1-2	**Magnification: 3.376**								
1	1.16	2.38	3.78	0.739	8	1.84	3.53	4.91	0.326
2	2.06	3.10	5.19	0.756	9	0.18	1.17	1.47	0.750
3	1.18	1.83	3.94	0.779	10	1.46	2.37	4.41	0.750
4	2.17	3.74	5.31	0.744	11	1.46	2.22	4.41	0.768
5	2.00	4.01	5.06	0.244	12	2.17	3.73	5.28	0.762
6	1.19	2.57	3.94	0.686	13	-	4.04	21.5	1.000
B1-3	**Magnification: 3.386**								
1	1.36	2.77	4.19	0.759	7	2.22	3.32	5.34	0.782
2	2.51	4.62	5.66	0.759	8	1.89	2.84	4.94	0.330
3	2.26	3.97	5.38	0.742	9	2.05	2.71	5.13	0.788
4	0.45	1.49	2.44	0.377	10	1.79	3.25	4.78	0.771
5	1.95	3.73	4.97	0.249	11	-	4.30	21.6	1.000
6	2.36	4.21	5.53	0.730					
B1-4	**Magnification: 3.400**								
1	0.51	1.36	2.56	0.756	8	2.18	3.48	5.34	0.352
2	2.19	3.24	5.28	0.762	9	1.79	2.54	4.91	0.335
3	2.28	3.51	5.38	0.750	10	2.23	3.39	5.41	0.744
4	1.92	3.27	4.90	0.744	11	1.23	2.03	3.97	0.756
5	1.74	2.50	4.72	0.300	12	1.02	1.96	3.66	0.762
6	1.24	2.07	4.00	0.260	13	1.27	2.11	4.22	0.762
7	0.24	0.93	1.78	0.750	14	-	4.65	20.7	1.000
B1-5	**Magnification: 3.376**								
1	2.26	3.08	5.41	0.750	8	2.24	3.53	5.38	0.762
2	0.78	1.75	3.25	0.773	9	2.04	3.34	5.22	0.779
3	1.08	1.81	3.72	0.750	10	1.41	2.77	4.28	0.297
4	2.26	3.66	5.38	0.779	11	2.29	3.07	5.41	0.750
5	1.67	3.20	4.66	0.326	12	1.84	2.88	4.88	0.739
6	0.84	1.46	3.38	0.733	13	-	3.57	20.7	1.000
7	1.40	2.31	4.25	0.297					

Table 8 (Continued)

Section Cell Number	S_p' in.^{2}	S_m' in.^{2}	Z_p' in.	r/R	Section Cell Number	S_p' in.^{2}	S_m' in.^{2}	Z_p' in.	r/R
Bl-6	Magnification: 3.350								
1	0.41	1.29	2.34	0.785	8	1.44	2.85	4.31	0.768
2	2.22	3.25	5.34	0.762	9	2.21	3.86	5.38	0.434
3	2.14	2.89	5.22	0.762	10	0.25	0.95	1.88	0.281
4	0.26	1.34	1.94	0.750	11	1.29	2.55	4.09	0.727
5	2.12	3.56	5.28	0.281	12	0.66	1.57	3.00	0.750
6	1.66	2.62	4.66	0.299	13	1.23	2.36	4.03	0.779
7	1.68	2.44	4.69	0.750	14	-	5.30	21.6	1.000
Bl-7	Magnification: 3.318								
1	2.28	3.00	5.31	0.733	7	2.31	3.59	5.41	0.290
2	1.76	2.79	4.69	0.734	8	2.07	2.92	5.13	0.728
3	0.93	1.98	3.41	0.266	9	1.94	2.77	4.94	0.769
4	2.22	4.13	5.34	0.414	10	2.26	2.96	5.34	0.745
5	1.86	3.17	4.91	0.728	11	0.47	1.04	2.47	0.757
6	1.91	2.75	4.88	0.751	12	-	4.12	21.1	1.000
Bl-8	Magnification: 3.304								
1	1.76	2.93	4.72	0.743	7	2.31	5.05	5.47	0.440
2	1.82	2.85	4.81	0.760	8	0.92	1.87	3.41	0.748
3	1.43	2.64	4.25	0.315	9	1.29	2.44	4.06	0.725
4	0.61	1.57	2.78	0.754	10	1.87	3.42	5.85	0.748
5	1.75	3.35	4.72	0.743	11	-	5.24	21.0	1.000
6	2.07	3.66	5.16	0.321					
Bl-9	Magnification: 3.304								
1	1.03	1.60	3.56	0.766	9	1.25	2.18	4.00	0.760
2	1.58	2.20	4.44	0.754	10	0.28	0.42	1.78	0.321
3	2.18	3.13	5.25	0.743	11	2.18	3.13	5.22	0.297
4	1.56	2.35	4.38	0.772	12	2.08	3.03	5.16	0.731
5	1.85	3.14	4.84	0.356	13	2.15	3.08	5.22	0.760
6	0.19	0.59	1.56	0.297	14	2.23	3.30	5.38	0.225
7	0.74	1.13	3.19	0.428	15	-	3.54	21.0	1.000
8	0.70	1.34	2.97	0.731					

Table 8 (Continued)

Section Cell Number	S_p' in.^{2}	S_m' in.^{2}	Z_p' in.	r/R	Section Cell Number	S_p' in.^{2}	S_m' in.^{2}	Z_p' in.	r/R
II. Bed C1, spheres									
C1-1	Magnification: 3.367								
2	1.02	1.64	3.63	0.839	13	1.21	2.54	3.91	0.344
4	0.85	1.43	3.22	0.536	15	0.40	0.81	2.25	0.478
5	1.26	1.90	3.94	0.536	17	0.43	1.19	2.25	0.839
6	1.32	1.88	4.06	0.828	18	0.94	1.59	3.47	0.472
9	1.17	1.90	3.81	0.186	19	0.85	1.72	3.28	0.822
11	0.88	1.27	3.38	0.828	21	1.25	2.22	4.00	0.828
12	1.18	1.81	3.81	0.833	22	-	2.81	21.4	1.000
C1-3	Magnification: 3.435								
1	0.41	0.99	2.25	0.834	14	0.25	0.91	1.72	0.480
3	0.52	0.86	2.56	0.663	16	1.05	1.79	4.81	0.463
4	1.02	2.03	3.63	0.606	17	0.82	1.45	3.25	0.486
5	0.51	1.02	2.69	0.828	18	0.68	1.63	2.94	0.811
7	1.01	1.61	3.53	0.480	20	1.07	1.66	3.59	0.817
11	1.19	1.84	3.94	0.828	22	1.16	1.51	3.78	0.811
12	0.97	1.60	3.47	0.326	23	-	3.06	21.3	1.000
C1-5	Magnification: 3.420								
1	1.31	1.88	4.13	0.826	12	1.27	2.41	4.03	0.614
3	1.17	2.19	3.88	0.821	15	1.08	1.94	4.03	0.471
4	0.96	1.72	3.53	0.585	18	1.08	1.64	3.72	0.570
5	0.78	1.41	3.22	0.425	19	0.52	0.91	2.63	0.471
6	0.32	0.82	2.09	0.430	20	0.94	1.72	3.50	0.809
7	0.74	1.43	3.13	0.836	21	1.23	1.56	4.03	0.821
11	1.17	1.82	3.88	0.453	22	-	3.46	21.9	1.000
C1-6	Magnification: 3.399								
1	1.04	1.59	3.78	0.802	21	0.48	0.92	2.41	0.496
3	1.03	1.62	3.63	0.802	22	0.77	1.07	3.09	0.514
4	1.27	1.62	3.97	0.802	23	1.08	1.61	3.66	1.820
14	1.21	1.76	3.81	0.214	24	0.37	0.84	2.06	0.843
15	1.34	2.01	4.13	0.595	25	1.01	1.50	3.53	0.843
17	0.90	1.53	3.38	0.208	26	0.13	0.47	1.28	0.820
18	1.24	1.69	3.88	0.849	27	1.18	1.62	3.81	0.826

Table 8 (Continued)

Section Cell Number	S_p' in.^{2}	S_m' in.^{2}	Z_p' in.	r/R	Section Cell Number	S_p' in.^{2}	S_m' in.^{2}	Z_p' in.	r/R
C1-8	Magnification: 3.421								
1	1.07	1.57	3.94	0.832	12	1.03	1.85	3.63	0.172
3	1.10	1.68	3.75	0.837	15	0.46	1.05	2.44	0.837
4	0.19	0.62	1.59	0.522	16	1.03	1.82	3.66	0.502
5	1.02	1.74	3.63	0.493	20	1.29	2.38	4.66	0.579
6	0.55	1.21	2.69	0.826	21	1.14	1.87	3.84	0.803
7	0.59	1.17	2.81	0.843	22	1.30	2.02	4.09	0.826
11	0.46	0.72	2.44	0.809	24	-	3.89	21.8	1.000
C1-9	Magnification: 3.406								
2	1.23	1.84	3.97	0.812	17	0.70	0.97	3.06	0.547
4	1.04	1.81	3.69	0.582	18	1.32	1.90	4.13	0.455
5	0.26	0.69	1.94	0.495	19	1.10	1.79	3.78	0.807
7	0.88	1.56	3.38	0.830	20	0.50	0.93	2.56	0.835
11	1.03	1.71	3.69	0.841	21	1.28	1.72	4.06	0.830
12	1.26	2.01	4.03	0.300	22	1.26	1.61	4.00	0.818
15	0.19	0.72	1.59	0.824	23	-	3.54	21.8	1.000
C1-12	Magnification: 3.451								
1	1.17	1.74	3.84	0.807	12	0.25	0.68	1.88	0.803
2	1.23	1.76	3.97	0.807	15	1.19	1.86	3.94	0.182
3	0.55	0.83	2.66	0.796	19	0.74	1.30	3.09	0.847
4	0.17	0.62	1.53	0.813	20	0.46	0.89	2.41	0.523
7	1.19	1.63	3.88	0.802	22	1.21	1.72	3.97	0.842
8	0.99	1.56	3.63	0.830	25	0.72	1.23	3.09	0.830
10	1.17	1.76	3.88	0.250	27	-	3.07	21.9	1.000
C1-14	Magnification: 3.406								
1	1.17	1.65	3.84	0.830	10	0.35	0.71	2.22	0.714
3	1.30	2.05	4.13	0.818	11	1.23	2.03	3.97	0.311
4	0.25	0.71	1.81	0.490	12	0.70	1.19	3.03	0.127
6	1.17	1.79	3.88	0.847	13	1.12	1.61	3.78	0.812
7	0.62	1.10	2.81	0.530	15	1.24	2.52	4.00	0.582
8	0.72	1.37	3.03	0.173	16	0.97	1.84	3.56	0.444
9	1.30	2.13	4.09	0.369	18	1.25	2.62	4.03	0.588

Table 8 (Continued)

Section Cell Number	S_p' in.^{2}	S_m' in.^{2}	Z_p' in.	r/R	Section Cell Number	S_p' in.^{2}	S_m' in.^{2}	Z_p' in.	r/R
III. Bed C3, spheres									
C3-1 Magnification: 2.168									
8	0.30	0.56	1.97	0.750	37	0.53	0.81	2.44	0.838
12	0.48	0.88	2.47	0.574	39	0.30	0.53	2.03	0.880
13	0.46	0.81	2.38	0.543	44	0.49	0.67	2.47	0.870
15	0.38	0.74	2.22	0.595	55	0.52	0.88	2.56	0.331
18	0.44	0.78	2.38	0.709	57	0.47	0.63	2.44	0.523
20	0.49	0.67	2.53	0.890	63	0.50	0.72	2.44	0.512
22	0.14	0.32	1.34	0.497	65	0.48	0.66	2.47	0.735
26	0.33	0.63	2.06	0.492	69	0.51	0.65	2.53	0.719
34	0.48	0.79	2.47	0.725	71	0.51	0.66	2.47	0.900
36	0.52	0.78	2.50	0.595	73	0.42	0.65	2.31	0.900
C3-3 Magnification: 2.142									
6	0.48	0.71	2.47	0.886	30	0.48	0.78	2.41	0.545
7	0.46	0.67	2.41	0.697	32	0.42	0.76	2.28	0.891
14	0.47	0.85	2.47	0.503	37	0.35	0.47	2.16	0.152
15	0.29	0.61	1.88	0.671	40	0.46	0.71	2.41	0.377
17	0.50	0.79	2.44	0.907	41	0.36	0.69	2.13	0.665
18	0.34	0.49	2.03	0.555	42	0.43	0.65	2.34	0.335
19	0.27	0.41	1.81	0.398	43	0.43	0.62	2.38	0.901
20	0.35	0.51	2.09	0.283	44	0.44	0.66	2.31	0.681
21	0.40	0.59	2.22	0.293	68	0.32	0.53	1.97	0.912
24	0.44	0.83	2.38	0.846	70	0.26	0.52	1.81	0.956
C3-5 Magnification: 2.144									
9	0.31	0.50	1.94	0.707	43	0.41	0.58	2.28	0.230
16	0.20	0.39	1.53	0.497	47	0.13	0.24	1.22	0.492
17	0.44	0.72	2.31	0.497	56	0.17	0.41	1.44	0.424
23	0.11	0.34	1.19	0.366	57	0.33	0.56	2.00	0.529
27	0.33	0.56	2.03	0.827	60	0.50	0.93	2.50	0.780
32	0.31	0.52	1.97	0.335	62	0.49	0.94	2.47	0.571
33	0.49	0.78	2.50	0.455	64	0.13	0.34	1.06	0.503
35	0.29	0.46	1.94	0.728	70	0.49	0.83	2.50	0.906
39	0.21	0.34	1.69	0.571	71	0.48	0.96	2.41	0.785
41	0.40	0.69	2.22	0.230	78	0.22	0.38	1.63	0.890

Table 6 (Continued)

Section Cell Number	S_p' in.^{2}	S_m' in.^{2}	Z_p' in.	r/R	Section Cell Number	S_p' in.^{2}	S_m' in.^{2}	Z_p' in.	r/R
C3-7	Magnification: 2.146								
1	0.41	0.62	2.25	0.889	36	0.48	0.98	2.44	0.680
3	0.13	0.35	1.31	0.879	37	0.35	0.63	2.09	0.387
15	0.43	0.75	2.31	0.701	45	0.36	0.58	2.19	0.915
16	0.31	0.53	1.94	0.544	46	0.46	0.91	2.38	0.607
17	0.083	0.32	1.03	0.418	51	0.40	0.86	2.28	0.915
19	0.44	0.73	2.38	0.471	61	0.11	0.32	1.16	0.554
21	0.42	0.76	2.25	0.706	63	0.30	0.52	1.94	0.533
23	0.49	0.83	2.47	0.900	71	0.33	0.50	2.03	0.717
24	0.48	0.72	2.44	0.350	74	0.42	0.62	2.31	0.920
28	0.46	0.70	2.41	0.476	76	0.41	0.55	2.25	0.920
C3-9	Magnification: 2.150								
2	0.21	0.33	1.56	0.903	33	0.49	0.87	2.50	0.345
3	0.14	0.28	1.25	0.903	37	0.11	0.27	1.19	0.308
11	0.50	0.77	2.47	0.887	42	0.24	0.44	1.75	0.177
12	0.49	0.83	2.47	0.705	46	0.33	0.55	2.06	0.334
15	0.24	0.40	1.75	0.908	51	0.51	0.89	2.50	0.371
16	0.38	0.55	2.19	0.705	53	0.38	0.63	2.22	0.433
17	0.50	0.73	2.50	0.527	63	0.10	0.26	1.16	0.371
21	0.40	0.72	2.25	0.637	66	0.26	0.49	1.78	0.720
28	0.34	0.64	2.06	0.689	71	0.52	0.73	2.53	0.898
32	0.13	0.39	1.25	0.553	74	0.42	0.61	2.31	0.893
C3-11	Magnification: 2.152								
3	0.47	0.69	2.34	0.887	37	0.44	0.65	2.34	0.714
5	0.47	0.61	2.38	0.714	38	0.38	0.57	2.13	0.542
7	0.37	0.64	2.19	0.761	41	0.50	0.89	2.50	0.245
14	0.48	0.78	2.44	0.553	47	0.52	0.79	2.50	0.725
15	0.33	0.68	2.06	0.678	48	0.43	0.75	2.31	0.464
16	0.22	0.41	1.66	0.887	49	0.24	0.38	1.69	0.334
23	0.37	0.53	2.13	0.323	51	0.46	0.78	2.38	0.402
25	0.44	0.69	2.34	0.605	55	0.49	0.72	2.44	0.892
29	0.50	0.71	2.44	0.605	64	0.33	0.55	2.03	0.902
33	0.48	0.75	2.44	0.511	71	0.16	0.30	1.44	0.897

Table 8 (Continued)

Section Cell Number	S_p' in.^{2}	S_m' in.^{2}	Z_p' in.	r/R	Section Cell Number	S_p' in.^{2}	S_m' in.^{2}	Z_p' in.	r/R
IV. Bed C4, spheres									
C4-3 Magnification: 2.343									
1	0.089	0.26	0.97	0.775	38	0.61	1.41	2.75	0.615
9	0.65	1.12	2.84	0.590	41	0.64	1.06	2.81	0.156
10	0.36	0.68	2.09	0.581	43	0.33	0.57	2.13	0.244
11	0.19	0.41	1.53	0.691	46	0.66	1.48	2.78	0.721
15	0.36	0.64	2.09	0.792	50	0.27	0.61	1.75	0.421
16	0.64	1.18	2.75	0.590	51	0.30	0.68	2.03	0.324
18	0.50	0.74	2.47	0.400	59	0.57	1.29	2.59	0.758
19	0.46	0.78	2.38	0.430	60	0.22	0.37	1.66	0.581
21	0.33	0.72	2.00	0.902	64	0.61	1.00	2.69	0.522
25	0.54	0.90	2.56	0.742	67	0.50	1.01	2.56	0.746
27	0.63	1.26	2.81	0.421	68	0.10	0.28	1.19	0.927
31	0.33	0.61	1.94	0.126	69	0.36	0.67	2.06	0.919
34	0.52	0.90	2.56	0.493	79	0.25	0.61	1.72	0.931
35	0.62	1.16	2.75	0.678	81	0.58	1.29	2.69	0.826
36	0.13	0.39	1.28	0.164	82	0.55	1.15	2.66	0.843
C4-6 Magnification: 2.340									
1	0.62	1.00	2.75	0.919	40	0.47	0.93	2.44	0.354
2	0.16	0.40	1.34	0.914	41	0.60	0.85	2.75	0.758
3	0.41	0.80	2.25	0.927	44	0.58	0.86	2.72	0.255
4	0.24	0.46	1.69	0.914	45	0.16	0.54	1.34	0.480
6	0.53	0.90	2.56	0.762	47	0.47	0.72	2.38	0.927
10	0.22	0.52	1.56	0.763	50	0.13	0.37	1.25	0.581
11	0.61	1.17	2.75	0.914	51	0.63	1.28	2.75	0.400
15	0.19	0.44	1.50	0.607	57	0.27	0.60	1.78	0.523
19	0.56	1.28	2.63	0.919	58	0.54	0.92	2.63	0.931
25	0.30	0.61	1.88	0.463	59	0.58	0.95	2.72	0.891
27	0.60	1.12	2.72	0.784	62	0.24	0.52	1.78	0.522
28	0.52	0.99	2.56	0.256	67	0.62	1.14	2.69	0.754
30	0.21	0.50	1.63	0.299	74	0.18	0.58	1.47	0.906
33	0.55	1.12	2.63	0.733	79	0.49	0.89	2.41	0.742
38	0.23	0.42	1.63	0.801	83	0.48	0.85	2.44	0.931

Table 6 (Continued)

Section Cell Number	S_p' in.^{2}	S_m' in.^{2}	Z_p' in.	r/R	Section Cell Number	S_p' in.^{2}	S_m' in.^{2}	Z_p' in.	r/R
C4-8	Magnification: 2.346								
1	0.61	0.89	2.78	0.935	34	0.33	0.66	2.00	0.438
3	0.51	0.90	2.47	0.931	37	0.63	1.22	2.78	0.333
5	0.32	0.61	1.94	0.935	38	0.49	0.86	2.50	0.455
6	0.63	1.06	2.81	0.795	44	0.59	1.11	2.75	0.377
11	0.11	0.32	1.13	0.725	45	0.59	1.02	2.75	0.135
12	0.34	0.84	2.03	0.741	50	0.52	0.88	2.59	0.914
15	0.19	0.39	1.56	0.851	53	0.54	0.91	2.62	0.632
16	0.55	0.81	2.56	0.615	56	0.52	0.65	2.56	0.324
17	0.63	0.88	2.84	0.560	57	0.63	1.11	2.78	0.308
24	0.30	0.45	1.97	0.577	59	0.52	0.88	2.63	0.468
25	0.36	0.55	2.13	0.447	68	0.59	1.08	2.69	0.527
26	0.44	0.72	2.31	0.421	74	0.64	1.10	2.81	0.910
28	0.38	0.69	2.19	0.649	77	0.10	0.34	1.19	0.678
31	0.61	0.80	2.72	0.927	86	0.33	0.60	2.00	0.927
32	0.13	0.29	1.19	0.750	88	0.37	0.64	2.13	0.931
C4-13	Magnification: 2.347								
1	0.61	1.13	8.69	0.931	37	0.57	0.89	2.66	0.919
4	0.12	0.44	1.22	0.935	38	0.21	0.46	1.59	0.784
7	0.62	1.18	2.78	0.792	41	0.27	0.67	1.84	0.101
9	0.58	0.84	2.72	0.742	45	0.47	0.78	2.47	0.758
10	0.50	0.79	2.44	0.746	50	0.56	1.00	2.63	0.354
13	0.55	0.94	2.63	0.603	51	0.35	0.62	2.03	0.518
15	0.64	1.18	2.84	0.506	52	0.26	0.47	1.81	0.687
17	0.58	1.51	2.72	0.792	58	0.24	0.69	1.75	0.375
19	0.54	1.02	2.63	0.615	59	0.59	0.81	2.78	0.417
23	0.61	0.98	2.78	0.447	62	0.60	1.05	2.72	0.914
25	0.36	0.67	2.13	0.737	64	0.58	1.07	2.75	0.754
29	0.52	1.00	2.59	0.624	67	0.59	0.93	2.69	0.527
30	0.58	0.97	2.72	0.434	71	0.59	1.04	2.78	0.927
34	0.36	0.70	2.06	0.624	74	0.53	0.84	2.56	0.771
36	0.22	0.50	1.69	0.910	75	0.40	0.73	2.22	0.927

Table 6 (Continued)

Section Cell Number	S_p' in.^{2}	S_m' in.^{2}	Z_p' in.	r/R	Section Cell Number	S_p' in.^{2}	S_m' in.^{2}	Z_p' in.	r/R
C4-16 Magnification: 2.340									
5	0.52	0.86	2.53	0.876	38	0.16	0.37	1.44	0.923
7	0.30	0.77	1.84	0.657	41	0.52	1.09	2.56	0.261
13	0.48	0.83	2.38	0.603	53	0.30	0.72	1.91	0.156
14	0.47	0.99	2.50	0.455	54	0.16	0.41	1.41	0.228
19	0.55	1.15	2.66	0.805	57	0.58	1.03	2.75	0.733
22	0.30	0.69	2.00	0.645	58	0.60	1.15	2.75	0.927
23	0.35	0.66	2.03	0.489	60	0.47	0.72	2.50	0.910
25	0.57	0.89	2.72	0.202	61	0.55	0.81	2.72	0.716
26	0.26	0.50	1.81	0.337	66	0.44	0.76	2.34	0.539
27	0.58	1.26	2.75	0.468	67	0.14	0.41	1.25	0.767
28	0.15	0.64	1.44	0.632	69	0.30	0.59	1.97	0.687
29	0.096	0.29	1.03	0.910	70	0.51	0.88	2.56	0.725
30	0.65	1.39	2.75	0.910	74	0.61	1.23	2.78	0.927
31	0.53	0.95	2.56	0.624	75	0.61	0.85	2.72	0.914
32	0.61	1.24	2.78	0.501	79	0.59	1.17	2.75	0.796
V. Bed D1, Raschig rings									
D1-1 Magnification: 2.049									
1	0.67	1.14	4.00	0.836	12	0.32	0.67	3.00	0.329
3	0.68	1.52	5.34	0.854	13	0.69	1.27	5.06	0.543
5	1.02	1.53	3.97	0.494	14	0.49	0.93	3.75	0.854
7	0.57	0.90	4.25	0.561	15	0.98	1.49	3.88	0.805
8	0.51	1.05	3.81	0.775	17	0.11	0.41	1.59	0.146
9	0.53	1.02	3.09	0.848	21	0.43	1.05	3.13	0.439
10	0.71	1.47	4.91	0.525	27	0.81	1.46	5.63	0.817
D1-2 Magnification: 2.054									
2	0.50	0.94	3.63	0.803	11	0.63	1.25	4.75	0.213
3	0.59	1.24	5.25	0.821	12	0.41	0.76	3.47	0.176
5	0.43	0.86	3.34	0.584	13	0.14	0.39	1.22	0.316
6	0.46	0.85	3.25	0.469	16	0.17	0.41	1.78	0.316
7	0.28	0.65	2.19	0.499	20	1.12	1.87	4.09	0.420
8	0.69	2.00	5.50	0.602	21	0.67	1.41	4.69	0.493
9	0.57	1.36	4.41	0.797	29	-	2.73	20.4	1.000

Table 6 (Continued)

Section Cell Number	S_p' in.^{2}	S_m' in.^{2}	Z_p' in.	r/R	Section Cell Number	S_p' in.^{2}	S_m' in.^{2}	Z_p' in.	r/R
D1-4	Magnification: 2.054								
1	0.79	1.35	3.66	0.797	13	0.29	0.80	2.19	0.821
2	0.49	1.12	3.75	0.785	14	0.32	0.59	2.25	0.669
3	0.33	0.88	2.44	0.834	16	-.62	1.29	4.53	0.158
4	0.59	1.25	4.44	0.475	18	0.50	0.82	3.19	0.529
5	0.65	1.37	3.78	0.669	19	0.22	0.57	1.91	0.797
11	0.36	0.63	5.47	0.298	21	0.32	0.61	2.38	0.487
12	0.25	0.50	1.91	0.201	23	0.50	0.93	4.25	0.444
D1-6	Magnification: 2.054								
1	0.38	0.87	2.44	0.828	12	0.32	0.66	2.72	0.146
3	0.66	1.89	4.28	0.651	14	0.82	2.07	6.47	0.602
4	0.63	1.55	5.38	0.779	16	0.41	0.91	3.47	0.475
6	0.23	0.46	2.06	0.335	18	1.03	1.75	4.00	0.274
9	0.14	0.34	1.78	0.493	19	0.83	1.95	6.28	0.609
10	1.07	1.80	4.00	0.657	20	1.03	1.51	4.06	0.815
11	0.56	1.22	4.25	0.377	21	0.67	1.48	5.00	0.627
D1-7	Magnification: 2.060								
6	1.07	1.94	4.09	0.813	15	1.03	1.48	3.91	0.194
7	0.61	1.47	4.91	0.607	16	0.98	1.45	3.88	0.522
8	0.48	0.94	3.75	0.291	17	0.98	1.45	3.88	0.843
10	0.52	1.34	5.13	0.303	18	0.28	0.71	2.44	0.825
11	0.77	1.78	6.47	0.801	20	0.27	0.67	2.76	0.509
13	0.43	1.05	3.47	0.516	21	0.55	0.94	3.94	0.522
14	0.48	0.90	3.38	0.382	23	0.39	0.76	2.41	0.776
D1-9	Magnification: 2.056								
1	0.17	0.59	1.84	0.815	13	0.44	1.05	2.75	0.353
2	0.61	1.75	5.97	0.632	15	0.70	0.88	3.41	0.839
4	0.71	1.56	4.72	0.754	18	0.78	1.73	6.31	0.152
6	0.34	0.63	2.63	0.839	21	0.34	0.59	3.06	0.839
8	0.60	1.31	4.44	0.298	25	0.52	0.78	3.81	0.444
10	0.34	0.71	3.16	0.821	28	0.33	0.63	2.53	0.827
11	0.50	0.98	3.63	0.462	30	0.70	1.33	5.38	0.809

Table 8 (Continued)

Section Cell Number	S_p' in.^{2}	S_m' in.^{2}	Z_p' in.	r/R	Section Cell Number	S_p' in.^{2}	S_m' in.^{2}	Z_p' in.	r/R
D1-10 Magnification: 2.060									
1	0.40	0.96	3.38	0.825	15	0.32	0.72	2.41	0.285
3	0.37	0.79	3.16	0.837	19	0.41	0.76	2.97	0.837
4	0.65	1.16	5.09	0.825	21	0.32	0.62	2.25	0.770
5	0.46	0.72	2.84	0.819	24	0.65	1.71	4.63	0.509
7	0.63	1.19	4.66	0.431	25	0.25	0.48	2.13	0.831
9	0.34	0.76	2.81	0.509	27	1.08	9.98	4.13	0.655
11	0.81	1.49	5.59	0.807	30	0.63	1.16	4.88	0.843
D1-12 Magnification: 2.050									
2	0.65	1.60	5.59	0.841	15	0.29	1.04	2.75	0.286
3	0.50	1.23	2.91	0.622	16	0.083	0.36	1.44	0.122
5	0.38	0.77	2.84	0.847	17	1.05	1.82	4.06	0.280
7	0.45	0.91	3.06	0.549	18	0.43	1.17	3.19	0.707
9	0.23	0.43	2.16	0.616	25	0.59	1.07	4.88	0.829
10	0.69	1.24	5.66	0.219	27	0.33	0.79	2.81	0.841
12	0.60	1.23	4.19	0.408	29	0.44	0.95	3.94	0.853
VI. Bed D2, Raschig rings									
D2-1 Magnification: 2.375									
1	0.74	2.11	3.59	0.523	14	0.86	2.23	5.72	0.190
2	0.96	2.22	5.88	0.855	15	0.72	1.57	5.75	0.443
3	0.93	2.28	5.97	0.833	16	0.43	1.15	3.41	0.797
6	0.49	1.09	3.53	0.390	19	0.17	0.34	2.03	0.860
8	0.65	1.65	4.63	0.549	20	0.32	1.79	2.91	0.865
9	0.95	2.36	6.16	0.691	21	0.83	2.28	3.75	0.411
10	1.14	1.88	4.38	3.839	23	1.46	2.31	4.74	0.549
11	0.29	0.86	2.25	0.622	25	0.53	1.40	3.38	0.839
13	0.13	0.58	1.50	0.169	28	-	5.86	23.5	1.000
D2-4 Magnification: 2.374									
1	0.95	2.03	5.66	0.839	13	0.84	1.64	3.81	0.870
2	0.88	2.31	7.18	0.860	16	0.62	1.48	4.19	0.185
3	0.86	2.22	5.69	0.823	17	1.34	1.99	4.72	0.844
5	0.13	0.51	1.53	0.522	18	1.01	1.77	4.69	0.433
6	0.13	0.54	1.78	0.512	20	1.37	2.36	7.13	0.485
7	0.66	2.00	4.00	0.680	21	0.81	1.78	5.63	0.833
9	0.70	1.54	4.31	0.554	22	0.20	0.81	2.22	0.860
11	1.12	2.51	7.31	0.396	24	1.40	2.30	4.75	0.754
12	0.81	1.79	4.84	0.760	25	0.17	0.56	2.00	0.812

Table 8 (Continued)

Section Cell Number	S_p' in.^{2}	S_m' in.^{2}	Z_p' in.	r/R	Section Cell Number	S_p' in.^{2}	S_m' in.^{2}	Z_p' in.	r/R
D2-6	Magnification: 2.378								
3	0.86	1.97	5.78	0.753	15	0.86	1.67	5.78	0.837
5	1.09	2.45	6.69	0.538	16	1.43	2.06	4.81	0.821
6	0.30	0.87	2.59	0.426	18	0.89	2.36	6.25	0.479
7	1.07	1.85	5.31	0.795	20	0.37	0.86	2.72	0.621
8	0.33	0.70	2.53	0.258	21	0.52	1.12	3.97	0.837
11	0.46	0.73	2.78	0.716	22	0.65	1.59	4.13	0.806
12	0.68	1.83	4.50	0.432	23	0.79	1.53	5.69	0.863
13	0.95	1.63	3.97	0.068	24	0.23	0.54	2.19	0.848
14	1.11	1.81	4.19	0.490	26	0.75	1.68	3.66	0.784
D2-7	Magnification: 2.376								
2	0.78	1.91	5.69	0.848	16	1.06	2.39	6.41	0.854
3	0.43	1.09	2.72	0.775	17	0.99	2.30	6.00	0.485
4	0.75	1.60	5.81	0.559	18	0.84	2.28	6.00	0.532
5	0.82	1.96	4.00	0.696	19	0.25	0.79	2.13	0.543
10	1.00	2.60	5.94	0.860	20	0.89	1.94	5.31	0.759
11	0.15	0.64	1.75	0.485	21	1.50	2.55	4.81	0.812
12	0.93	1.88	5.91	0.153	22	0.46	0.85	3.19	0.848
14	0.97	1.68	4.00	0.474	23	0.55	1.01	3.53	0.843
15	1.41	2.19	4.75	0.827	24	0.81	1.73	3.97	0.833
D2-9	Magnification: 2.377								
3	0.72	1.50	4.94	0.848	13	0.47	1.14	3.19	0.622
4	0.31	1.17	2.72	0.822	14	0.20	0.47	1.91	0.232
5	0.42	0.97	2.56	0.775	15	0.70	1.60	6.03	0.854
6	0.78	1.73	3.91	0.506	17	1.05	2.59	4.84	0.364
7	0.84	2.76	5.91	0.458	18	0.95	2.69	6.19	0.711
8	0.86	2.32	7.03	0.843	19	0.91	1.96	6.25	0.840
9	0.91	2.04	6.19	0.353	20	1.44	3.09	4.72	0.796
10	0.59	2.05	4.41	0.047	21	1.05	2.22	4.19	0.769
12	0.31	1.26	2.25	0.848	22	-	5.37	23.5	1.000
D2-11	Magnification: 2.375								
1	1.11	2.90	7.25	0.844	12	0.44	1.14	2.91	0.174
2	0.61	1.47	3.78	0.855	13	0.65	1.71	4.69	0.317
4	0.92	1.85	6.09	0.839	14	0.72	1.87	4.31	0.781
5	0.13	0.72	1.53	0.749	15	0.15	0.44	1.69	0.369
6	1.03	2.53	6.44	0.443	17	0.41	1.34	2.56	0.833
8	1.48	2.50	4.72	0.491	18	0.40	1.14	3.25	0.870
9	1.06	1.94	5.41	0.76-	19	0.72	1.80	5.50	0.849
10	0.89	2.76	5.91	0.844	21	0.53	1.41	2.94	0.839
11	0.95	3.17	6.28	0.353	22	-	5.69	23.5	1.000

Table 8 (Continued)

Section Cell Number	S_p' in.^{2}	S_m' in.^{2}	Z_p' in.	r/R	Section Cell Number	S_p' in.^{2}	S_m' in.^{2}	Z_p' in.	r/R
D2-12 Magnification: 2.374									
1	0.35	0.84	2.47	0.886	11	0.03	3.01	7.69	0.807
2	0.41	1.04	2.81	0.812	14	0.067	0.46	1.06	0.116
3	0.79	1.59	4.16	0.818	15	0.84	2.52	4.44	0.528
4	0.47	1.04	3.31	0.849	17	1.04	2.08	6.63	0.855
5	1.04	2.49	5.28	0.765	18	1.20	2.53	7.06	0.491
6	0.30	0.69	2.09	0.876	20	0.89	2.73	6.19	0.364
7	0.75	2.04	4.81	0.564	21	1.09	2.85	5.53	0.802
8	0.52	1.46	2.91	0.855	23	0.21	0.59	2.06	0.797
9	0.60	1.51	3.34	0.359	25	0.47	1.15	3.84	0.570
VII. Bed E1, cylinders									
E1-2 Magnification: 2.384									
3	0.99	1.57	3.75	0.865	24	0.22	0.52	2.00	0.184
4	0.69	1.14	3.25	0.635	25	0.76	1.32	3.38	0.115
5	0.44	0.76	2.59	0.635	27	0.91	1.43	3.56	0.614
7	0.59	1.19	2.75	0.876	29	0.86	1.28	3.69	0.886
11	0.26	0.57	2.00	0.299	32	0.59	0.87	3.00	0.325
12	0.72	1.24	3.09	0.441	34	0.46	0.78	2.75	0.881
17	0.78	1.28	3.50	0.226	35	0.17	0.37	2.00	0.635
19	0.47	1.11	3.88	0.472	36	0.97	1.23	3.72	0.577
21	0.61	1.22	2.97	0.876	39	0.37	0.62	2.44	0.886
22	0.35	0.58	2.22	0.656	42	0.35	0.84	2.38	0.813
23	0.20	0.41	2.78	0.608					
E1-3 Magnification: 2.389									
3	0.64	1.08	2.81	0.874	24	0.20	0.35	1.97	0.141
5	0.76	1.26	3.47	0.832	27	0.30	0.68	2.25	0.586
7	0.17	0.54	1.72	0.633	28	0.38	0.72	2.47	0.707
8	0.96	1.35	3.94	0.827	29	0.73	1.08	3.13	0.890
13	0.68	1.00	2.94	0.853	33	0.82	1.21	3.59	0.267
15	0.52	0.94	2.75	0.565	35	0.44	1.01	2.88	0.670
16	0.48	0.85	2.69	0.356	37	0.88	1.34	3.44	0.859
17	0.72	1.25	3.22	0.073	39	0.87	1.17	3.72	0.544
20	0.47	0.73	2.72	0.859	40	0.78	1.18	3.38	0.853
21	0.72	1.04	3.22	0.623	44	0.12	0.38	1.38	0.628
23	0.41	0.82	2.56	0.319					

Table 8 (Continued)

Section Cell Number	S'_p in.^{2}	S'_m in.^{2}	Z'_p in.	r/R	Section Cell Number	S'_p in.^{2}	S'_m in.^{2}	Z'_p in.	r/R
El-6	Magnification: 2.383								
5	0.29	0.69	2.16	0.793	30	0.21	0.45	1.88	0.163
10	0.70	1.01	2.91	0.614	31	0.59	0.89	2.97	0.257
11	0.81	1.31	3.38	0.520	32	0.93	1.44	3.59	0.210
12	0.83	1.42	3.47	0.788	36	0.77	1.13	3.44	0.882
13	0.56	0.79	2.75	0.882	37	0.61	1.04	3.09	0.851
16	0.65	1.16	3.25	0.352	38	0.85	1.34	3.75	0.625
19	0.42	0.76	2.53	0.830	39	0.58	0.93	3.00	0.494
20	0.60	0.83	3.19	0.651	40	0.84	1.25	3.56	0.525
23	0.70	1.01	2.94	0.788	45	0.32	0.64	2.38	0.851
26	0.096	0.32	1.25	0.667	49	0.34	0.77	2.34	0.788
27	0.78	1.18	3.34	0.425					
El-8	Magnification: 2.390								
2	0.63	0.91	3.16	0.838	23	0.81	1.20	3.53	0.230
4	0.58	0.95	2.94	0.848	26	0.43	0.78	2.63	0.832
5	0.23	0.53	1.97	0.738	27	0.85	1.33	3.59	0.408
6	0.16	0.37	1.59	0.849	28	0.56	0.95	2.94	0.105
9	0.43	0.82	2.56	0.524	30	0.79	1.18	3.94	0.890
10	0.19	0.57	1.69	0.607	31	0.72	1.45	3.53	0.644
11	0.13	0.46	1.59	0.565	34	0.82	1.18	3.41	0.701
13	0.06	1.08	2.84	0.874	37	0.72	1.34	3.31	0.639
14	0.44	0.84	2.59	0.764	46	0.27	0.54	2.16	0.827
17	0.80	1.23	3.59	0.476	47	0.75	1.13	3.09	0.864
19	0.32	0.67	2.59	0.811					
El-9	Magnification: 2.382								
2	0.83	1.22	3.44	0.872	26	0.62	1.11	3.09	0.667
3	0.45	0.82	2.63	0.882	28	0.72	1.23	2.88	0.515
7	0.63	0.93	3.00	0.583	31	0.70	1.22	3.13	0.383
10	0.64	0.94	3.28	0.861	34	0.72	1.17	3.48	0.830
15	0.89	1.19	3.59	0.641	35	0.15	0.38	1.63	0.651
16	0.62	1.04	2.78	0.872	37	0.47	0.70	2.66	0.389
17	0.58	0.95	2.99	0.672	39	0.92	1.70	3.75	0.735
19	0.37	0.59	2.44	0.200	41	0.52	0.66	2.69	0.893
22	0.16	0.31	1.66	0.494	42	0.67	1.31	3.16	0.809
23	0.89	1.26	3.75	0.305	45	0.81	1.21	3.19	0.877
24	0.53	0.75	2.81	0.000					

Table 8 (Continued)

Section Cell Number	S_p' in.^{2}	S_m' in.^{2}	Z_p' in.	r/R	Section Cell Number	S_p' in.^{2}	S_m' in.^{2}	Z_p' in.	r/R
E1-11 Magnification: 2.377									
2	0.24	0.46	2.00	0.873	20	0.95	1.55	3.50	0.679
3	0.17	0.42	1.56	0.868	21	0.80	1.66	3.63	0.663
5	0.41	0.66	2.50	0.842	23	0.13	0.34	1.38	0.021
6	0.73	1.16	3.38	0.821	25	0.85	1.18	3.72	0.416
7	0.32	0.58	2.34	0.642	29	0.82	1.17	3.53	0.284
8	0.64	0.87	3.25	0.494	30	0.65	1.04	3.28	0.284
9	0.74	1.05	3.41	0.584	38	0.70	1.04	3.03	0.500
12	0.64	1.01	2.88	0.868	39	0.11	0.35	1.56	0.584
15	0.57	0.85	2.88	0.363	41	0.79	1.12	3.19	0.847
18	0.33	0.61	2.28	0.363	46	0.52	0.79	3.16	0.642
19	0.11	0.26	1.44	0.558					
VIII. Bed E2, cylinders									
E2-2 Magnification: 3.313									
1	0.22	0.57	2.09	0.824	9	1.09	2.53	4.03	0.794
2	1.62	1.97	4.56	0.812	10	0.96	1.76	3.88	0.800
3	1.67	2.86	5.00	0.587	11	1.82	2.63	5.00	0.444
4	1.40	2.08	4.19	0.356	12	0.23	1.18	2.06	0.332
5	1.39	2.07	4.88	0.723	14	1.40	2.18	4.38	0.824
6	1.55	2.52	4.50	0.450	15	0.97	1.88	3.78	0.545
7	0.43	0.90	2.81	0.403	17	-	4.04	20.9	1.000
8	0.87	1.67	3.66	0.036					
E2-4 Magnification: 3.321									
1	1.59	2.65	5.00	0.768	10	1.74	3.21	4.69	0.225
2	1.65	2.91	5.31	0.662	11	0.25	0.70	2.25	0.810
3	1.56	2.28	4.53	0.349	12	1.76	2.47	4.91	0.762
4	0.58	1.10	3.09	0.260	13	1.31	1.91	4.44	0.762
5	0.47	0.98	2.88	0.585	14	1.57	2.21	4.94	0.762
7	1.11	2.43	5.16	0.768	15	1.14	1.66	3.94	0.810
8	1.37	2.11	4.56	0.426	16	-	3.87	21.1	1.000
9	1.68	2.53	5.13	0.721					

Table 8 (Continued)

Section Cell Number	S_p' in.^{2}	S_m' in.^{2}	Z_p' in.	r/R	Section Cell Number	S_p' in.^{2}	S_m' in.^{2}	Z_p' in.	r/R
E2-5	Magnification: 3.328								
1	0.46	1.06	2.75	0.825	11	0.15	0.52	2.00	0.224
2	1.73	2.64	5.22	0.731	12	1.62	7.35	4.66	0.377
3	1.26	1.61	4.13	0.778	13	1.42	2.24	4.25	0.808
4	1.73	2.51	5.09	0.737	14	0.47	1.27	2.75	0.796
6	0.19	0.69	2.00	0.253	15	0.79	1.26	3.50	0.472
7	1.58	2.79	4.88	0.342	16	1.66	2.36	4.69	0.814
8	0.96	1.74	3.81	0.702	18	1.97	3.22	5.56	0.713
9	1.72	2.80	5.31	0.365					
E2-7	Magnification: 3.328								
1	0.60	1.50	3.00	0.837	10	1.88	2.80	5.09	0.766
2	0.87	2.50	3.81	0.825	11	1.85	3.43	5.44	0.477
3	1.35	2.62	4.13	0.495	13	0.59	0.95	3.03	0.436
4	0.11	0.52	1.63	0.271	15	0.73	1.18	3.38	0.796
5	1.54	2.76	4.66	0.519	16	1.31	1.99	4.50	0.619
6	0.49	1.17	2.91	0.802	17	0.88	1.48	3.59	0.749
8	1.25	1.85	3.97	0.819	18	0.27	0.83	2.03	0.625
9	0.65	1.24	3.28	0.495					
E2-10	Magnification: 3.328								
2	1.21	1.91	4.19	0.595	10	1.45	1.96	4.25	0.790
3	1.86	2.69	5.28	0.725	11	1.10	1.64	4.00	0.271
4	1.65	2.69	4.78	0.595	12	0.98	1.55	4.94	0.377
5	0.70	1.10	3.34	0.808	13	0.081	0.58	1.19	0.625
6	1.82	2.53	5.41	0.348	14	1.88	2.77	5.47	0.678
7	0.58	1.26	3.19	0.153	15	1.23	1.75	4.00	0.784
8	1.14	2.14	4.25	0.472	16	1.45	2.44	4.84	0.790
9	1.79	2.62	5.28	0.796					
E2-11	Magnification: 3.322								
1	1.71	2.35	5.03	0.762	14	1.21	1.93	4.51	0.732
2	0.31	0.81	2.28	0.797	15	1.11	1.85	3.94	0.407
3	1.25	2.07	4.78	0.744	16	1.74	2.68	5.03	0.774
4	1.48	2.10	4.47	0.679	17	0.68	1.67	3.31	0.803
6	1.46	2.36	4.75	0.348	18	0.32	0.82	2.28	0.573
8	0.34	0.90	2.28	0.809	19	0.95	1.76	4.03	0.791
10	1.27	1.59	4.06	0.821	20	0.13	0.50	1.75	0.803
12	1.65	2.64	4.63	0.331					

Table 8 (Continued)

Section Cell Number	S_p' in.^{2}	S_m' in.^{2}	Z_p' in.	r/R	Section Cell Number	S_p' in.^{2}	S_m' in.^{2}	Z_p' in.	r/R
E2-14	Magnification: 3.309								
2	0.90	1.73	4.03	0.688	13	1.81	2.51	4.91	0.468
3	1.64	2.14	4.81	0.771	14	1.42	2.08	4.59	0.255
4	0.90	1.68	3.69	0.368	15	1.34	2.10	4.38	0.451
5	0.55	1.03	2.94	0.409	16	0.59	1.65	3.22	0.783
6	0.69	1.26	3.38	0.735	17	0.67	1.23	3.28	0.806
7	1.33	1.78	4.16	0.818	18	0.68	1.51	3.59	0.789
9	0.23	0.70	2.03	0.225	19	1.79	2.92	5.34	0.729
11	0.35	0.89	2.50	0.801					
E2-16	Magnification: 3.316								
1	0.27	0.90	2.22	0.841	10	1.99	3.35	5.63	0.687
3	1.68	2.57	5.00	0.568	11	0.27	0.63	2.31	0.260
4	0.33	0.67	2.56	0.403	12	0.73	1.17	3.38	0.474
5	1.65	2.81	5.16	0.604	13	1.92	2.75	5.80	0.497
6	1.28	1.79	4.00	0.817	14	1.31	2.11	4.63	0.710
7	1.26	1.79	4.13	0.225	15	0.30	0.88	2.38	0.764
8	1.52	2.14	4.47	0.166	17	1.08	1.67	4.09	0.793
9	1.64	2.56	4.59	0.752					